



UNIVERSITETET I AGDER

# Modelling, Simulation, and Testing of an Active Heave Compensation Winch

Silje Gunvaldsen  
Tonje Gunvaldsen

## Supervisors

Michael R. Hansen  
Øyvind Solli

*This Master's Thesis is carried out as a part of the education at the University of Agder and is therefore approved as a part of this education. However, this does not imply that the University answers for the methods that are used or the conclusions that are drawn.*

University of Agder, 2013  
Faculty of Technology and Science  
Department of Engineering

# Abstract

Modelling and simulation play an important role in modern engineering. This is partly because simulation generally is less expensive, safer and more time efficient compared to experimental testing and prototyping. There are a variety of modelling and simulation tools on the market today. This report concerns the development of a dynamic simulation model for an active heave compensation winch system, using the software tool 20-sim. The model is developed in cooperation with the company Cargotec that is a world leading company within manufacturing of large offshore load handling equipment.

The winch system has been analyzed and a dynamic simulation model has been developed. To optimize and confirm the validity of the model, experimental testing was performed by the support of Cargotec. The optimization was based on several test runs using varying input parameters. Model parameters were estimated by comparing simulated and experimental data. Simulation results indicate that the proposed model is in accordance with the experimental results.

The motion controller used in this work consist of a feedforward control and a feedback controller. Three different feedforward strategies were evaluated and tested on the winch system. One feedforward which was explored is the model-based prediction of input. A model-based feedforward dependent on pressure measurements was successfully implemented.

Based on the quality of the developed simulation model it is concluded that it can be used to study system behavior under different operating conditions. In addition, it can be used to analyze and design controllers for the system.

# Acknowledgements

This study would not have been possible without the guidance and the support of several individuals. First and foremost, the authors would like to express their gratitude to Prof. Dr. Michael Rygaard Hansen, for his supervision. He offered valuable assistance in the field of hydraulics and modelling of hydraulic systems.

The authors would also like to thank supervisor Øyvind Solli at Cargotec, for his support, commitment and active interest.

Finally, the authors would like to thank everybody who was involved with the experimental work performed at Cargotec. Many thanks go in particular to Børge Christian Mosgren at Cargotec, for his assistance and support with the PLC programming.

June, 2013

Silje Gunvaldsen

Tonje Gunvaldsen

# List of Figures

2.1	Principle diagram of a passive heave compensator . . . . .	4
2.2	Electro-hydraulic controlled 4/3-way proportional directional control valve . . . . .	5
2.3	4/4-way proportional directional control valve . . . . .	6
2.4	Different valve lapping when the spool is in neutral position . . . . .	6
2.5	Flow-signal graph of different center types . . . . .	6
2.6	Typical flow-signal curves . . . . .	7
3.1	Schematic drawing of system . . . . .	9
3.2	Hydraulic Diagram . . . . .	10
3.3	Parker F12-60 Hydraulic Motor . . . . .	12
3.4	Parker Hannifin D3FP Direct Operated Control Valve . . . . .	13
3.5	Parker Hannifin VCD Technology . . . . .	13
4.1	Drum dimensions . . . . .	17
4.2	FBD of the payload . . . . .	18
4.3	The mechanical system . . . . .	20
4.4	Payload diagrams . . . . .	20
4.5	FBD's of the different wire mass sections . . . . .	22
4.6	FBD of sheave . . . . .	23
4.7	FBD's and KD's showing rotary dynamics . . . . .	24
4.8	Hydraulic motor driving a positive load . . . . .	26
4.9	Hydraulic motor driving a negative load . . . . .	26
4.10	Schematic drawing of a pressure compensator . . . . .	31
4.11	Velocity profiles of laminar and turbulent flows . . . . .	32
4.12	Viscosity of typical hydraulics fluids . . . . .	34
4.13	Variation of fluid stiffness with temperature and pressure . . . . .	35
4.14	Variation of effective stiffness with respect to fluid-air mixture at 40°C . . . . .	36
5.1	Feedforward control . . . . .	39
5.2	Final control loop . . . . .	42
6.1	Illustration of wave motion . . . . .	44
6.2	20-sim model of the mechanical system . . . . .	45
6.3	20-sim model of the hydraulic system . . . . .	47
6.4	Hydraulic motor block . . . . .	48
6.5	20-sim model of the motor and the gearbox . . . . .	49
6.6	Symbol of the proportional valve in 20-sim . . . . .	50
6.7	Different possible spool positions of the servo valve . . . . .	50
6.8	Frequency response $\pm 5\%$ and $\pm 90\%$ of command signal. . . . .	51

6.9	Bode diagram of servo valve spool dynamics . . . . .	52
6.10	Flow characteristic of D3FP valve . . . . .	53
6.11	Model used to verify the flow characteristics of the D3FP valve . . . . .	54
6.12	Flow characteristic at $\Delta p = 35$ bar per metering edge . . . . .	54
6.13	Laminar Resistance Block . . . . .	55
6.14	PI-controller with feedforward . . . . .	56
6.15	Steady state simulation results . . . . .	57
6.16	Simulation results with heave disturbance . . . . .	58
6.17	Simulation results with angular drum velocity and heave disturbance . . . . .	59
6.18	20-sim model of the hydro-mechanical system . . . . .	60
6.19	Simulation results of active heave compensation . . . . .	61
6.20	Simulation results of active heave compensation . . . . .	62
7.1	System Components . . . . .	64
7.2	Experimental setup . . . . .	65
7.3	Sensors . . . . .	66
7.4	Siemens S7 modular PLC . . . . .	66
7.5	PR card . . . . .	67
7.6	ServiceLab worksheet . . . . .	70
8.1	Import of data in 20-Sim . . . . .	75
8.2	Control signals from tests (payload of 500 kg) . . . . .	75
8.3	Control signals from tests (payload of 200 kg) . . . . .	76
8.4	Measured supply pressure . . . . .	76
8.5	Measured tank port pressure . . . . .	77
8.6	Workport pressures with "Heave 1" (Load case1) . . . . .	78
8.7	Payload position and position error with "Heave1" (Load case 1) . . . . .	79
8.8	Payload position and position error with "Heave2" (Load case 1) . . . . .	80
8.9	Workport pressures with "Heave 1" (Load case 2) . . . . .	81
8.10	Payload position and position error with "Heave1" (Load case 2) . . . . .	81
8.11	Pressure drop across the motor with a payload of 500 kg . . . . .	82
8.12	Validation of implemented friction model . . . . .	83
8.13	Measured and ideal mean value of PT4 and PT3 . . . . .	84
8.14	Asymmetry curve . . . . .	85
8.15	Pressures as a result of asymmetry . . . . .	86
8.16	Pressures as a result of asymmetry and external motor leakage . . . . .	86
8.17	Flow characteristics of servo valve . . . . .	87
8.18	Motor flow with different flow characteristics . . . . .	87
8.19	Measured input signal versus valve feedback signal . . . . .	88
8.20	Measured control effort and deviation . . . . .	90
8.21	Measured feedback control . . . . .	91
8.22	Simulated. Load 200kg. . . . .	92

# List of Tables

2.1	Application fields of servo and proportional valves . . . . .	8
3.1	Wire data . . . . .	12
3.2	Hydraulic motor data . . . . .	13
3.3	Servo valve data . . . . .	14
3.4	PVG 120 data . . . . .	14
3.5	Hydraulic oil properties . . . . .	15
4.1	System Parameters . . . . .	16
4.2	Results Winch Calculations . . . . .	18
4.3	Torque Estimation . . . . .	19
4.4	Hydraulic Motor Efficiencies . . . . .	28
4.5	Computed bandwidths . . . . .	38
6.1	Different spool positions and the flow direction . . . . .	50
6.2	Characteristic frequencies of Parker D3FP valve . . . . .	51
6.3	Lookup table . . . . .	53
6.4	Static Analysis vs. Simulation . . . . .	58
7.1	Sensors . . . . .	64
7.2	PLC Components . . . . .	67
7.3	Signal voltage - PVES . . . . .	68
7.4	PLC Blocks . . . . .	68
7.5	I/O table for PLC . . . . .	69
7.6	ServiceLab - Process Variables . . . . .	70
7.7	Test Procedure . . . . .	72
7.8	Pre-Startup Checks . . . . .	73
D.1	Hose table . . . . .	140

# Abbreviations

<b>AHC</b>	Active Heave Compensation
<b>DB</b>	Data Block
<b>FB</b>	Function Block
<b>FBD</b>	Free Body Diagram
<b>FC</b>	Function
<b>FFW</b>	Feedforward
<b>HPU</b>	Hydraulic Power Unit
<b>KD</b>	Kinetic Diagram
<b>MRU</b>	Motion Reference Unit
<b>M&amp;S</b>	Modelling and Simulation
<b>OB</b>	Organization Block
<b>PCD</b>	Pitch Circle Diameter
<b>PHC</b>	Passive Heave Compensation
<b>PLC</b>	Programmable Logic Controller
<b>PR-Card</b>	Permanent Resident Card
<b>PVG</b>	Proportional Valve Group
<b>PT</b>	Pressure Transmitter
<b>VCD</b>	Voice Coil Drive

# Contents

<b>List of Figures</b>	<b>iii</b>
<b>List of Tables</b>	<b>v</b>
<b>Abbreviations</b>	<b>vi</b>
<b>1 Introduction</b>	<b>1</b>
1.1 Motivation	1
1.2 Problem Statement	1
1.3 Report Outline	2
<b>2 Theoretical Background</b>	<b>3</b>
2.1 Heave Compensation	3
2.1.1 Passive Heave Compensators	3
2.1.2 Active Heave Compensators	4
2.1.3 Combined Passive/Active Heave Compensation Systems	4
2.2 Directional Control Valves	5
2.2.1 Classification of Spool Type Valves	5
2.2.2 Types of Valve Center	6
2.2.3 Proportional Valves versus Servo Valves	7
<b>3 System Information</b>	<b>9</b>
3.1 Introduction	9
3.2 System Overview	9
3.3 Hydraulic Winch	12
3.4 Hydraulic Motor	12
3.5 Servo Valve	13
3.6 Proportional Valve	14
3.7 Hydraulic Power Unit	15
3.8 Accumulator	15
3.9 Hydraulic Fluid	15
<b>4 System Analysis</b>	<b>16</b>
4.1 Introduction	16
4.2 Winch Calculations	17
4.3 Static Analysis of the Mechanical System	18
4.3.1 Wire Force	18
4.3.2 Torque Estimation	19



4.4	Dynamic Analysis of the Mechanical System . . . . .	19
4.4.1	Linear Dynamics . . . . .	19
4.4.2	Rotary Dynamics . . . . .	23
4.5	Analysis of the Hydraulic System . . . . .	25
4.5.1	Motor . . . . .	25
4.5.2	Control Valves . . . . .	29
4.5.3	Hydraulic Lines . . . . .	31
4.5.4	Hydraulic Fluid Properties . . . . .	34
4.5.5	Fluid Compressibility Effects . . . . .	36
4.6	Eigenfrequency of the Hydro-Mechanical System . . . . .	37
<b>5</b>	<b>Control Design</b>	<b>39</b>
5.1	Introduction . . . . .	39
5.2	Feedforward Control . . . . .	39
5.3	Feedforward plus Feedback Control . . . . .	42
<b>6</b>	<b>Modelling and Simulation</b>	<b>43</b>
6.1	Introduction . . . . .	43
6.2	20-sim . . . . .	43
6.3	Heave Motion . . . . .	44
6.4	Mechanical System . . . . .	45
6.4.1	Payload . . . . .	45
6.4.2	Drum and Sheave . . . . .	46
6.4.3	Wire . . . . .	46
6.5	Hydraulic System . . . . .	47
6.5.1	Hydraulic Power Unit . . . . .	47
6.5.2	Motor . . . . .	47
6.5.3	Gearbox . . . . .	49
6.5.4	Parker D3FP Valve . . . . .	49
6.5.5	Hose Lines . . . . .	55
6.6	Control System . . . . .	56
6.7	Verification of Model by Simulation . . . . .	57
6.7.1	Mechanical Model . . . . .	57
6.7.2	Hydro-Mechanical Model . . . . .	60
<b>7</b>	<b>Experimental Work</b>	<b>63</b>
7.1	Introduction . . . . .	63
7.2	Electrical Instrumentation . . . . .	63
7.2.1	Sensors . . . . .	63
7.2.2	Programmable Logic Controller . . . . .	66
7.2.3	PR-Card / Isolation Amplifier . . . . .	67
7.2.4	Joystick . . . . .	68
7.3	PLC Programming . . . . .	68
7.4	Data Logging in ServiceLab . . . . .	69
7.5	Testing . . . . .	71
7.5.1	Test Cases . . . . .	71
7.5.2	Test Procedure and Checklist . . . . .	72

<b>8</b>	<b>Model Calibration and Validation</b>	<b>74</b>
8.1	Introduction . . . . .	74
8.2	Model Inputs . . . . .	74
8.3	Comparison of Simulated and Measured Test Data . . . . .	77
8.3.1	Load Case 1 . . . . .	77
8.3.2	Load Case 2 . . . . .	80
8.4	Parameter Identification and Optimization . . . . .	82
8.4.1	Motor Friction . . . . .	82
8.4.2	Valve Asymmetry and Leakage . . . . .	84
8.4.3	Valve Area-Opening Relationship . . . . .	86
8.4.4	Valve Dynamics . . . . .	87
8.5	Key findings . . . . .	88
8.6	Using the Calibrated Model . . . . .	89
8.6.1	Evaluation of Control Strategies . . . . .	89
8.6.2	Importance of valve bandwidth . . . . .	92
<b>9</b>	<b>Conclusion and Further Work</b>	<b>94</b>
	<b>Bibliography</b>	<b>95</b>
<b>A</b>	<b>20-sim Model</b>	<b>96</b>
<b>B</b>	<b>Electrical Loop Diagrams</b>	<b>112</b>
<b>C</b>	<b>PLC Program</b>	<b>118</b>
<b>D</b>	<b>Hose Table</b>	<b>139</b>
<b>E</b>	<b>Technical Datasheets</b>	<b>141</b>
E.1	Parker Hydraulic Motor . . . . .	141
E.2	Parker Servo Valve . . . . .	147
E.3	Sauer Danfoss PVG120 . . . . .	154
E.4	Brevini Hydraulic Winch . . . . .	161



# Chapter 1

## Introduction

### 1.1 Motivation

The use of modelling and simulation (M&S) within engineering is well recognized. This is because simulation studies generally are less expensive and safer than experimenting with the real system. By M&S the systems can be tested in a different manner than what is possible in real test and the system limits can be verified without the risk of damage. M&S could therefore increase the quality of products and systems and reduce the change of failure.

Cargotec, a cargo handling solutions provider, is aware of the major potential and application of M&S. Currently they want to invest in M&S in their engineering divisions. This study was performed in this context.

### 1.2 Problem Statement

This master thesis deals with modelling, simulation and testing of an active heave compensation (AHC) winch. The problem tasks of the study are:

1. Analyze the AHC winch system.
2. Create a dynamic model of the real system using 20-sim.
3. Perform tests and measurements to use for calibration and validation of the dynamic simulation model.
4. Evaluate different control strategies.
5. If time allows: Evaluate the potential to use simpler and less expensive control valves.

## 1.3 Report Outline

**Chapter 2** provides basic information about heave compensation and directional control valves. Three kinds of heave compensation systems are explained. The directional control valves are studied since these valves are important in active heave compensation systems.

**Chapter 3** provides an overview of the experimental system. The hydraulic diagram and the system components are presented in this chapter.

**Chapter 4** presents the system analysis. This analysis comprises winch calculations, static and dynamic analysis of the mechanical system, analysis of the hydraulic system and eigen-frequency calculations. The main purpose of the system analysis was to derive and set up equations to use in the modelling of the experimental system.

**Chapter 5** presents the control system. Feedforward control and combined feedforward plus feedback control are discussed. One implementation of feedforward that are explored, is the model-based prediction of input.

**Chapter 6** concerns the modelling and simulation of the experimental system. Modelling of the system require three main parts; mechanical modelling, hydraulic modelling and control system. The building of the model in 20-sim is systematically explained. At the end of this chapter, the hydro-mechanical model is verified by simulation.

**Chapter 7** presents the experimental work. Information about the electrical instrumentation, the PLC programming and the testing are presented in this chapter.

**Chapter 8** is all about the calibration and validation of the 20-sim model. First, the simulated and measured test data are compared. Thereafter, model parameters are estimated using the experimental data. At the end of this chapter, the calibrated model is used to evaluate control strategies and the importance of valve bandwidth.

**Chapter 9** presents the conclusion and suggestions for further work.

# Chapter 2

## Theoretical Background

### 2.1 Heave Compensation

Ships and floating offshore installations are subjected to ocean wave induced heave motion. The vessel's heave motion has a significant effect on several marine applications, such as subsea lifting operations. During deep-water lifting operations, heave compensation may be used to control the vertical motion of the payload and to reduce the dynamic loads in the hoisting system. This improves the accuracy of the positioning of the load.

In general, heave compensation can be divided into three kinds of system [1]:

- passive heave compensators
- active heave compensators
- combined passive/active heave compensation systems

#### 2.1.1 Passive Heave Compensators

A passive heave compensator is in principle a pure spring damper system that do not require any input of energy during operation [1]. Passive heave compensation (PHC) systems absorb energy created by the motion of the vessel and store this as potential energy.

A principle diagram of a passive heave compensator system is given in Fig. 2.1. The system is installed onto the wire of a winch. It consists of a hydraulic cylinder provided with a wire sheave on top. The bottom end of the cylinder is connected via a medium separator to a number of pressure tanks. The tanks absorbs the energy when the floating piston is forced upwards.

PHC systems reduce dynamic loads, and is mainly used in situations where the load is positioned on the seabed, for example as a drill string compensator. However, it can also be used for motion compensation [2].

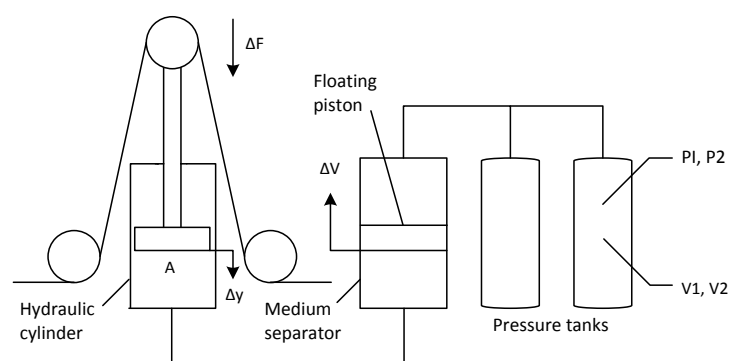


Figure 2.1: Principle diagram of a passive heave compensator

### 2.1.2 Active Heave Compensators

Active Heave Compensation (AHC) can be used to control the relative position of a load to a fixed object. AHC differs from PHC by having a control system, for example a Programmable Logic controller (PLC), that actively tries to compensate for any movement. The control system requires the knowledge about the vessel's heave motion. AHC systems often use a Motion Reference Unit (MRU) which measures the vessel's heave, pitch and roll motion [1].

AHC systems are controlled by reference signals. Examples of input values [1]:

- wire tension
- crane top motion
- winch or hydraulic piston motion
- position of lifted object
- vessel motion
- wave height/ current velocity

AHC systems makes the hoisting, lowering and handling of loads on floating vessels safer. Without such systems many operations performed on rough sea would not be possible. AHC systems are widely used to minimize unwanted drill string movement.

### 2.1.3 Combined Passive/Active Heave Compensation Systems

In a combined system the active system is working in parallel with the passive. Such systems use advantages from both methods. The combined system can be designed with cylinder and winch based technology. A combination of passive and active heave compensation with hydraulic cylinders results in limited power consumption. [2]

## 2.2 Directional Control Valves

The most common form of directional control valve is the spool valve. Proportional valves and servo valves are spool type control valves. These valves can be adjusted to an infinite number of positions within their range, making these valves a combination of a pure directional valve and a flow control valve. The movement of the spool restricts the flow, thus controlling the fluid flow. Since directional control valves are the main part of the control process in AHC systems, such valves have been studied. This section presents the characteristics and the principal function of directional control valves.

### 2.2.1 Classification of Spool Type Valves

Typical spool valve configurations are classified by the number of ways (ports) flow can enter and leave the valve and the number of switching positions. Four-way valves are most common, and are usually used for double sided control of pistons or hydraulic motors. They direct inlet flow from the pump to the system through one of two outlet ports. They usually have a pressure port (P) which is connected to the pump, a tank port (T) which are connected to the reservoir, and two working ports (A,B) which are connected to an actuator unit. The number of switching positions on a spool varies from one in a primitive valve to two or three. Special valves may have more [3].

Spool control valves may also be classified according to the actuation method available to control the spool position. External signal commands (electrical, manual, pilot pressure), and internal signal commands (pilot pressure, spring force) may be applied to shift the position of the spool [3]. Fig. 2.2 displays a 4/3-way proportional directional control valve. The symbol displays an electro-hydraulic controlled valve in the center position, centered by springs. At this position the flow between the ports are blocked.

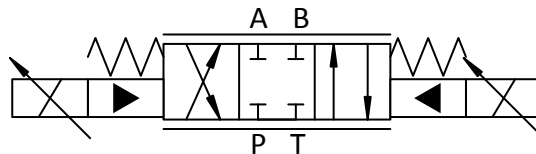


Figure 2.2: Electro-hydraulic controlled 4/3-way proportional directional control valve

The fundamental principle of operating a proportional valve is based on a proportional solenoid. This moves the valve spool to the desired position. Many proportional directional control valves, such as the valve displayed in Fig. 2.2, have two solenoids, one solenoid at each end of the valve. Other proportional directional valves have only one coil. These valves typically have four rather than three positions. Fig. 2.3 gives a schematic of a 4/4-way single coil proportional valve. Such valves are usually high performance valves, and are by some manufacturers termed as servo-proportional valves. This because of their higher dynamic performance. The higher dynamic performance can be explained by the fact that the displacement of the spool is not affected by the hysteresis typical of the centering springs found in a dual coil proportional valve. [4]



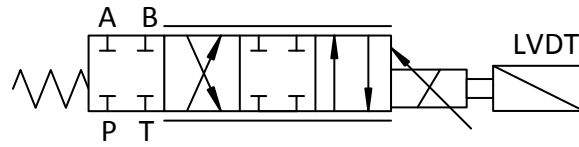


Figure 2.3: 4/4-way proportional directional control valve

### 2.2.2 Types of Valve Center

For a spool directional control valve, the spool slides axially in a bore or sleeve. The type of valve center (open, closed, critical) is defined by the width of the spool lands relative to the width of the ports in the valve bore or sleeve, when the valve spool is in neutral position. A key characteristic is the amount of valve lap. As shown in Fig. 2.4, there are three possible lap configurations: under-lap, over-lap, or zero-lap. The two control valves included in the experimental setup have different types of valve centers. The servo valve has a critical center (zero-lap), while the proportional valve has a closed center (over-lap).

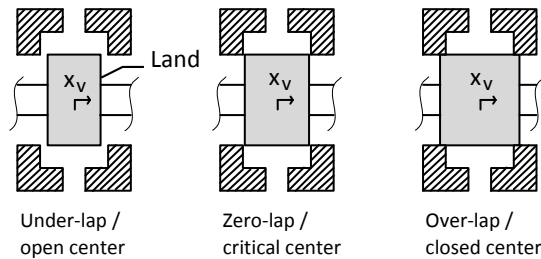


Figure 2.4: Different valve lapping when the spool is in neutral position

The flow characteristics of a valve are related to the type of valve center. Fig. 2.5 illustrates the theoretically flow gain characteristics of the different center types. As seen from the figure, the flow gain is constant through null for an ideal zero-lapped valve. If the spool is over-lapped, the valve flow gain is reduced at null. Likewise, an under-lap produces higher valve flow gain. However, for a practical valve the flow gain varies depending on non-linearities and hysteresis. [3]

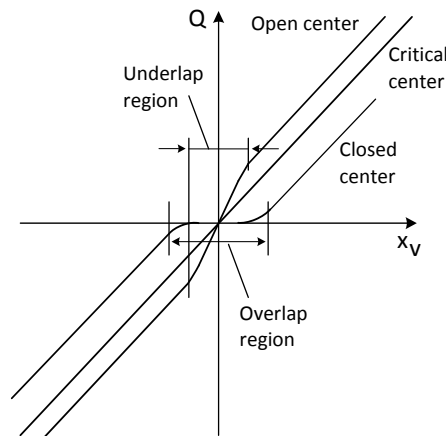


Figure 2.5: Flow-signal graph of different center types [3]

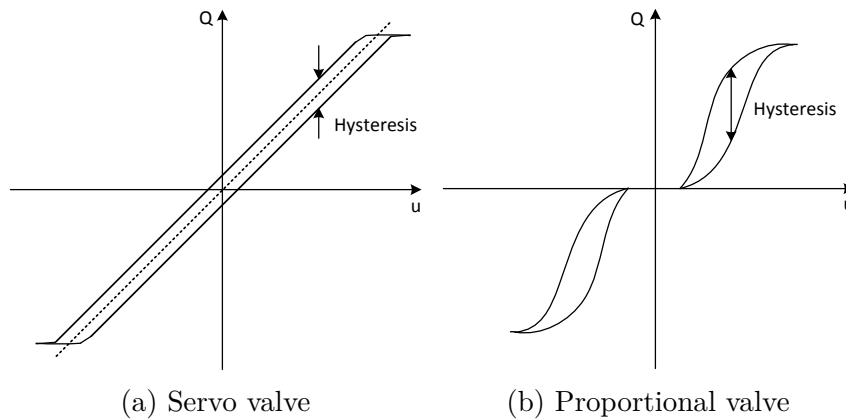


Figure 2.6: Typical flow-signal curves [3]

Qualitative examples illustrating the effect of hysteresis on the flow characteristics are presented in Fig. 2.6. As seen, the hysteresis is more consistent for a servo valve.

A majority of commercially available servo valves are manufactured with a critical center because of the emphasis with the linear flow gain. Such valves are suitable for position control systems because they deliver seamless control of flow to an actuator.

Closed center valves are not desirable because of the dead-band characteristics near neutral in the flow gain. There is no flow when the spool is in the dead-band region. Thus, the spool must move a certain distance (equal to the overlap dimension) before any flow is delivered to the actuator ports. Most proportional valves are designed and manufactured with a targeted amount of overlap. Some valves have dead-bands as great as 20%, which simply means that the controller must output a 20% control signal to overcome the lap. These valves can be a problem in applications where the spool must be shifted back and forth across the null position to hold a position or pressure. Many motion controllers have dead-band parameters and can compensate for the dead-band region. However, the spool still takes time to shift the spool through the dead-band.

Open center valves has a higher flow gain near neutral. The benefit for open center valves are faster response with a cost of high leakage flows. Such valves are normally preferred in applications which require a continuous flow. [3]

### 2.2.3 Proportional Valves versus Servo Valves

Servo valves are complex valves with very high performance, which are frequently used in closed-loop arrangements. These valves are precisely machined spool-type directional control valves, capable of controlling the oil flow rapidly and accurately. They are electrically controlled by an internal sensing and control mechanism, and have a sleeve and spool assembly in the main stage. The sleeve allows for simpler machining of the sleeve lands in comparison to machining the internal body lands of a typical proportional valve. Because of the tight manufacturing tolerances, servo valves tend to be expensive. [3][4]

Table 2.1: Application fields of servo and proportional valves, as presented in [3]

Application fields	Servo Valve	Proportional Valve
Closed-loop/open-loop control	Closed-loop control	Open-loop control Closed-loop control (refined)
Position/angle and force/-torque control	Well suited	Not possible due to non-smooth flow-signal curve (dead band) Possible (refined)
Velocity/speed control	Well suited	Possible

Proportional valves are not manufactured by such precision as servo valves. Typical proportional valves consist of a proportional spool that slides in a cast housing, i.e. no sleeve/spool in the main stage (unlike a servo valve). "Unrefined" proportional valves are usually less expensive than servo valves with larger values of hysteresis and dead-bands. They also tend to be limited in their dynamic performance. They are mainly used for open-loop control. However, highly sophisticated proportional valves are also available today, which show very good dynamic characteristics similar to those of servo valves. These valves are known as "refined" proportional valves, and are well suited for closed-loop control. [3]

However, the definitions of servo valve and proportional valve and the distinction between the two have become more and more vague and overlapping [3]. The application fields of servo and proportional valves are given in Table 4.1.

# Chapter 3

## System Information

### 3.1 Introduction

In this chapter, the hydraulic winch system and its components are presented. A schematic drawing of the mechanical parts of the system is given in Fig. 3.1. As illustrated, the wire run from a winch drum over a wire sheave and down to a load, where it is attached. The hydraulic system capable of actuating the mechanical system is presented in the next section. Technical data sheets can be found in Appendix E.

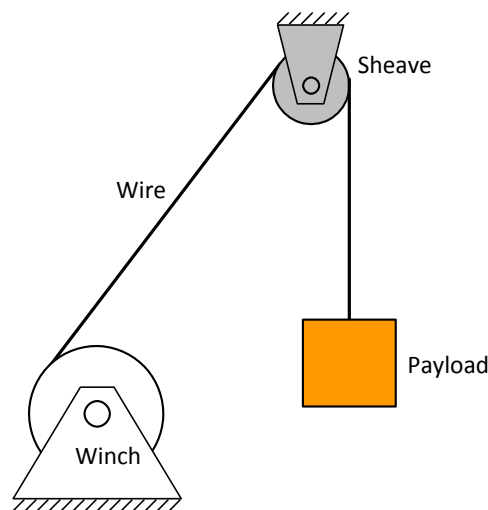


Figure 3.1: Schematic drawing of system

### 3.2 System Overview

The hydraulic system studied in this project consists of a hydraulic motor, a control valve, an accumulator and a hydraulic power unit (HPU) with a variable displacement pump. The hydraulic schematic of the test setup is presented in Fig. 3.2. As shown in the figure, two

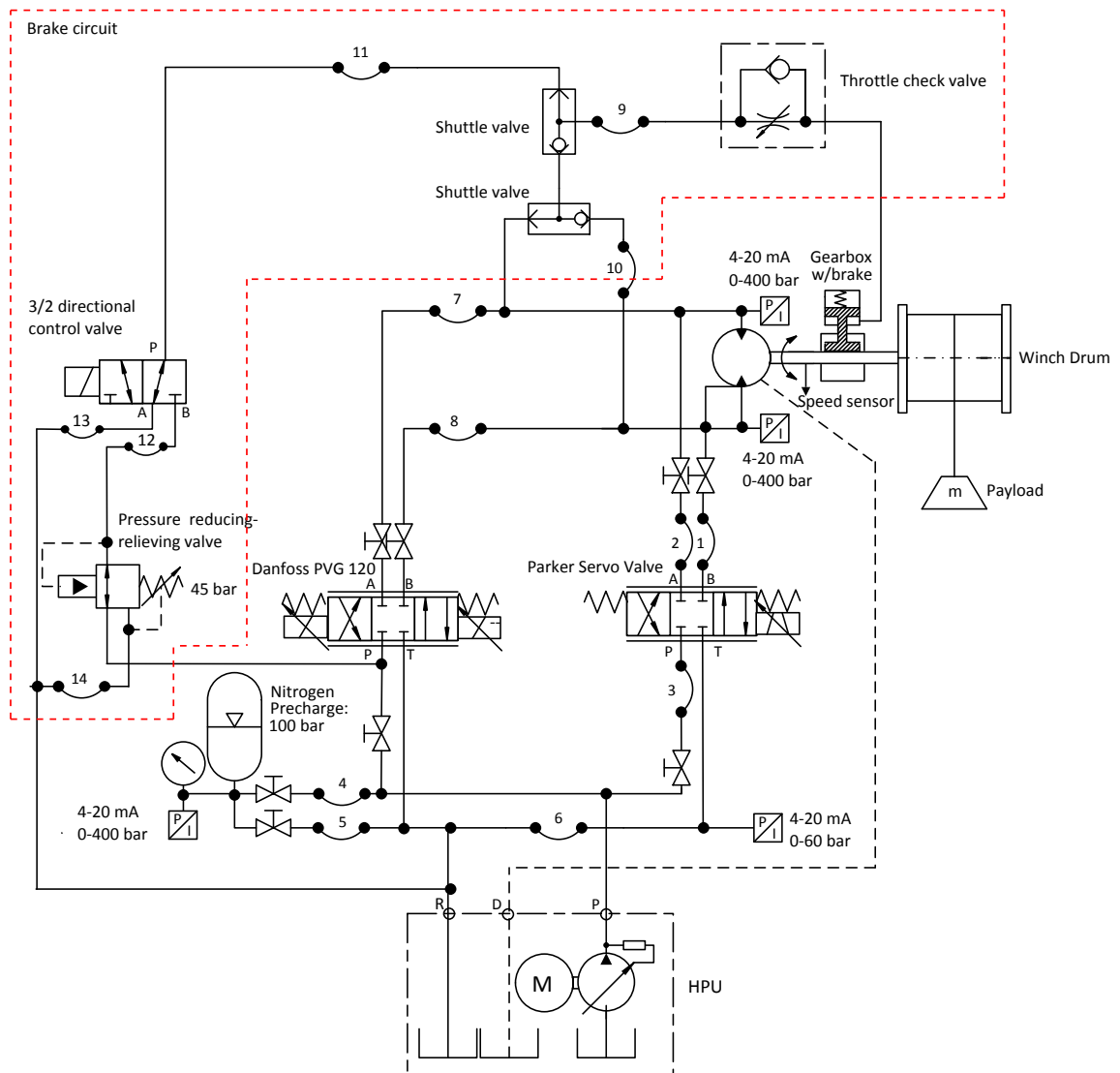


Figure 3.2: Hydraulic Diagram

control valves are included in the setup; Danfoss PVG120 and Parker Servo Valve. These will not be activated at the same time.

The hydraulic system also includes a brake circuit, as shown in the diagram. This circuit includes a pressure reducing-relieving valve, a 3/2 directional control valve, shuttle valves and a throttle check valve (flow control valve with reverse free flow). The purpose of the brake circuit is to enable/disable the brake. However, this circuit is not included in the modelling of the system, because it is not a part of the hydraulic actuation system.

As illustrated in the diagram, the winch is directly operated by a hydraulic motor in a closed loop hydraulic system. In normal operation mode or in AHC mode, one of the control valves receive a control signal from a joystick or a control system, causing the main spool to move. The spool is moved in opposite directions to control oil flow to and from a pair of work ports. When the valve receive a positive control signal, the motor will hoist the payload. In this case the oil flow from port P to port A, through the motor and back through the control

valve to tank. In the opposite case, when the valve receive a negative control signal, the oil flow from port P to port B, through the motor and back to the control valve to tank. In this case the motor will lower the payload.

### 3.3 Hydraulic Winch

The studied winch is a Brevini tugger winch of type TNE5600, with a 4 ton line pull capacity and 16 mm diameter wire. The wire is a non-rotating 35\*7 flexpack wire rope. Technical wire data is listed in Table 3.1.

The Brevini gearbox which is attached to the winch drum is of type ET3055. It is a two-stage planetary gearbox with a total transmission ratio of 35.

Table 3.1: Wire data

Technical Data	
Nom. Rope Diameter	16 mm
Minimum Breaking Force (MBF)	255 kN
Weight in Air	1.24 kg/m
Modulus of Elasticity	$1.36 \times 10^{11}$ N/m <sup>2</sup>
Fill factor	0.75

### 3.4 Hydraulic Motor

The hydraulic motor used to drive the winch, is a fixed displacement bent-axis motor from Parker of type F12-60. It is capable of bidirectional operation, and the displacement of the motor is rated to 59.8 cm<sup>3</sup>/rev. Specifications of the hydraulic motor are listed in Table 3.2.

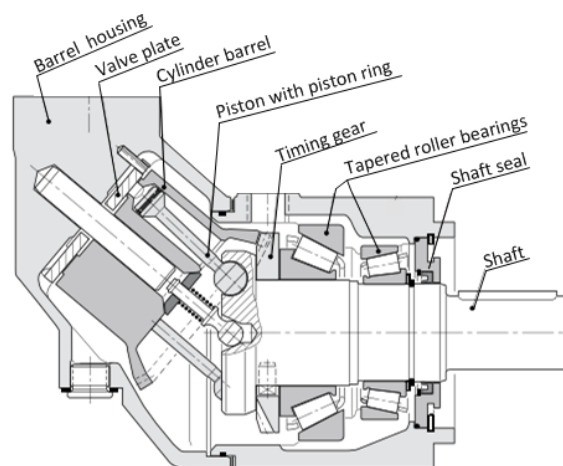


Figure 3.3: Parker F12-60 Hydraulic Motor

Table 3.2: Hydraulic motor data

Technical Data	
Displacement	59.8 cm <sup>3</sup> /rev
Max continuous speed	5300 rpm
Max continuous input flow	317 l/min
Mass moment of inertia	0.005 kg m <sup>2</sup>

### 3.5 Servo Valve

The servo valve included in the test setup is a direct-operated control valve (one-stage valve) in the DF plus series from Parker Hannifin. Technical data are given in Table 3.3.

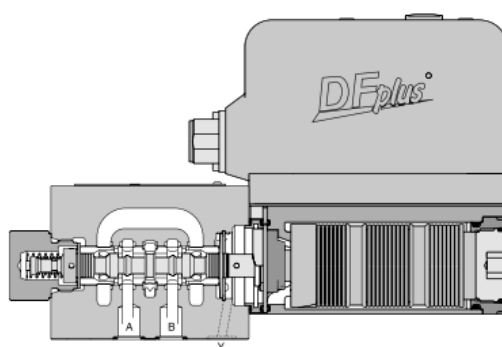


Figure 3.4: Parker Hannifin D3FP Direct Operated Control Valve

The D3FP valve features a precision spool/sleeve design, and shows extremely high dynamics combined with high flow. It is driven by Parkers VCD (Voice Coil Drive) technology. An illustration of the VCD is given in Fig. 3.5. In contrast to standard proportional solenoid drives, this technology actuates the spool by a movable coil. The spool is rigidly connected to the coil able to move back and forth on the outside of a permanent magnetic cylinder. When the coil is energized, the spool is moved to the desired position. The spool position is fed back into the control electronics through an integrated feedback system. While, at power-down, the spool is driven by a spring to a defined position. [5]

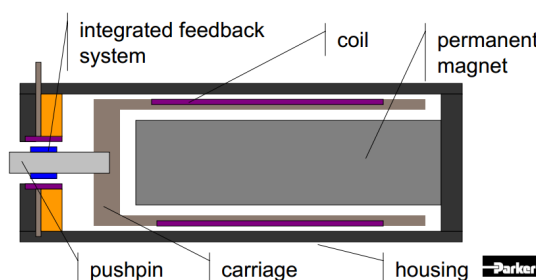


Figure 3.5: Parker Hannifin VCD Technology



Table 3.3: Servo valve data

Technical Data	
Size	D3FP (NG10)
Flow nominal at $\Delta p=35\text{bar}$ per control edge	100 l/min
Frequency response ( $\pm 5\%$ signal)	200 Hz (amp. ratio -3dB), 200 Hz (phase lag $-90^\circ$ )
Hysteresis	$<0.05\%$
Input signal (voltage)	10...0...-10 V

### 3.6 Proportional Valve

The proportional valve included in the test setup is a Sauer Danfoss PVG120 (Proportional Valve Group). The PVG120 has a modular design providing a wide range of configuration possibilities. The valve group consisting of the following modules: PVP (pump side module), PVB (basic module), PVM (mechanical actuation) and PVE (electrical actuation).

The PVB module contains the main spool and a compensator valve. The function of the main spool is to direct the correct amount of flow to an actuator. The purpose of the compensator valve is to keep the pressure drop across the main spool constant, so that the flow rate essentially only depend on the position of the spool and thereby the orifice area. The compensator will compensate whenever the pressure at the load changes. The primary function of the actuator modules (PVM and PVE) are to move the main spool, and thereby open the valve for work flow.

The PVG120 is a 4/3 valve, which means that it has four ports connected to the valve, and three different positions the spool can move between. In the test setup, a PVB module with a closed center spool is used. Thus, when the spool is in neutral position, the flow between the ports are blocked. The spool is actuated by a PVE module, of type PVES. This module features closed loop control, through on board electronics and an integrated feedback transducer that measures spool movement. The PVES type is characterized by low hysteresis, typically less than 0.5%.

Table 3.4: PVG 120 data

Technical Data	
Oil flow	180 l/min
Spool travel	$\pm 8$ mm
Dead band ( $\pm 25\%$ )	$\pm 2$ mm
Hysteresis	$<0.5\%$
Input signal (voltage)	$0.25 \cdot \text{UDC}$ to $0.75 \cdot \text{UDC}$

### 3.7 Hydraulic Power Unit

The hydraulic power unit (HPU) consists of an electric motor, a variable displacement pump, a tank, filters and valves. The electric motor has a constant speed of 1500 rpm. The pump has a pressure controlled compensator that can be set to a specific value. The HPUs main function is to supply the required amount of pressurized hydraulic fluid.

### 3.8 Accumulator

The accumulator included in the system has a volume of 50 l and is a bladder type accumulator, precharged with nitrogen gas. The precharge pressure is 100 bar. Bladder-type accumulators are commonly used for energy storage, shock and vibration absorption, compensation of leakage losses and volume compensation. The high compressibility of nitrogen is utilized in this type of accumulators.

### 3.9 Hydraulic Fluid

RANDO HDZ 32 hydraulic oil is used in the experimental test setup. Physical properties of this oil are listed in Table 3.5.

Table 3.5: Hydraulic oil properties

Typical Test Data	
Manufacturer, type	Hydra Texaco, RANDO HDZ 32
Kinematic viscosity at 40°C / 100°C	32.0 cSt / 6.3 cSt
Density, 15°	0.867 kg/l

# Chapter 4

## System Analysis

### 4.1 Introduction

This chapter presents the analysis that forms the basis for the modelling of the experimental system. The analysis includes winch calculations, static and dynamic analysis of the mechanical system, analysis of the hydraulic system and eigenfrequency calculations. Table 4.1 presents important system parameters, that are included in various calculations presented in this chapter.

Table 4.1: System Parameters

Component	Description	Parameter	Value	Units
Drum	Drum diameter	$d_D$	266.0	mm
	Drum width	$w_D$	433.5	mm
	Drum thickness	$t_D$	40.0	mm
	End disk diameter	$d_{DE}$	472.4	mm
	End disk thickness	$t_{DE}$	13.0	mm
Wire	Wire diameter	$d_w$	16.0	mm
	Wire mass	$m_w$	1.24	kg/m
	Modulus of elasticity	$E_w$	1.36e11	N/m <sup>2</sup>
Payload	Mass	$m_{PL}$	2000	kg
Sheave	Mass	$m_{sh}$	15.0	kg
	Inner diameter	$d_{sh,i}$	75.0	mm
	Outer diameter	$d_{sh,o}$	280.0	mm
Gear	Reduction ratio	$i$	35:1	-
Motor	Displacement	$D_M$	59.8	cm <sup>3</sup> /rev
Servo Valve	Nominal flow	$Q_M$	100	l/min

## 4.2 Winch Calculations

The most important drum dimensions are shown in Fig. 4.1. Based on this figure, the pitch circle diameter (PCD) of the drum can be calculated from:

$$PCD = d_D + d_w + 2 \cdot (n - 1) \cdot 0.8 \cdot d_w \quad (4.1)$$

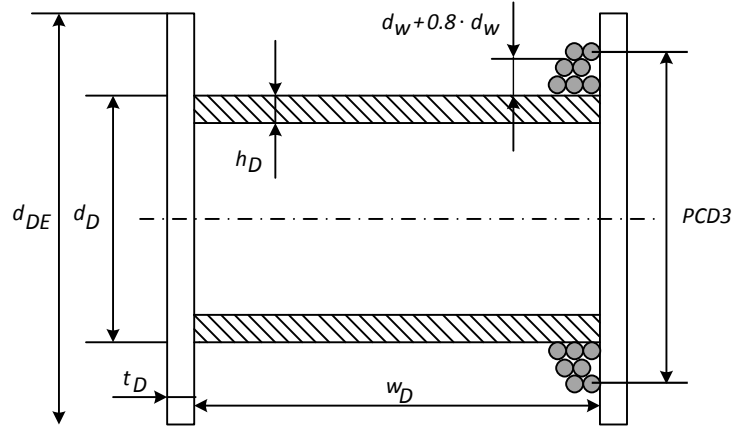


Figure 4.1: Drum dimensions

where the parameter  $n$  is the number of layers of wire on the drum. In addition to calculating the PCD, it is also beneficial to estimate number of turns on each layer. This can be achieved by using the following relationship:

$$n_{turns} = \frac{w_D}{d_w} \quad (4.2)$$

Consequently,  $n_{turns} = 27$ . Furthermore, the wire length on each layer can be estimated by using the following equation:

$$L_w = \pi \cdot PCD \cdot n_{turns} \quad (4.3)$$

Table 4.2 presents the results from the winch calculations. The total length of wire on the drum ( $L_{Tot}$ ), depending on the total number of layers on the drum, is also listed in the table. This parameter is estimated by summing the appropriate  $L_{w_n}$ . As an example, the total length of wire can be written as <sup>1</sup>:

$$\sum_{n=1}^5 L_w \quad (4.4)$$

<sup>1</sup>In this example it is assumed that there are five layers of wire on the drum.

Table 4.2: Results Winch Calculations

Layers of wire	PCD [mm]	$L_w$ [m]	$L_{Tot}$ [m]
1	282.0	25.3	25.3
2	307.6	27.4	52.7
3	333.2	29.6	82.3
4	358.8	31.8	114.1
5	384.4	34.0	148.1

### 4.3 Static Analysis of the Mechanical System

To estimate the wire force and the drum torque, a static force analysis is performed. The results from this analysis are used when the dynamic model is analyzed and verified. Following simplifications are taken:

- The system is in equilibrium, i.e. no dynamics are involved
- The wire is considered as massless non-elastic rods

#### 4.3.1 Wire Force

A free body diagram (FBD) of the payload is presented in Fig. 4.2. As illustrated, the forces acting on the payload in steady state are gravity and wire force. If the payload is submerged in water, buoyancy force is also acting on the payload<sup>2</sup>. The equivalent equation for the FBD is given below. In this equation  $G_{PL} = m_{PL} \cdot g$ . By assuming a 2000 kg payload the wire force  $F_W$  is calculated to 19 620 N.

$$\sum F = F_W - G_{PL} = 0 \quad (4.5)$$

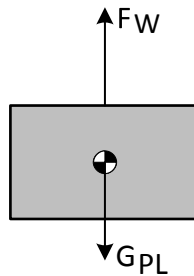


Figure 4.2: FBD of the payload

<sup>2</sup>The buoyancy force on a submerged body is directed in the opposite direction of gravity.

### 4.3.2 Torque Estimation

The drum torque can be estimated by multiplying the estimated wire force ( $F_W$ ) by the pitch circle radius ( $PCD/2$ ). Eq. 4.6 is used to estimate the drum torque on each layer of wire on the drum. The results from these calculations are presented in Table 4.3.

$$T_D = F_W \cdot \frac{PCD}{2} \quad (4.6)$$

Table 4.3: Torque Estimation

Layers of wire	$T_D$ [Nm]
1	2766.4
2	3017.6
3	3268.7
4	3519.8
5	3771.0

## 4.4 Dynamic Analysis of the Mechanical System

The dynamic analysis is divided into two parts: linear dynamics and rotary dynamics. Linear dynamics concerns objects moving in a line and includes quantities as force, mass(linear inertia), displacement, velocity, acceleration and momentum. Rotational dynamics concerns rotating objects or objects moving in a curved path and includes quantities as torque, moment of inertia, angular displacement, angular velocity, angular acceleration and angular momentum. Simplifications include assuming a constant wire mass. This can be justified by the limited movement that the system will undergo. A schematic drawing of the mechanical system is given in Fig. 4.3.

### 4.4.1 Linear Dynamics

Free body diagrams (FBDs) and kinetic diagrams (KDs) are drawn, and equations of motion are set up for the mechanical system.

#### Payload

FBD and KD of the payload are presented in Fig. 4.4. As shown, the buoyancy force and the hydrodynamic drag force are included in this analysis. This is only to show how these forces affects the system, if the payload is submerged in water. It should be stressed that the buoyancy force and the drag force will not be included in the dynamical modelling of

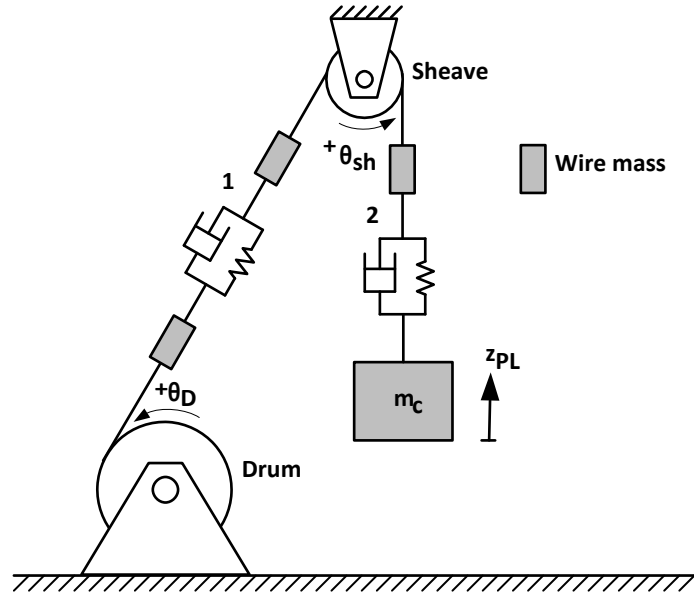


Figure 4.3: The mechanical system

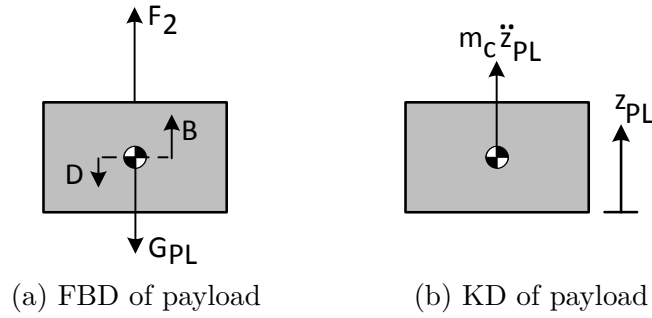


Figure 4.4: Payload diagrams

system, since the payload will not be submerged in water during testing. The equivalent equation for the diagrams in Fig. 4.4 is:

$$\sum F = F_2 + B - G - D = m_c \cdot \ddot{z}_{PL} \quad (4.7)$$

where  $F_2$  is the wire force,  $B$  is the combined buoyancy force,  $G$  is the gravitational force and  $D$  is the drag force. The latter three variables are calculated using Eq. 4.8, 4.9 and 4.10, respectively.  $\ddot{z}_{PL}$  is the vertical acceleration of the payload.

$$B = \rho_{sw} \cdot \frac{m_c}{\rho_{material}} \cdot g \quad (4.8)$$

$$D = \frac{1}{2} \cdot \rho_{sw} \cdot \dot{z}_{PL}^2 \cdot C_D \cdot A_{PL} \quad (4.9)$$

$$G = m_c \cdot g \quad (4.10)$$

The buoyancy force on a submerged body is directed in the opposite direction of gravity. In Eq. 4.8 the combined buoyancy force comprises the sum of the wire buoyancy and payload buoyancy. The parameter  $\rho_{sw}$  is the density of seawater ( $1030 \text{ kg/m}^3$ ).

The drag force,  $D$ , is given by Eq. 4.9, where  $\dot{z}_{PL}$  is the velocity of the payload,  $C_D$  is the drag coefficient - a dimensionless coefficient related to the objects geometry, and  $A_{PL}$  is the projected area.

The gravitational force,  $G$ , is given by Eq. 4.10, where  $m_c$  is the combined mass. This parameter is defined as the sum of the payload mass and the lower wire section mass of the wire attached to the payload:

$$m_c = m_{pl} + \frac{1}{2}m_{w2} \quad (4.11)$$

where the wire mass is given by multiplying the appropriate wire length  $l_{w2}$  with the wire mass  $m_w = 1.24 \text{ kg/m}$ .

### Wire Forces

The wire can be seen as an elastic rod and therefore modeled as a spring. In order to account for internal friction in the wire, damping is also added to this model. Thus, the general wire force is given by this equation:

$$F_n = F_s + F_d \quad (4.12)$$

where the spring force is derived from Hooke's law:  $F_s = k\delta$ . The damping force is  $F_d = c\dot{\delta}$ . This yields the following equations:

$$F_1 = k_1\delta_1 + c_1\dot{\delta}_1 \quad (4.13)$$

$$F_2 = k_2\delta_2 + c_2\dot{\delta}_2 \quad (4.14)$$

The spring coefficient  $k$  is given by  $k_n = EA/L$ , where  $E$  is the Young modulus,  $A$  is the effective cross section area of the wire and  $L$  is the wire length. This implies that the  $k$ -value will vary as the length of the wire changes. The effective cross section area of a wire line is found by Eq. 4.15, where  $c_F$  is the fill-factor of wire rope and  $d_w$  is the rope diameter (see Table 3.1).

$$A = \frac{\pi \cdot d_w^2}{4} \cdot c_F \quad (4.15)$$

The damping coefficient  $c$  is however more problematic to determine. In the modelling this vaule is set to 10% of the spring coefficient, as a rough estimate.



In order to calculate the wire force, the wire elongation  $\delta$  and the wire rate  $\dot{\delta}$  must be found. The wire elongation in the first wire section can be modelled by Eq. 4.16, while the elongation in the second wire section can be modelled by Eq. 4.17. In this equation the elongation is determined by the angular displacement of the sheave and the difference between the heave motion  $z(t)_{heave}$  and the motion of the payload  $z(t)_{PL}$ .

$$\delta_1 = \theta_D r_D - \theta_{sh} r_{sh} \quad (4.16)$$

$$\delta_2 = \theta_{sh} r_{sh} + z_{heave} - z_{PL} \quad (4.17)$$

Eq. 4.16 and 4.17 are valid for  $\delta_n \geq 0$ , since no wire compression is modelled. Furthermore, the wire rate can be found by differentiate the above equations with respect to time. This yields the following equations:

$$\dot{\delta}_1 = \dot{\theta}_D r_D - \dot{\theta}_{sh} r_{sh} \quad (4.18)$$

$$\dot{\delta}_2 = \dot{\theta}_{sh} r_{sh} + \dot{z}_{heave} - \dot{z}_{PL} \quad (4.19)$$

### Wire weight

The wire mass is divided into upper and lower sections, as illustrated in Fig. 4.6. The lower mass section of wire section 2 has been combined with the payload, while the other wire mass sections are seen as separate bodies. This is a simplification, which allows the effect of wire elongation to be shown. Ideally the wire should be divided into several small masses with a spring damper in-between.

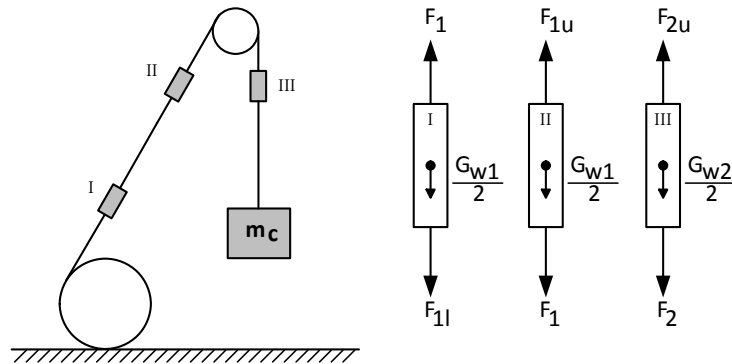


Figure 4.5: FBD's of the different wire mass sections

Based on the FBDs in Fig. 4.6 the following equations are derived. Here  $G_{w1}$  and  $G_{w2}$  are the gravity of the two wire sections.

$$F_1 - \frac{G_{w1}}{2} - F_{1l} = 0 \quad (4.20)$$

$$F_{1u} - \frac{G_{w1}}{2} - F_1 = 0 \quad (4.21)$$

$$F_{2u} - \frac{G_{w2}}{2} - F_2 = 0 \quad (4.22)$$

### Sheave

The sheave is fixed to the test tower. This means that it has no acceleration relative to the overall system, hence no KD needs to be drawn in the linear analysis. An FBD of the sheave is presented in Fig. 4.7b. The equivalent equation for the FBD is:

$$\sum F = \begin{bmatrix} R_x \\ R_y \end{bmatrix} + \begin{bmatrix} 0 \\ -F_{2u} \end{bmatrix} + \begin{bmatrix} -F_{1u} \cos(\phi) \\ -F_{1u} \sin(\phi) \end{bmatrix} + \begin{bmatrix} 0 \\ -m_{sh}g \end{bmatrix} = 0 \quad (4.23)$$

By rewriting this equation, the reaction forces  $R_x$  and  $R_y$  and the normal force can be found.

$$\begin{bmatrix} R_x \\ R_y \end{bmatrix} = \begin{bmatrix} 0 \\ F_{2u} \end{bmatrix} + \begin{bmatrix} F_{1u} \cos(\phi) \\ F_{1u} \sin(\phi) \end{bmatrix} + \begin{bmatrix} 0 \\ m_{sh}g \end{bmatrix} \quad (4.24)$$

$$N = \sqrt{R_x^2 + R_y^2} \quad (4.25)$$

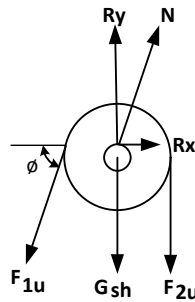


Figure 4.6: FBD of sheave

## 4.4.2 Rotary Dynamics

### Drum

The FBD and the KD of the drum showing the rotary dynamics are presented in Fig. 4.7a. From these diagrams Eq. 4.26 is derived. The inertia of the drum  $I_D$  is calculated by Eq.

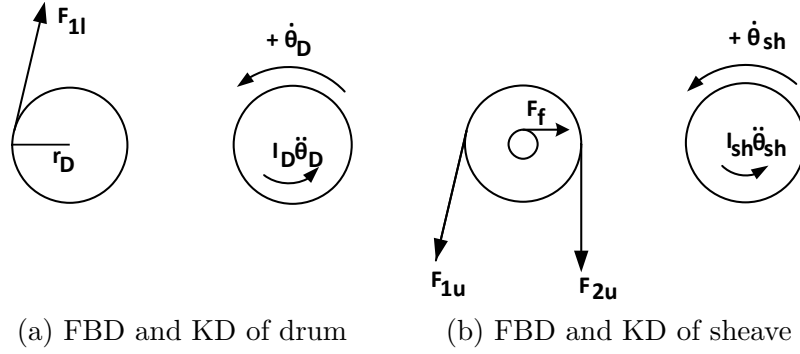


Figure 4.7: FBD's and KD's showing rotary dynamics

4.27 and includes the inertia of a thick-walled cylinder and two solid disks. In this equation  $I_1 = \frac{1}{2}m_D(r_D^2 + r_{Di}^2)$  and  $I_2 = mr_{ED}^2$ . The parameter  $m_D$  is the mass of the drum, including the mass of the wire that is on the drum. The outer radius,  $r_D$ , is the half of the PCD and the inner radius,  $r_{Di}$ , is the radius of the winch minus the thickness of the drum.

$$-F_{1l} \cdot r_D = I_D \cdot \ddot{\theta}_D \quad (4.26)$$

$$I_D = I_1 + 2I_2 \quad (4.27)$$

## Sheave

The dry friction between the bearing of the sheave and the pin can be modeled by the coulomb friction equation; Eq. 4.28. Coulomb friction is an approximate model used to calculate the force of dry friction. In this equation  $\mu$  is the coefficient of friction, and  $N$  is the normal force between the surfaces. The friction coefficient is assumed to be 0.1.

$$F_f = \mu N \quad (4.28)$$

The FBD and the KD of the sheave is presented in Fig. 4.7b. Based on these diagrams, the following equation is set up:

$$\sum T = (F_{1u} - F_{2u})r_{sh} - F_f r_{sh,i} \cdot \text{sign}(\theta_{sh}) = I_{sh}\ddot{\theta}_{sh} \quad (4.29)$$

The sign of the friction force is determined by the rotational direction of the sheave. Positive angular velocity yields a positive output from  $\text{sign}()$  and vice versa. Thus, the friction force will work in negative direction, and conversely. The parameter  $r_{s,h,i}$  is the radius of the bearing/the inner radius of the sheave.

The sheave is considered a thick-walled cylinder. The equation for the inertia of the sheave  $I_{sh}$  is therefore:

$$I_{sh} = \frac{1}{2}m_{sh}(r_{sh}^2 + r_{sh,i}^2) \quad (4.30)$$

where  $m_{sh}$  is the mass of the sheave,  $r_{sh}$  is the outer diameter and  $r_{sh,i}$  is the inner radius.

## 4.5 Analysis of the Hydraulic System

In this section the behavior of the key hydraulic components are analyzed. The main purpose of the hydraulic analysis is to identify the equations needed to develop a simulation model of the system. The theoretical information presented in this section is mainly based on the textbook of Merritt [6], the textbook of Jelali and Croll [3], and the compendium of Hansen and Andersen [7].

### 4.5.1 Motor

In this section the steady-state behavior of hydraulic motors are analyzed. Both ideal and practical motors are examined.

#### Basic Equations

Ideal motors are defined by the relations between fluid pressure drop  $\Delta p$  and flow  $Q$ , and shaft torque  $T$  and velocity  $\omega$ . For an ideal motor, input and output power is conserved. The power balance for a motor is:

$$Power = \Delta p Q = T \omega \quad (4.31)$$

The motor displacement  $D_M$ , defined as the amount of fluid that is displaced through the motor for each revolution of the shaft, is the only parameter that defines the operating characteristics of an ideal motor. It relates to the ideal motor flow,  $Q_{tM}$ , as follows:

$$Q_{tM} = D_M \cdot n = \frac{D_M \cdot \omega}{2\pi} \quad (4.32)$$

The theoretical hydraulic torque in motor,  $M_{tM}$ , is approximated by:

$$M_{tM} = \frac{D_M \cdot \Delta p_M}{2\pi} \quad (4.33)$$

In steady state conditions, the torque delivered to the output shaft,  $M_{tM}$ , is opposite in direction but in size with the load torque on the shaft,  $M_L$ .

$$M_{tM} = M_L \quad (4.34)$$

The direction of the load torque, relative to the motor speed, depends on whether the motor is subjected to a positive or a negative load. In the hydraulic system being analyzed, the motor is subjected to a positive load during hoisting, and to a negative load during lowering of the load (i.e. the motor will operate as a motor or as a pump depending on the position of the control valve).

As illustrated in Fig. 4.8, the load torque,  $M_L$ , is opposite to the direction of the motor speed,  $n$ , whenever the motor is subjected to a positive load (i.e. when the motor is said to be motoring).

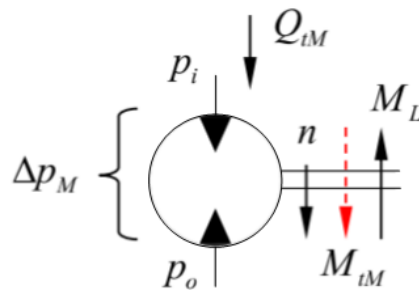


Figure 4.8: Hydraulic motor driving a positive load [7]

For the opposite case, whenever the motor is subjected to a negative load (i.e. when the motor is being driven as a pump by the external load), the load torque,  $M_L$ , is in the same direction as the speed,  $n$ . This is illustrated in Fig. 4.9. In this case  $p_o > p_i$ .

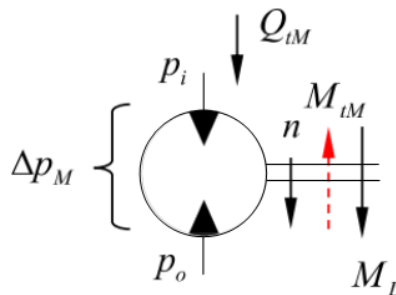


Figure 4.9: Hydraulic motor driving a negative load [7]

### Motor Efficiencies

Leakage flows and friction are the sources of losses in a motor. Hydraulic motors have an overall efficiency  $\eta$ , which is the product up of the volumetric  $\eta_{vM}$  and the hydro-mechanical

$\eta_{hmM}$  efficiencies:

$$\eta = \eta_{vM} \cdot \eta_{hmM} \quad (4.35)$$

The influence of the efficiencies depend on whether the motor is subjected to a positive load or a negative load. A motor subjected to a positive load requires more flow than theoretically expected, on account of leakage. This is expressed by means of a volumetric efficiency:

$$\eta_{vM} = \frac{Q_{tM}}{Q_M} = \frac{Q_{tM}}{Q_{tM} + Q_{leak}} \quad (4.36)$$

where  $Q_{tM}$  is the theoretical flow of the motor calculated from the motor's speed,  $Q_M$  is the actual flow of the motor, and  $Q_{leak}$  is the leakage flows.

There are two primary leakage paths within a hydraulic motor: (1) internal or cross-port leakage between the lines, and (2) external leakage from each motor chamber to case drain. In the literature, these leakage flows are assumed to be laminar and therefore proportional to the first power of pressure. The internal leakage is proportional to the pressure drop across the motor, and may be described by Eq. 4.37. In this equation,  $K_{im}$  is the internal leakage coefficient and  $\mu$  is the dynamic viscosity of the fluid.

$$Q_{im} = K_{im} \cdot \frac{\Delta p_M}{\mu} \quad (4.37)$$

The external leakage in each motor chamber is proportional to the particular chamber pressure (assuming negligible drain pressure  $p_T$ ) and may be expressed by Eq. 4.38 and Eq. 4.39. In these equations  $p_A$  is the pressure at motor port A and  $p_B$  is the pressure at motor port B. The external leakage coefficient  $K_{em}$  can be assumed to be the same for each chamber.

$$Q_{emA} = K_{em} \cdot (p_A - p_T) \quad (4.38)$$

$$Q_{emB} = K_{em} \cdot (p_B - p_T) \quad (4.39)$$

The fact that a motor subjected to a positive load delivers less output torque than theoretically expected is expressed by means of a hydro-mechanical efficiency:

$$\eta_{hmM} = \frac{M_M}{M_{tM}} = \frac{M_{tM} - M_{loss}}{M_{tM}} \quad (4.40)$$

where  $M_{tM}$  is the theoretical output torque from the motor, and  $M_M$  is the actual output torque from the motor. The total torque loss,  $M_{loss}$ , comprises of losses due to mechanical friction, viscous friction, turbulent friction and static friction:

$$M_{loss} = K_{mech} \cdot \Delta p_M + K_{visc} \cdot \mu \cdot n + K_{turb} \cdot n^2 + K_{cst} \quad (4.41)$$

For a positive load, the flow demand and motor torque can be calculated from:

$$Q_M = \frac{1}{\eta_{vM}} \cdot \frac{D_M \cdot \omega}{2\pi} \quad (4.42)$$

$$M_M = \eta_{hmM} \cdot \frac{D_M \cdot \Delta p_M}{2\pi} \quad (4.43)$$

However, for a negative load, the definition of the efficiencies are reversed (as with hydraulic pumps):

$$\eta_{vM} = \frac{Q_M}{Q_{tM}} \quad (4.44)$$

$$\eta_{hmM} = \frac{M_{tM}}{M_M} \quad (4.45)$$

Consequently, the flow demand and motor torque for a negative load can be calculated from:

$$Q_M = \eta_{vM} \cdot \frac{D_M \cdot \omega}{2\pi} \quad (4.46)$$

$$M_M = \frac{1}{\eta_{hmM}} \cdot \frac{D_M \cdot \Delta p_M}{2\pi} \quad (4.47)$$

Table 4.4 summarizes the efficiency equations for hydraulic motors. When a motor is subjected to a negative load (as is the case when lowering the payload) the efficiencies are reversed, i.e. the motor works as a pump.

Table 4.4: Hydraulic Motor Efficiencies

Positive Load	Negative Load
$\eta_{vM} = Q_{tM}/Q_M$	$\eta_{vM} = Q_M/Q_{tM}$
$\eta_{hmM} = M_M/M_{tM}$	$\eta_{hmM} = M_{tM}/M_M$
$\eta = \eta_{vM}\eta_{hmM}$	$\eta = \eta_{vM}\eta_{hmM}$

## Pressure Dynamics in Motor Chambers

In the steady-state analysis it is assumed that the pressure transients that results from fluid compressibility are negligible. This assumption is valid for a system design in which the transmission lines between the valve and the actuator are short and in which small volumes of fluid exist on either side of the motor. The volumetric flow rates in and out (port A and B) of the actuator are then assumed to be equal:  $Q_A = Q_B$ .

By taken into account the effects of compressibility in fluid flows, the pressure dynamics in the motor chambers can be expressed by Eq.4.48. The fluid compressibility effects are discussed in Section 4.5.5.

$$\dot{p}_A = \frac{\beta}{V} \cdot (Q_A - Q_B) \quad (4.48)$$

## 4.5.2 Control Valves

The studied hydraulic system includes two control valves, one servo valve (critical center/zero-lap) and one proportional valve (closed center/over-lap). Equations describing the behavior of such valves are presented below.

### Flow Equations

Fluid flow through the sharp-edged orifices<sup>3</sup> of a spool valve are described by the orifice equation (Eq. 4.49). In this equation,  $C_D$  is the discharge coefficient,  $A$  is the discharge area,  $\rho$  is the mass density of the fluid and  $\Delta p$  is the pressure drop across the orifice. Theoretically,  $C_D = \pi/(\pi + 2) = 0.611$  [3].

$$Q = C_D \cdot A \cdot \sqrt{\frac{2}{\rho} \cdot \Delta p} \quad (4.49)$$

By taking the direction of the pressure drop (flow direction) into account, the flow rate  $Q$  can be expressed by:

$$Q = C_D \cdot A \cdot \sqrt{\frac{2}{\rho} \cdot |\Delta p|} \cdot \text{sign}(\Delta p) \quad (4.50)$$

The absolute value of the pressure difference will always give a positive number, while the *sign* function take care of the direction as follows:

$$\text{sign}(\Delta p) = \begin{cases} 1 & \text{if } \Delta p > 0 \\ 0 & \text{if } \Delta p = 0 \\ -1 & \text{if } \Delta p < 0 \end{cases} \quad (4.51)$$

For proportional and servo directional control valves the discharge area is not a constant but varies with spool travel. For a critical center valve, the orifice area is a function of spool displacement,  $A = A(x_v)$  where  $x_v$  is the valve spool displacement from null position. If the

---

<sup>3</sup>An orifice is a sudden restriction of short length in a flow passage.



area  $A$  varies linearly with the position of the spool, the flow  $Q$  can be expressed by the following equation:

$$Q = C_D \cdot w \cdot x_v \cdot \sqrt{\frac{2}{\rho} \cdot |\Delta p|} \cdot \text{sign}(\Delta p) \quad (4.52)$$

where  $w$  [ $m^2/m$ ] is the area gradient of the valve, or the rate of change of orifice area with stroke (i.e.  $A = wx_v$ ).

For a over-lapped spool valve, the orifice area is a function of spool valve displacement and over-lap,  $A = A(x_v, x_o)$  where  $x_v$  is the valve spool displacement and  $x_o$  is the valve over-lap. The orifice area is zero until the valve has moved the full overlap distance. The flow  $Q$  can be expressed by Eq. 4.53 and Eq. 4.54.

$x_v \geq 0$ :

$$Q = C_D \cdot w \cdot \left( \frac{x_v - x_o}{1 - x_o} \right) \cdot \sqrt{\frac{2}{\rho} \cdot |\Delta p|} \cdot \text{sign}(\Delta p) \quad (4.53)$$

$x_v < 0$ :

$$Q = C_D \cdot w \cdot \left( \frac{-x_v - x_o}{1 - x_o} \right) \cdot \sqrt{\frac{2}{\rho} \cdot |\Delta p|} \cdot \text{sign}(\Delta p) \quad (4.54)$$

## Valve Dynamics

Nowadays, manufacturers' catalog information usually provides the well-known step responses and/or frequency responses for various sizes and types of valve. Therefore, it is useful to use this information to develop simple model approximations of valves. Inspection of step responses and frequency responses suggest an approximation of these valves by a second-order model. If hysteresis is negligible, then the valves spool position's second order transfer function can be expressed as:

$$G(s) = \frac{\omega_0^2}{s^2 + 2\zeta\omega_0 s + \omega_0^2} \quad (4.55)$$

where  $\omega_0$  is the natural frequency and  $\zeta$  is the damping coefficient. These parameters can be extracted from the manufacturer's catalog information. The natural frequency is best associated with the  $90^\circ$  phase point, and the damping ratio with the amplitude characteristic. The valve dynamic approximations by a second order linear transfer function are commonplace in industry and is well established.

## Pressure Compensated Control Valves

An illustration of a 2-way flow control valve, called the pressure compensator, is shown in Fig. 4.10. The underlying principle of a pressure-compensated flow-control valve is that a

constant pressure drop is maintained across the control orifice (ports 1 and 3 of the pressure compensator), so that the flow rate is essentially only dependent on the orifice area. The compensator orifice modulates its opening in order to maintain a constant pressure drop across the control orifice. Thus, if the load pressure decreases the compensator will reduce its orifice area and vice versa.

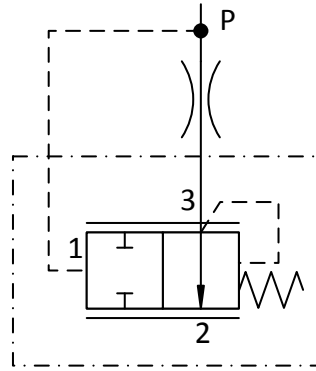


Figure 4.10: Schematic drawing of a pressure compensator

In the PVG120 a pressure compensator is added upstream, and will try to maintain a constant pressure drop across the main spool, given that the difference between the pump pressure and port pressure is greater than or equal to this value. The pressure compensator in PVG120 will try to obtain  $p_{set} = p_P - p_{A/B} = 10$  bar.

### 4.5.3 Hydraulic Lines

The hydraulic system's components are connected by hose lines. The flow of oil through hydraulic hoses can result in energy losses due to internal fluid friction and the friction against the walls of the hose.

#### Friction Loss

Friction is the main cause of loss of fluid energy as the fluid flows through a line. The energy loss is due to friction between the fluid and the pipe/hose wall and internal friction within the fluid itself. The internal friction in a real fluid is called viscosity, and is a measure of fluid's resistance to flow and movement. In a hydraulic system the frictional loss is seen as a pressure drop in the direction of flow. Thus any significant temperature change in the fluid is due to heat transfer.

Friction loss that occur during fluid flow have to be evaluated from a mixture of analytical and empirical results. Two types of flow regime exist, depending on whether inertia or viscous forces dominate. Flow dominated by viscosity forces is said to be laminar, while flow dominated by inertia forces is said to be turbulent. Figure 4.11 illustrates the velocity profile of the two flow regimes. Laminar flow is characterized by a smooth, parallel line motion of the fluid, while turbulent flow is characterized by irregular and chaotic fluid particle motions. Turbulent flow is usually not desirable, as the flow resistance increases and thus the hydraulic losses increase.

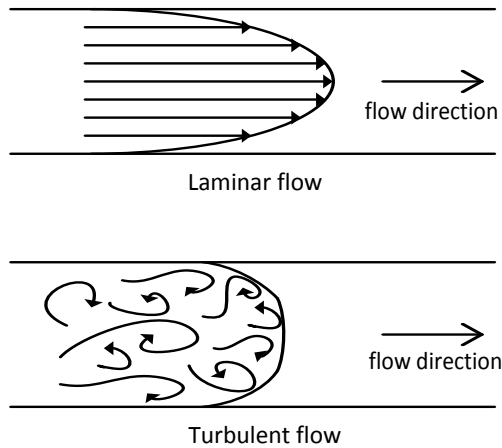


Figure 4.11: Velocity profiles of laminar and turbulent flows

The Reynolds number, the non-dimensional ratio of inertial to viscous forces in the fluid, is commonly used to characterize the flow. For a hydraulic hose or pipe, the Reynolds number can be expressed as:

$$Re = \frac{V_{avg}D}{\nu} \quad (4.56)$$

where  $V_{avg}$  is the average fluid velocity,  $D$  is the inner diameter of the line and  $\nu$  is the kinematic viscosity of the fluid.

The Reynolds number at which the flow becomes turbulent is different for different geometries and flow conditions. For flow in circular lines (pipes and hoses), it is generally accepted to use  $Re_T = 2300$  as a threshold for the transition from laminar to turbulent flow regime. This means that the flow in a circular line is laminar for  $Re \leq 2300$ , and turbulent for  $Re > 2300$ .

Theoretical analysis shows that the pressure drop,  $\Delta p$ , for a laminar flow can be expressed as:

$$\Delta p = \frac{128\nu\rho LQ}{\pi D^4} \quad (4.57)$$

where  $Q$  is the flow rate through the line,  $\nu$  is the kinematic viscosity of the fluid,  $\rho$  is the fluid mass density,  $L$  is the length of the line and  $D$  is the inner diameter of the line. This equation shows that for smooth flow, the pressure drop is proportional to the flow.

However, as the flow changes from laminar to turbulent, Eq. 4.57 is no longer valid. The pressure drop,  $\Delta p$ , for all types of flows can be found directly by using the following equation, known as Darcy's equation:

$$\Delta p = \frac{\lambda L \rho V_{avg}^2}{2D} \quad (4.58)$$

where  $L$  is the length of the line,  $D$  is the inner diameter of the line,  $\rho$  is the fluid mass density,  $V_{avg}$  is the average fluid velocity, and  $\lambda$  is a dimensionless friction factor to be determined.

There are different formulas for the friction factor depending on the Reynolds number and the surface roughness of hose or pipe. For a laminar flow, the friction factor depends only on the Reynolds number. For turbulent flow, the friction factor depends both on the Reynolds number and the surface roughness of the circular line. However, for hydraulic systems it is often assumed that the line conditions are smooth. Under these conditions, the following expressions can be used to calculate the friction factor:

$$\lambda = \begin{cases} \frac{64}{Re} & \text{Re} \leq 2300 \\ \frac{0.3164}{Re^{0.25}} & \text{Re} > 2300 \end{cases} \quad (4.59)$$

Thus the pressure drop,  $\Delta p$ , along a smooth line where turbulent flow is present may be calculated from:

$$\Delta p = 0.242 \frac{L \mu^{0.25} \rho^{0.75} Q^{1.75}}{D^{4.75}} \quad (4.60)$$

### Hose sizing

The hoses need to be selected to provide a sufficient diameter to give an allowable pressure drop along the hose. Under-sized hoses can cause turbulent flow and excessive pressure drops in form of heat buildup. Over-sized hoses can add cost, size and weight to a system and decrease the rate of flow.

The size of a hydraulic hose is based on its inside diameter. A hose can be dimensioned by the following formula, where  $d_{hose}$  is the inner diameter of a hose,  $Q$  is the fluid flow and  $V_{avg}$  is the average velocity of the fluid:

$$d_{hose} = \sqrt{\frac{4Q}{\pi V_{avg}}} \quad (4.61)$$

### Bends and Fittings

In practical hydraulic systems, flow goes typically through right-angle fittings and short sections of bent, flexible hoses. The pressure drops in these pathways can be determined. Engineers generally use tabulated values of dimensionless loss coefficients  $K$  for each component. The pressure drop across the component can be expressed by the following equation:

$$\Delta p = K \frac{\rho}{2} V_{avg}^2 = K \frac{\rho}{2A^2} Q^2 \quad (4.62)$$

where  $A$  is the area of the fitting. As expressed, the pressure drop is proportional to the flow squared.

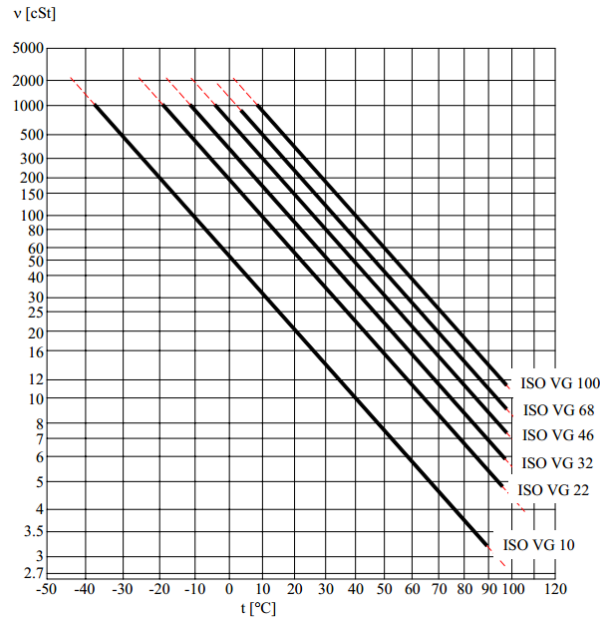


Figure 4.12: Viscosity of typical hydraulics fluids. The ISO VG standard refers  $\nu$  at 40°C

#### 4.5.4 Hydraulic Fluid Properties

The primary purpose of any hydraulic fluid is to transfer the hydraulic power. To ensure stable operation of the hydraulic components, the fluid must flow easily. In this section, important physical properties of hydraulic fluids that affect system behavior are presented.

##### Viscosity

The viscosity is a measure of a fluids resistance to flow. It is the most important property of a hydraulic fluid and has a significant impact on the operation of the system. The dynamic viscosity is the shearing resistance of the fluid. The symbol for dynamic viscosity is  $\mu$ , and the SI unit is the Pascal-second ( $Pa - s$ ). The more common unit is however centipoise ( $cP$ ), with  $1cP = 0.001Pa - s$ . For practical purposes, however, it is more common to report the kinematic viscosity of a fluid. The kinematic viscosity  $\nu$  is defined as:

$$\nu = \frac{\mu}{\rho} \tag{4.63}$$

where  $\mu$  is the dynamic viscosity [ $Pa - s$ ] and  $\rho$  is the fluid density [ $kg/m^3$ ]. The common unit used for  $\nu$  is centistoke ( $cSt$ ), with  $1cSt = 10^{-6}m^2/s$ .

A fluid with low viscosity corresponds to a "thin" fluid, while a fluid with high viscosity corresponds to a "thick" fluid. The viscosity changes with the temperature. It is well known, as fluid warms up it flows more easily. Fig. 4.12 illustrates how viscosity changes for typical hydraulic fluids.

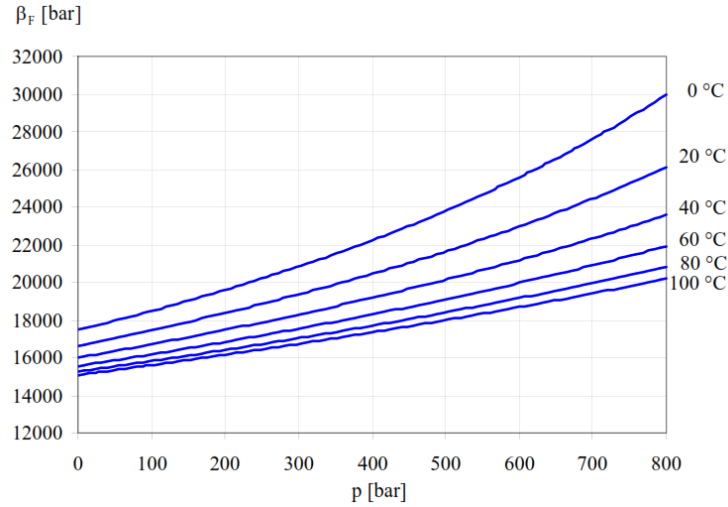


Figure 4.13: Variation of fluid stiffness with temperature and pressure [7]

## Bulk Modulus

The bulk modulus of a fluid is the property that indicates the stiffness of the fluid. The bulk modulus is a measure of a fluid's resistance to being compressed. If a fluid has a high bulk modulus, then it is difficult to compress. The bulk modulus,  $\beta$ , is defined as follows:

$$\beta = \frac{\Delta p}{\Delta V/V_0} \quad (4.64)$$

$V_0$  is the volume corresponding to the initial pressure.  $\Delta V$  is the change in volume of the fluid when subjected to a pressure change of  $\Delta p$ . Because  $\Delta V/V_0$  is dimensionless, units of the bulk modulus are the same as pressure ( $Pa$ ,  $N/m^2$ ).

The bulk modulus varies with fluid pressure, temperature and air content. The variation of the fluid stiffness with temperature and pressure is illustrated in Fig. 4.13. As shown, the bulk modulus increases with increasing pressure and decreases with increasing temperature. When air-bubbles are entrapped in the hydraulic oil, the bulk modulus drops and the fluid becomes springy. Fig. 4.14 displays how the bulk modulus of a fluid changes with pressure for different volumetric ratios ( $\epsilon_{A0}$ ) of air entrapped in the oil. As illustrated, the variation of the stiffness is dramatic for small pressure levels. The higher the air content the more spongy the system (lower bulk modulus). A low bulk modulus lowers the response time of a system.

The bulk modulus is an important property in determining the dynamic properties of a hydraulic system, and should be determined/predicted as precisely as possible. As a rule of thumb, the bulk modulus used for modeling a system should not be set above 10.000 bar, unless verified by means of testing [7]. In the modelling of the system, the bulk modulus is set to 8000 bar.

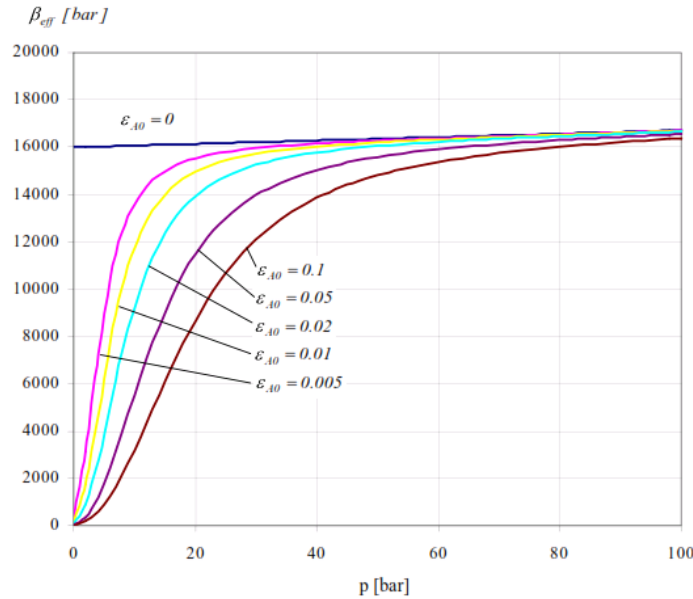


Figure 4.14: Variation of effective stiffness with respect to fluid-air mixture at 40°C [7]

## Vapor Pressure

Another way that the fluid can change properties is if the pressure fall below the vapor pressure of the fluid causing the formation of vapor bubbles. Areas with low local pressures are for example suction lines, metering ports, etc. When a vapor bubble collapse, it causes pressure shocks which erode metal components. This phenomenon is often referred to as cavitation. Cavitation damage can be a problem for fluid power pumps with the erosion greatly shortening the lifetime of components.

### 4.5.5 Fluid Compressibility Effects

It is commonly assumed that the fluid density does not change much with pressure and a conservation of volumetric flow approach may be used with sufficient accuracy for most hydraulic circuit analysis. For a steady-state flow, the principle of conservation of mass can be expressed by the following equation:

$$Q_{in} = Q_{out} \quad (4.65)$$

No liquid is fully incompressible. The effect of compressibility is accounted for when considering bulk volumes of fluid undergoing pressure change. In hydraulic circuits, volumes of fluid exist between components. There will be a flow of fluid in and out of this volume. The fact that the fluid volume may change with time can be accounted for by making  $V$  vary with time. At any instant of time, the rate at which the fluid in a control volume<sup>4</sup>  $V$  is being

<sup>4</sup>A control volume is an arbitrary volume in space through which the fluid flows.

compressed can be expressed by:

$$\frac{dV}{dt} = Q_{in} - Q_{out} \quad (4.66)$$

If the control volume is fixed ( $V = V_0$ ), the pressure build up equation is obtained (Eq. 4.67). This equation is fundamental for the description of the pressure dynamics in hydraulic compartments.

$$\dot{p} = 0 = \frac{\beta}{V} \cdot (Q_{in} - Q_{out}) \quad (4.67)$$

## 4.6 Eigenfrequency of the Hydro-Mechanical System

The eigenfrequency of the hydro-mechanical system composed of the lines to and from the motor, the motor and the mechanical system represented by the effective mass moment of inertia, may be computed by [7]:

$$\omega_n = \sqrt{\frac{k_\theta}{J_{eff}}} \quad (4.68)$$

$$k_\theta = \frac{\beta_{eff} \cdot D_M^2}{\pi^2 \cdot (D_M + V_L)} \quad (4.69)$$

In Eq. 4.69  $\beta_{eff}$  is the effective stiffness of the fluid that depends on temperature, dissolved air, hoses and tubings,  $D_M$  is the motor displacement and  $V_L$  is the total volume of the fluid lines leading to and from the motor.

The effective mass moment of inertia,  $J_{eff}$ , may be computed as:

$$J_{eff} = \frac{2E_{kin}}{\dot{\theta}_m^2} \quad (4.70)$$

In Eq. 4.70  $E_{kin}$  is the kinetic energy of the mechanical system. This parameter is determined by:

$$E_{kin} = \frac{1}{2} J_m \dot{\theta}_m^2 + \frac{1}{2} J_{dr} \dot{\theta}_{dr}^2 + \frac{1}{2} J_{sh} \dot{\theta}_{sh}^2 + \frac{1}{2} m_w v_w^2 + \frac{1}{2} m_{pl} v_{pl}^2 \quad (4.71)$$

Consequently, the effective mass moment of inertia related to the output shaft of the motor can be computed as:

$$J_{eff} = J_m + \left(\frac{1}{i}\right)^2 \cdot J_{dr} + \left(\frac{r_{dr}}{r_{sh}i}\right)^2 \cdot J_{sh} + \left(\frac{r_{dr}}{i}\right)^2 \cdot m_w + \left(\frac{r_{dr}}{i}\right)^2 \cdot m_{pl} \quad (4.72)$$



Table 4.5: Computed bandwidths

Payload weight:	2000kg	500kg	200kg
Effectiv mass moment of inertia ( $J_{eff}$ )	0.0601 kg/m	0.0235 kg/m	0.0160 kg/m
Hydro-mechanical eigenfrequency ( $f_n$ )	10.7 Hz	17.2 Hz	20.8 Hz
Valve bandwidth ( $f_v$ )	32.1 Hz	51.6 Hz	62.4 Hz

The effective stiffness of the system was calculated to  $k_\theta = 274.0$  N/rad, assuming  $V_L = 1.0$  l,  $\beta_{eff} = 800$  MPa and  $D_M = 59.8$  cm<sup>3</sup>/rad. Furthermore, the effective mass moment of inertia and the eigenfrequency of the hydro-mechanical system were calculated for different loads (see Table 4.5). As shown in the table, the eigenfrequency increases with decreasing load weight.

The eigenfrequency of the hydro-mechanical system is important when choosing a servo valve. Experience shows that the servo valve must be faster than the hydro-mechanical system. This means that the valve should be able to operate at frequencies higher than the lowest eigenfrequency of the hydro-mechanical system. A basic rule of thumb is that the valve bandwidth should be three times larger than the eigenfrequency of the hydro-mechanical system:  $f_v = 3 \cdot f_n$  [Hz]. In Table 4.5 required valve bandwidth frequencies for three load cases are presented, applying the rule of thumb. According to these results, the servo valve bandwidth should be above 60 Hz with a 2000 kg payload. The actual servo valve has a bandwidth well above this.

The eigenfrequency of a real system may be substantially smaller than the one computed for the system. According to Merritt, computed values of  $f_n$  are typically 40% or so higher than measured values. The discrepancy is mainly because the computed stiffness typically is higher than the actual stiffness of the system. Experimental work can reveal the actual eigenfrequency of the system. This has not been a part of this project.

It should be stressed that the mechanical system is considered to be infinitely rigid in the computation of  $f_n$ . The flexibility of the wire, the drum and the sheave block are not considered. It is therefore reasonable to assume that the computed stiffness is higher than the actual stiffness of the system. In the computation of the hydraulic spring stiffness  $k_\theta$ , the parameters  $D_M$ ,  $V_L$  and  $J_{eff}$  are well defined and do not vary significantly in value. It is however difficult to determine the value of the effective bulk modulus  $\beta_{eff}$  other than by direct measurements. Hence,  $\beta_{eff}$  may be a source of the discrepancy. The effective bulk modulus is viewed as a series interconnection of the “stiffness” of the oil, of the hoses and of entrapped air volume in the oil.

# Chapter 5

## Control Design

### 5.1 Introduction

Active Heave Compensation (AHC) systems commonly use a Motion Reference Unit (MRU) to measure movements of the vessel, caused by wave action. Using the real-time signals from the MRU, the control system operates the winch to compensate for the vessel movement. The winch will pay in or pay out wire rope to keep the load at a constant elevation. When the vessel moves downwards, the winch will pay in wire. Hence the drive operates as motor and use energy. When the vessel moves upwards, the winch will pay out wire. In this case the drive operates as a pump in generator mode.

In the experimental setup, the winch is directly operated by a hydraulic motor in a closed loop hydraulic system. Dynamic control of the system is achieved using a Siemens Programmable Logic Computer (PLC). In this chapter, three control strategies are proposed. These were used in the simulation and tested in real life.

### 5.2 Feedforward Control

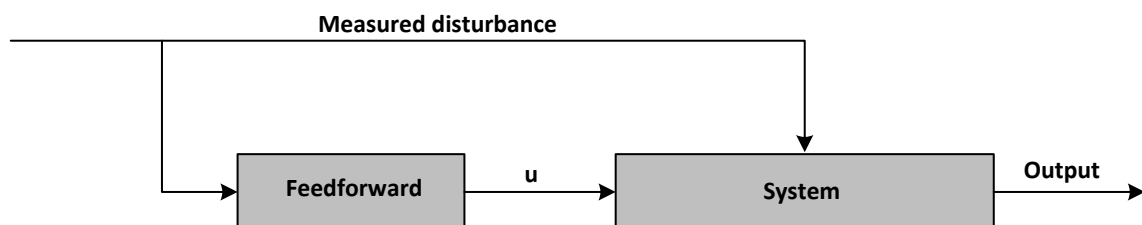


Figure 5.1: Feedforward control

Feedforward (FFW) control is used to compensate for measured disturbance. In AHC systems this type of control is frequently used to compensate for heave disturbance. The FFW signal  $u$  is then given by:

$$u = \dot{z}_{heave} \cdot K \quad (5.1)$$

where  $\dot{z}_{heave}$  is the measured disturbance and  $K$  is the FFW gain. This gain is typically a constant value. One implementation of FFW which will be explored is the model-based prediction of input. Ideally this FFW controller consists of an exact inverse model of the plant.

The three FFW strategies that will be explored in this work:

1. One constant FFW gain.
2. Two constant FFW gains,  $K_l$  and  $K_h$ , for lowering and hoisting respectively.
3. Model-based FFW, dependent of pressure measurements (see Eq. 8.7).

The third FFW strategy is the model-based prediction of input. To use this control strategy, the system response must be predictable. Since this is the case, it is possible to estimate the control effort needed for desired output. The desired output / the desired flow rate can be calculated by Eq. 5.2. In this equation,  $\eta_{vM}$  is the volumetric efficiency of the motor,  $n$  is the rotational speed of the motor (rev/s) and  $D_M$  is the motor displacement (m<sup>3</sup>/rev). The latter equation is only valid for a positive load. For a negative load the efficiency is reversed. The expression for  $n$  is given by Eq. 5.3.

$$Q^{(ref)} = \frac{1}{\eta_{vM}} \cdot n \cdot D_M \quad (5.2)$$

$$n = \frac{\dot{z}_{heave} \cdot i}{\pi \cdot PCD} \quad (5.3)$$

The supplying flow rate to the motor can be determined by the orifice equation. Introducing a flow gain coefficient  $K_v$  to the orifice equation, the valve orifice equation can be represented as follows:

$$Q = K_v \cdot u \cdot \sqrt{\Delta p} \quad (5.4)$$

$$K_v = C_d \cdot A \cdot \sqrt{\frac{2}{\rho}} \quad (5.5)$$

The control input signal  $u$  can then be expressed by:

$$u = \frac{Q}{K_v \cdot \sqrt{\Delta p}} \quad (5.6)$$

The control input needed for desired output can be found by setting  $Q=Q^{ref}$ . It is also possible to determine the control input needed for desired output, from Eq. 5.7. This equation gives the desired flow in percent of  $Q_x$ , where  $Q_x$  is the flow rate for different  $\Delta p$  per control edge (P-to-A orifice when hoisting and P-to-B orifice when lowering).

$$\%Q = \frac{Q^{(ref)}}{Q_x} \cdot 100 \quad (5.7)$$

$$Q_x = Q_{Nom.} \cdot \sqrt{\frac{\Delta p_x}{\Delta p_{Nom.}}} \quad (5.8)$$

By assuming a linear flow gain, the required control signal can be found from Eq. 5.7. The following expression is derived:

$$u = \frac{Q^{(ref)}}{Q_{Nom.} \cdot \sqrt{\frac{\Delta p_x}{\Delta p_{Nom.}}}} \quad (5.9)$$

This equation will be used to determine the required feedforward control. The expression is chosen over the one presented in Eq. 5.6. By using Eq. 5.9, it is not necessary to assume any values. The parameters  $Q_{Nom.}$  and  $p_{Nom.}$  are given in the servo valve's data sheet.

Finally, a model-based FFW is proposed. This FFW consists of two gains, one for hoisting and one for lowering. These gains are found by substituting Eq. 5.2 into Eq. 5.9, and using the relationship presented in Eq. 5.1.

$$K_h = \frac{i \cdot D_M}{\eta_{vM} \cdot 2\pi \cdot r_{drum} \cdot Q_{Nom.} \cdot \sqrt{\frac{(p_p - p_b)}{\Delta p_{Nom.}}}} \quad (5.10)$$

$$K_l = \frac{\eta_{vM} \cdot i \cdot D_M}{2\pi \cdot r_{drum} \cdot Q_{Nom.} \cdot \sqrt{\frac{(p_p - p_a)}{\Delta p_{Nom.}}}} \quad (5.11)$$

The nonlinear flow characteristic of the control valve is not accounted for in this FFW design. However, in the modelling this is included in the FFW by a look-up table.

### 5.3 Feedforward plus Feedback Control

The final control loop consist of both a velocity feedforward loop and a position feedback loop (see Fig. 5.2). The position feedback loop is included to counteract deviation in position.

The use of a feedforward control is well recognized as a compliment to the feedback controller in order to compensate the effect of a measurable disturbance. Feedforward control is a strategy used to compensate for disturbances in a system before they affect the controlled variable. In contrast, the feedback control takes corrective action as soon as the controlled variable deviates from the command. A feedback control system is required to track setpoint changes and to suppress unmeasured disturbance.

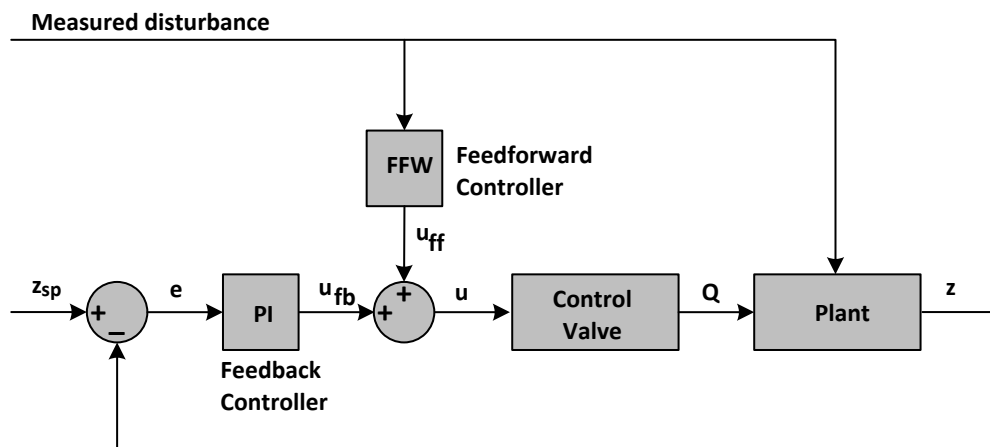


Figure 5.2: Final control loop

# Chapter 6

## Modelling and Simulation

### 6.1 Introduction

Modelling is the process of creating a model of a system of interest. This model should be a close approximation to the real system and include most of its key features. The challenge is to capture all relevant detail and to avoid superfluous features. [8]

Simulation is a tool to evaluate the performance of a system, existing or proposed, over a predefined period of time. It is used to optimize system performance, to reduce the chances of failure and to prevent under or over-utilization of resources. The model can be reconfigured and experimented with. This is convenient, since often this is impossible, too expensive or impractical to do in the real system it represents. [8]

In this chapter, the modelling of the AHC winch system is presented. The model is created in 20-sim and the complexity of the model has been increased iteratively. The model is calibrated and validated in Chapter 8. Techniques to validate the model include simulating the model under known input conditions and subsequently comparing model output with measured test data.

Modelling of the system require three main parts; mechanical modelling, hydraulic modelling and control system. The mechanical model includes the drum, sheave, wire and payload. These components are important to the overall dynamics. The hydraulic model consist of the hydraulic circuit that actuates the mechanical system. This is also where the control element, ie. the servo valve, is located. The control system regulates the hydro-mechanical system.

### 6.2 20-sim

20-sim (v.4.3) is the modelling and simulation program used in this study. 20-sim is originally developed by the University of Twente, but is now commercially developed and distributed by Controllab. With this program it is possible to simulate the behavior of dynamic systems

(electrical, mechanical and hydraulic systems or any combination of these). 20-sim consists of two main windows (Editor and Simulator) and many tools. In the Editor models are entered and compiled. Dynamics models of systems can be modelled using equations, state space descriptions, bond graphs, block diagrams, and iconic diagrams (components). These representations may be combined in one model. [9]

20-sim supports unlimited hierarchical modelling. The highest level consist of graphical models (e.g. block diagrams or iconic diagrams), while the lowest level in a 20-sim model is formed by equations. Hence, equations are the foundation for all models in 20-sim. All equations used in 20-sim are described in the language SIDOPS+. In most cases the SIDOPS+ language is equal to standard mathematical notation. [9]

After entering a model in the Editor, it is possible to check and compile it. This is performed automatically (in the background), when opening the Simulator. The Simulator is used for simulation and analysis of the model. The Simulation results can be shown in plots and animations. [9]

### 6.3 Heave Motion

The AHC winch system is assumed to be located at a floating vessel that is subject to wave motion. This wave motion is assumed to be sinusoidal. An illustration of the wave motion is given in Fig. 6.1.

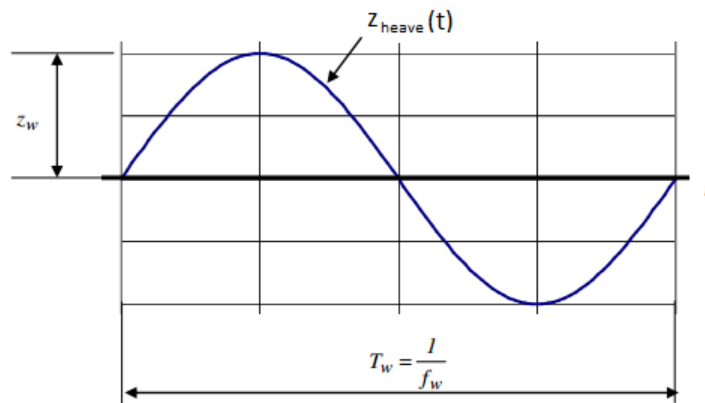


Figure 6.1: Illustration of wave motion

The AHC winch should be compensated for the wave motion. This means that the wave motion must be included in the 20-sim model. This is achieved by using a sine wave generator, from the block library in 20-sim. The block is called "HeaveMotion" and contains the following equations for wave motion and wave velocity:

$$z_{heave}(t) = z_w \sin(2\pi f t) \text{ [m]} \quad (6.1)$$

$$\dot{z}_{heave}(t) = 2\pi f \cos(2\pi f t) \text{ [m/s]} \quad (6.2)$$

where  $z_w$  is the peak amplitude of the wave and  $f$  is the frequency in hertz (Hz). The wave velocity is obtained by derivating Eq. 6.1. Because the wave motion is sinusoidal, the wave velocity is given by a cosine function. A cosine function at  $t=0$  equals one, and thus the load has an initial speed. In order to prevent the system to start with an initial speed, the wave equations are ramped up in the simulation model.

## 6.4 Mechanical System

The modelling of the mechanical system is based on the system analysis, presented in Chapter 4. The system is modelled by using iconic diagrams (components) and equations, see Fig. 6.2. Detailed code of the different model blocks are available in Appendix A.

As presented in Fig. 6.2, the model consist of components named "Payload", "Drum" and "Sheave". It also consists of blocks to calculate wire forces, wire elongation, wire rate, bearing/pin friction and spring stiffness. As the model was developed, it became apparent that it was preferable to do the calculations in separate blocks, and write the results to global variables. Consequently, these variable can be used throughout the system.

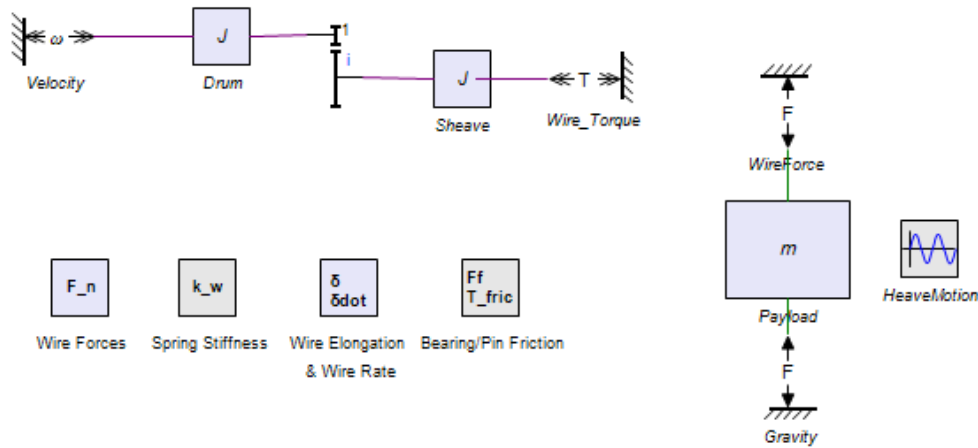


Figure 6.2: 20-sim model of the mechanical system

### 6.4.1 Payload

The iconic diagram "Mass" is used to model the payload. The graphical representation of the payload and the forces acting thereon, is shown in Fig. 6.2. As shown, the wire force and the gravity are forces acting on the payload. In order to account for the initial displacement of the payload, Eq. 6.3 is implemented.

$$z_0 = -\frac{m_c g}{k_2} [m] \quad (6.3)$$



where  $m_c$  is the combined payload mass which includes the lower section mass of the wire,  $g$  is the gravitational acceleration and  $k_2$  is the wire spring coefficient. In order to calculate the combined payload mass, Eq. 4.11 is included in the payload block.

### 6.4.2 Drum and Sheave

The drum and sheave are modelled by rotational inertia blocks, which are found in the mechanical library. The inertia of the these two blocks are calculated by Eq. 4.27 and Eq. 4.30, respectively.

As shown in Fig. 6.2, the drum-gear transmission is modelled by use of an ideal gear. The equations for the output torque and the output speed are modified to:

$$p_{out.T} = \frac{p_{in.T} \cdot r_{sh}}{r_{drum}} \text{ [Nm]} \quad (6.4)$$

$$p_{out.omega} = \frac{p_{in.omega} \cdot r_{drum}}{r_{sh}} \text{ [rad/s]} \quad (6.5)$$

Here,  $r_{drum}$  corresponds to the pitch circle diameter of the drum and  $r_{sh}$  to the sheave radius. The torque exerted on the sheave by the payload and wire, is also included in the model. The component named "WireTorque" contains the following equation:

$$p.T = -F_{2u} \cdot r_{drum} - T_f \text{ [Nm]} \quad (6.6)$$

where  $F_{2u}$  is the sum of the wire force and the upper wire weight (see Eq. 4.22) and  $T_f$  is the friction torque. Consequently, the implementation of the earlier derived Eq. 4.29 is complete. The following equations are implemented to model the torque friction:

$$F_f = \mu \cdot |2 \cdot F_{2u} + m_{sh} \cdot g| \text{ [N]} \quad (6.7)$$

$$T_f = F_f \cdot r_b \cdot \tanh(t_{gain} \cdot \dot{\theta}_{sh}) \text{ [Nm]} \quad (6.8)$$

where  $\mu$  is the friction coefficient,  $m_{sh}$  is the sheave mass and  $r_b$  is the bearing radius/the inner radius of the sheave. The  $\tanh$  is a function which determines the direction of the friction force by a continuous sloped step from -1 to 1.  $t_{gain}$  decides the gradient of the  $\tanh$  slope.

### 6.4.3 Wire

Equations presented in the dynamic analysis (see Section 4.4) are implemented in order to model the wire elasticity. The wire between the sheave and the payload is divided into an

upper and a lower wire section, which allows the effect of wire elongation to be shown. The weight of the lower wire section is combined with the mass of the payload, while the weight of the upper wire section is taken into account in the upper wire force. This solution proved to be an acceptable approximation.

## 6.5 Hydraulic System

The modelling of the hydraulic system is based on the hydraulic system analysis, presented in Section 4.5. The hydraulic system is modelled by using iconic diagrams (model building blocks) from the hydraulic library. The equations embedded in the model building blocks are rewritten and additional parameters are included inside the standard blocks. The code within the different model blocks are available in Appendix A.

An illustration of the hydraulic model is shown in Fig. 6.3. The model consists of blocks for the different components.

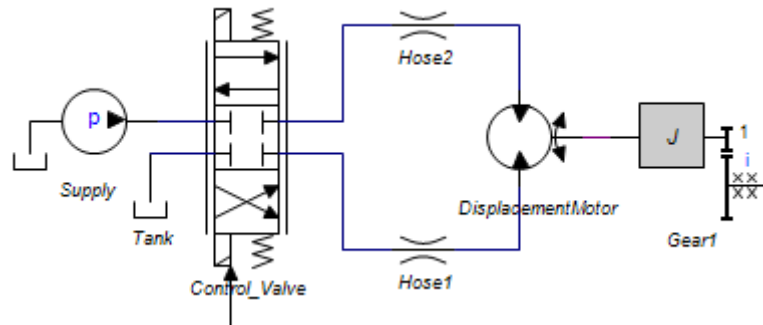


Figure 6.3: 20-sim model of the hydraulic system

### 6.5.1 Hydraulic Power Unit

The hydraulic power unit (HPU) is assumed to maintain a constant pressure at the valve inlet. Therefore, a constant pressure source is included in the simulation model.

### 6.5.2 Motor

The block "HydraulicMotor-Leakage" (see Fig. 6.4), found in the library, is used to model the hydraulic motor. This model describes a motor with internal and external leakage. The block's positive direction is from port A to port B. This means that the flow rate flowing through the motor from A to B rotates the shaft in positive direction, and positive pressure drop  $p = p_A - p_B$  creates positive torque at the motor shaft.

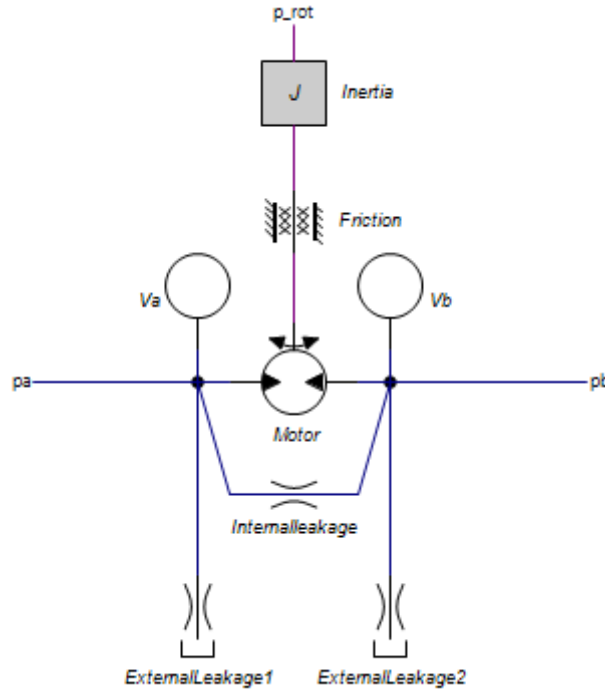


Figure 6.4: Hydraulic motor block

In the motor model, the leakage flows are modeled by laminar resistances. Within the laminar resistances the conductance  $G$  needs to be determined. It turned out that it was not possible to get good simulation results using the default values. Hence it was decided to use a more common approach to model these hydraulic losses; the leakage flows are determined by a volumetric efficiency.

Hydro-mechanical losses are represented with a friction torque applied to the motor shaft. Default, the friction is represented as a linear viscous friction torque. The following equation is implemented:

$$p.T = d \cdot p.\omega [Nm] \quad (6.9)$$

where  $d$  is the viscous coefficient (Nms/rad) which needs to be determined. However, this coefficient is motor dependent and difficult to determine without any experimental data. Therefore, the viscous coefficient is set to zero, and the friction is accounted for by including a hydro-mechanical efficiency.

Information regarding the motor efficiencies are provided by the manufacturer, see Appendix. In reality, the motor efficiencies will change with the working conditions (depend on pressure rise across the motor, the motor speed and the viscosity). As a simplification, the efficiencies are set as parameters. The volumetric and the hydro-mechanical efficiency are both set to 0.96.

As discussed in Section 4.5.1, the motor efficiencies depend on whether the motor is subjected to a positive or negative load. The motor is subjected to a positive load when the motor is

hoisting the payload, and to a negative load when the motor is lowering the payload. When the motor is subjected to a negative load, the motor works as a pump, hence the efficiencies are reversed. During hoisting, Eq. 4.42 and Eq. 4.43 are used, and in the case of lowering Eq. 4.46 and Eq. 4.47 are used.

The inertia block represents an ideal rotational inertia. Inside the block, the mass moment of inertia of the motor  $J$  must be determined. For the studied motor, the inertia is set to  $0.005 \text{ kgm}^2$ , as given in the product sheet.

### 6.5.3 Gearbox

The motor and gearbox assembly is shown in Fig. 6.5. The implemented gearbox block includes rotational inertia and power loss. The inertia is defined at the input axis, while the power loss is represented by the gearbox efficiency. In total, three parameters need to be defined within the gearbox block. The gearbox ratio is set to 35, the gearbox efficiency to 94.09 % (two stage gearbox with 3% power loss per stage) and the rotational inertia to  $0.00001 \text{ kgm}^2/\text{rad}$ . The gearbox ratio is found from the manufacturer data sheet, while the gearbox efficiency and the moment of inertia are assumed values.

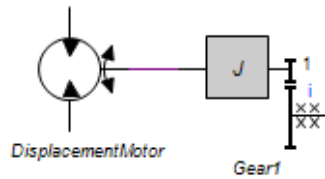


Figure 6.5: 20-sim model of the motor and the gearbox

The torque calculation depends on the direction of rotation. During hoisting the gearbox ratio is multiplied with the gearbox efficiency. In the opposite case (during lowering), the efficiency is reversed due to a reversed motor speed. This is accomplished by including the following equation in the code:

$$u\_0 = 1/eff + (1/2 \cdot \tanh(1e3 \cdot p\_in.\omega) + 1/2) \cdot (eff - 1/eff) [-] \quad (6.10)$$

### 6.5.4 Parker D3FP Valve

The servo valve is implemented as a four-three way proportional valve with a closed-center configuration, illustrated in Fig. 6.6. Some modifications of the standard block were required; the equations embedded in the block is rewritten and additional valve parameters are included.

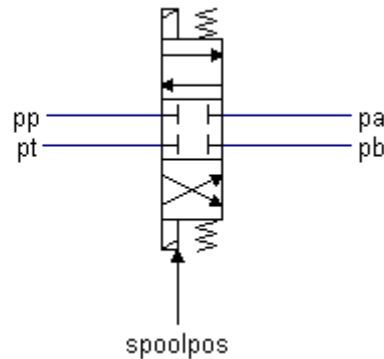


Figure 6.6: Symbol of the proportional valve in 20-sim

The flow through the valve depends on the position of the spool. This is illustrated in Fig. 6.7. The spool will change position, depending on the input signal of the valve. In 20-sim the valve input signal is limited to the range between -1 and 1. In the neutral position ( $sp=0$ ) there will be no flow. If the input signal is positive, the flow will go from the pressure port P to actuator port A and from actuator port B to tank port T. Opposite case, if the input signal is negative, the flow will go from pressure port P to port B and from port A to tank port T.

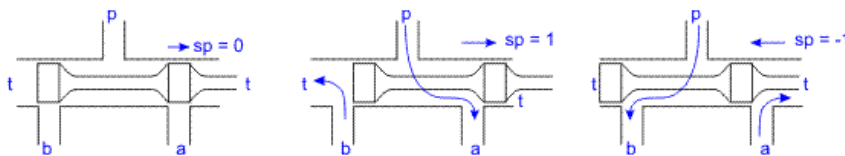


Figure 6.7: Different possible spool positions of the servo valve

For the D3FP valve, the input signal is  $0 \dots \pm 10V$ . All possible states are given in Table 6.1.

Table 6.1: Different spool positions and the flow direction

Control signal $u$	Action of the servo valve
$u = -10V$	Flow from pump to B and A to tank
$-10V < u < 0V$	Partial flow from pump to B and A to tank
$u = 0V$	No flow
$0V < u < 10V$	Partial flow from pump to A and B to tank
$u = 10V$	Flow from pump to A and B to tank

### Valve Spool Dynamics

The spool dynamics relate the valve spool position to the input signal. In the 20-sim model, the spool dynamics is modelled by a second order transfer function. The transfer function

is characterized by the bandwidth frequency ( $\omega_0$ ) and the damping coefficient ( $\zeta$ ):

$$G(s) = \frac{\omega_0^2}{s^2 + 2\zeta\omega_0 s + \omega_0^2} \quad (6.11)$$

The bandwidth frequency and the damping coefficient have to be determined. They are found by reading the frequency response characteristics of the valve (see Fig. 6.8). As seen, the frequency response is expressed by the amplitude ratio in decibels (dB) and phase angle in degrees ( $^\circ$ ) over a specific frequency range. The bandwidth frequencies for  $\pm 5\%$  and  $\pm 90\%$  of the input signal are summarized in Table 6.2. As presented, the valve has a much higher bandwidth if only a certain percentage of the total spool travel is activated.

The  $90^\circ$  phase lag frequency is often called the valve bandwidth, and is the defining characteristics of a valve. In the valve block, the natural frequency  $\omega_0$  is set to 150 Hz, assuming a spool travel of  $\pm 40\%$ . The damping coefficient  $\zeta$  is set to 0.7. The damping coefficient is found by comparing the bode plot of the valve with a standard second order bode plot. Using Eq. 8.9, the second-order transfer function becomes:

$$G(s) = \frac{8.883e5^2}{s^2 + 1319s + 8.883e5^2} \quad (6.12)$$

Fig. 6.9 presents the bode diagram of the transfer function describing the spool dynamics, given in Eq. 6.12.

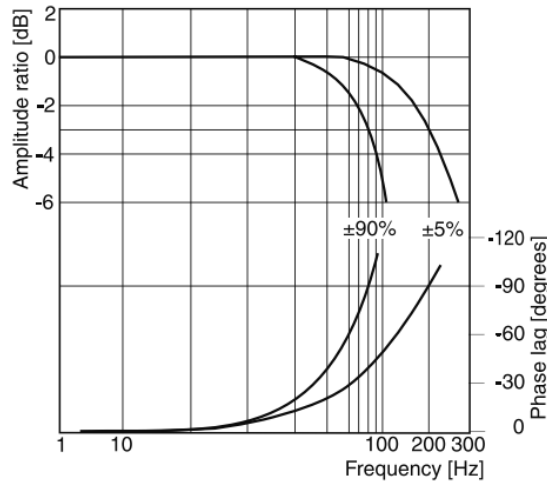


Figure 6.8: Frequency response  $\pm 5\%$  and  $\pm 90\%$  of command signal.

Table 6.2: Characteristic frequencies of Parker D3FP valve

Input signal	Frequency response (phase lag $-90^\circ$ )
$\pm 5\%$	200 Hz
$\pm 90\%$	80 Hz

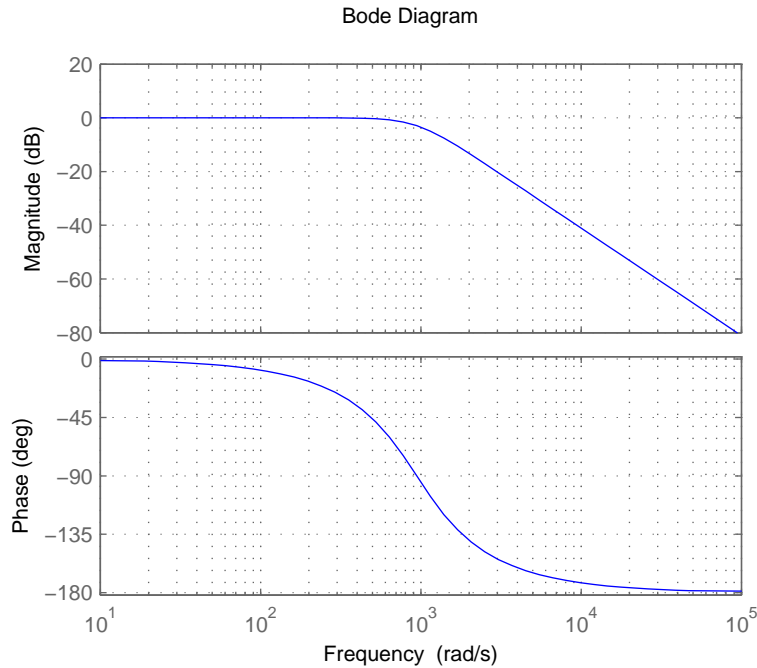


Figure 6.9: Bode diagram of servo valve spool dynamics

## Flow Rate

In the standard valve block, it is assumed that the relationship between the orifice area and the orifice opening is linear. For a zero-lapped valve, the orifice area  $A$  can be expressed by:

$$A = x_v \cdot A_{max} \quad (6.13)$$

where  $x_v$  is the spool position of the servo valve (-1 to 1), and  $A_{max}$  is the maximum orifice area. The parameter  $A_{max}$  is estimated from manufacturer data for the rated flow,  $Q_r$ , and the rated pressure difference,  $\Delta p_r$ , using the following equation (the orifice equation):

$$A_{max} = \frac{Q_r}{\sqrt{C_d \cdot \frac{2}{\rho} \cdot \Delta p_r}} \quad (6.14)$$

The flow characteristic provided in the manufacturer data sheet is shown in Fig. 6.10. The characteristic defines the relationship between the flow capacity and the valve opening under constant pressure. The flow rate are measured in the external valve loop with a pressure drop of 35 bar per metering edge. The characteristic represents the relationship between valve flow capacity and valve opening when there are no system effects involved. As seen from the figure, the relationship between the flow and the command signal is not completely linear (for spool type E50).

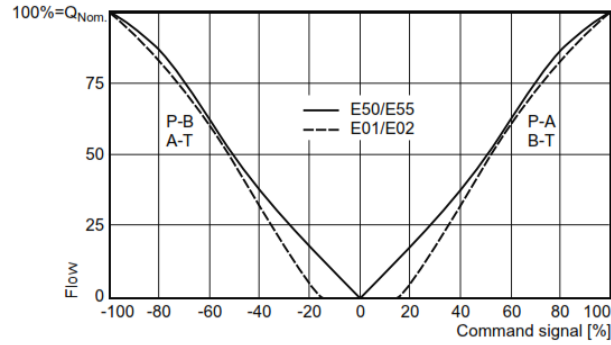


Figure 6.10: Flow characteristic of D3FP valve

To include the nonlinear flow characteristics given in the manufacturer's data sheet, the linear area-opening relationship is replaced by a nonlinear lookup table function  $A=A(x_v)$ . The characteristic is symmetrical, therefore only the P-A branch is considered. 11 points are extracted from the flow curve, and by dividing these values by 100, the set of data points presented in Table 6.3 are obtained. The tabulated values  $Q_{Tab}$  and  $sp_{Tab}$  represent the flow and spool position respectively.

Table 6.3: Lookup table

<b>spTab</b>	0.0	0.1	0.2	0.3	0.4	0.5	0.6	0.7	0.8	0.9	1.0
<b>QTab</b>	0.0	0.0897	0.180	0.269	0.372	0.487	0.628	0.756	0.872	0.949	1.0

The lookup table function is implemented with linear interpolation. Linear interpolation is a straight line fit between two data points. If the two known points are  $(x_1, y_1)$  and  $(x_2, y_2)$ , then the value  $y$  for some value  $x$  is given by:

$$y = (x - x_1) \cdot \frac{(y_2 - y_1)}{(x_2 - x_1)} + y_1 \quad (6.15)$$

Within the valve block, a dimensionless flow rate factor is computed by interpolating the actual spool position against the tabulated values presented in Table 6.3. This flow factor has a range between 0 and 1. The relationship between flow rate and orifice area is directly proportional. The orifice area,  $A$ , is computed by multiplying the flow factor,  $qpp$ , with the maximum orifice area,  $A_{max}$ , as follows:

$$A = qpp \cdot A_{max} \quad (6.16)$$

To verify that the servo valve model provides the desired flow characteristics, simulations were conducted. The outputs of the simulations were compared to the flow curves at  $\Delta p = 35$  bar metering edge, given by the manufacturer. A ramp signal was used as input signal, and the pressure at each port was set by use of ideal hydraulic pressure sources, see Fig. 6.11.



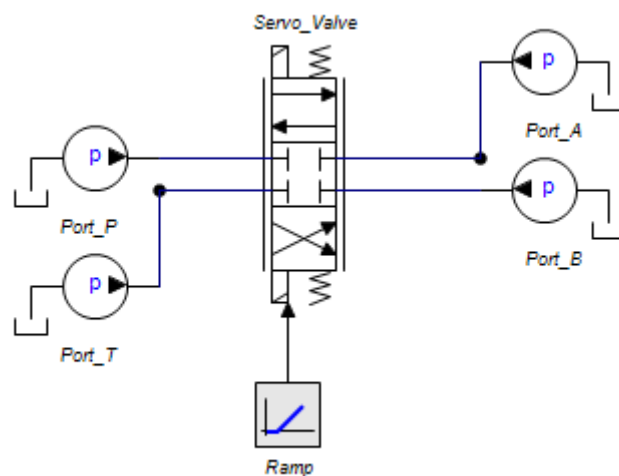
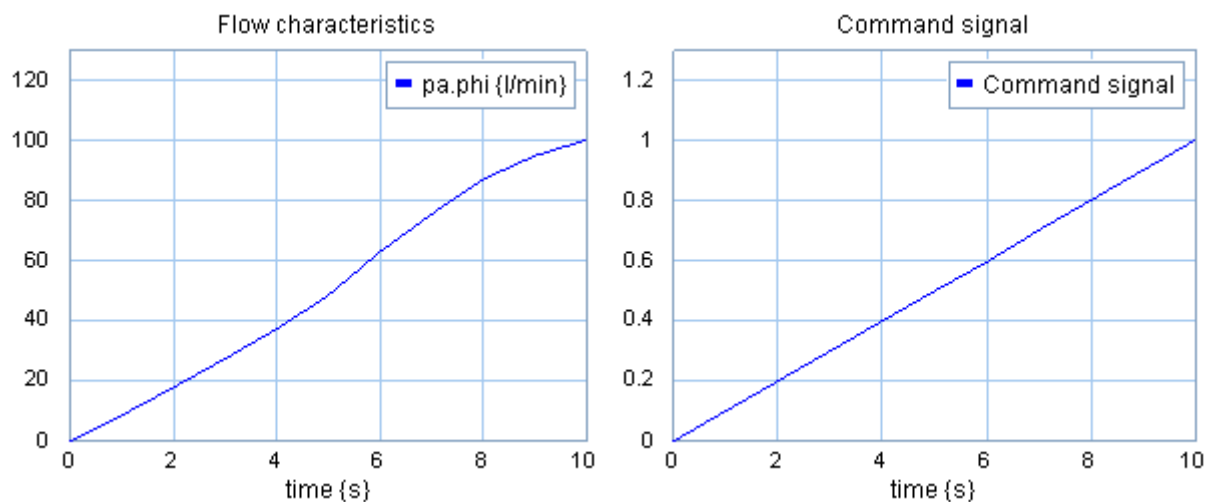


Figure 6.11: Model used to verify the flow characteristics of the D3FP valve

In the simulation model the pressure sources were set to:

- Port P: 70 bar
- Port A: 35 bar
- Port B: 35 bar
- Port T: 0 bar

The simulation time was set to 10 seconds, and the slope of the ramp signal was chosen to  $\pm 0.1$ , providing either positive or negative command signals. Fig. 6.12 shows the results of the simulation for a positive command signals. As illustrated, the flow characteristic is no longer linear, but match the characteristic given in the data sheet.

Figure 6.12: Flow characteristic at  $\Delta p = 35$  bar per metering edge

### 6.5.5 Hose Lines

The hose lines between the control valve and the hydraulic motor are included in the model. The friction loss, as well as the compressibility effect are taken into consideration.

#### Friction Loss

The pressure loss due to friction is modeled by a laminar resistance block (see Fig. 6.13). The following equation are used:

$$Q = G \cdot \Delta p \quad (6.17)$$

Assuming a laminar flow, the pressure drop can be calculated by Eq. 4.57. In the model block, the conductance  $G$  is expressed by:

$$G = \frac{128\nu\rho L}{\pi D^4} \quad (6.18)$$

The validity of laminar flow is checked by the Reynolds number ( $Re \leq 2300$  if laminar).

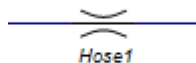


Figure 6.13: Laminar Resistance Block

#### Compressibility effect

In the modelling, volume blocks located within the servo valve block and the motor block are used to give the hoses a volume. The volume of each line is calculated by:

$$V = \frac{\pi}{4} d^2 l \quad (6.19)$$

In 20-sim, a volume block describes the capacitive part of hydraulics. The effect of compressibility is accounted for with the following formula (assuming small pressure variations):

$$p = \frac{\beta}{V} \cdot \text{int}(Q) \quad (6.20)$$

where  $V$  is the oil volume,  $\beta$  is the bulk modulus of the hydraulic fluid, and  $Q$  is the flow rate. The bulk modulus is a very uncertain parameter. This parameter depends not only on the compressibility of the fluid, but the effect of entrained air and vapor and the expansion

of the hose walls. These effects are very hard to compute directly but they result in an increased compressibility (reduced bulk modulus). Default in 20-Sim the bulk modulus is set to 1.6 GPa. This value is too high. The oil stiffness is reduced to 800 MPa. Want to make the simulation model less “high frequency”.

## 6.6 Control System

A control loop for the control valve was included in the 20-sim model. The control loop consists of a feedforward plus feedback control, as illustrated in Fig. 6.14. The motor position is fed back to the PI-controller, by means of a position sensor.

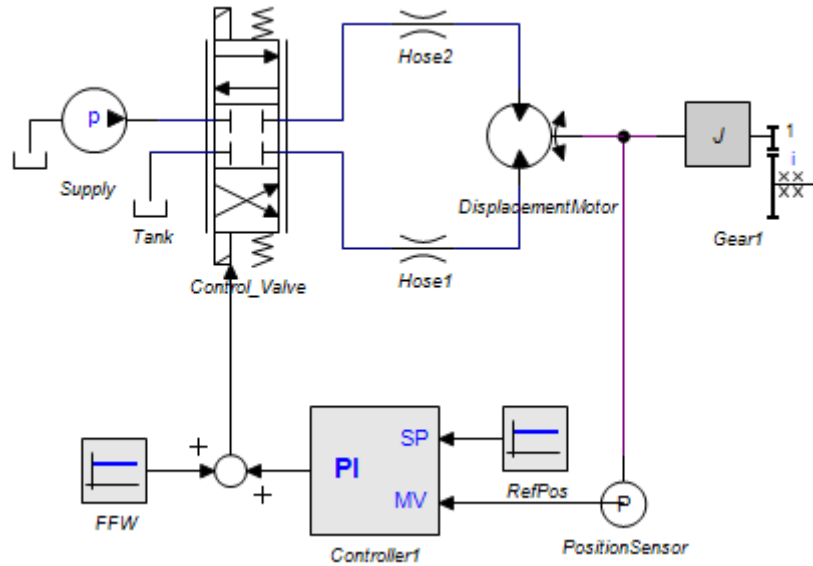


Figure 6.14: PI-controller with feedforward

The output  $U$  of the PI-controller (in s-domain) is given by:

$$U = K \cdot \left( 1 + \frac{1}{s \cdot Ti} \right) \cdot E \quad (6.21)$$

where  $K$  is the proportional gain,  $Ti$  is the integral time constant and  $E$  is the difference between the set point and the measured variable (SP-MV).

The set point (SP), i.e the reference position, is calculated by the following equation:

$$\theta_{motor,ref} = -z_{heave} \cdot \frac{i_{gear}}{r_{drum}} \quad (6.22)$$

## 6.7 Verification of Model by Simulation

To verify the dynamical model and check if the equations were properly implemented, series of simulation tests were conducted. The tests were performed under different load conditions and motion profiles to confirm that the system acted as expected. The simulation results presented in this section, are obtained with a payload of 2000 kg and a supply pressure of 200 bar. It is assumed that there is three layers of wire on the winch.

### 6.7.1 Mechanical Model

In this section the mechanical model is examined. Fig. 6.15 shows the simulations results obtained when the system is in steady state. In this simulation test the drum is locked and no wave motion is present. To verify that the model gives realistic results, the simulation results were compared with the results from the static analysis, see Table 6.4.

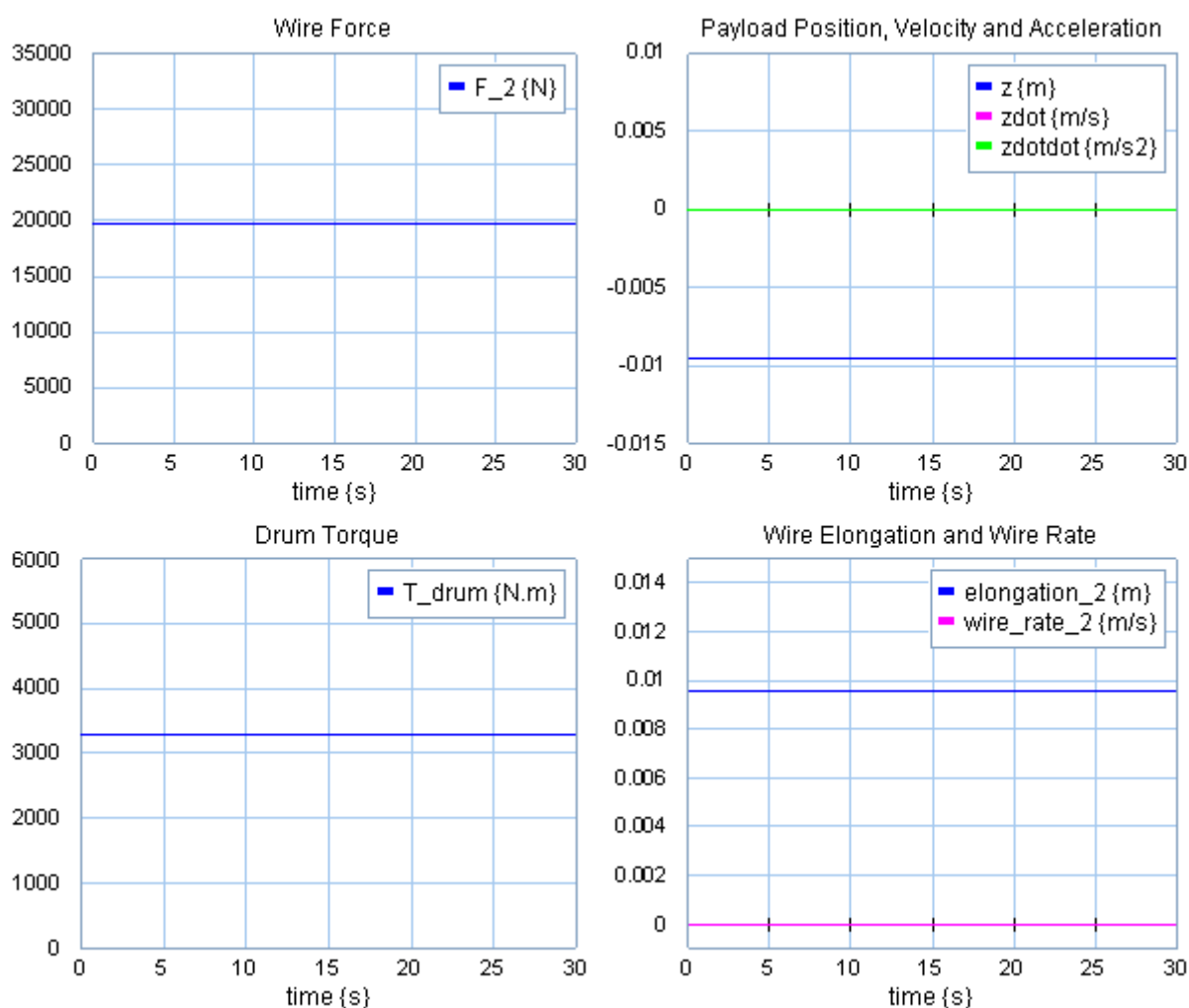


Figure 6.15: Steady state simulation results

Table 6.4: Static Analysis vs. Simulation

	Values Static Analysis	Simulated values
Wire Force [N]	19620.0	19680.8
Drum Torque [Nm]	3268.7	3289.0

The simulated values are slightly higher than the values obtained in the static analysis. This is because the mass of the wire is included in the simulation model. The initial displacement of the payload is simulated to -9.6 mm, due to the wire elasticity. This value was verified by using Eq. 6.23.

$$\frac{WL}{AE} [m] \tag{6.23}$$

In this equation  $W$  is the weight on the wire in [N],  $L$  is the length of the wire in [m],  $A$  is the effective area of the wire in [m<sup>2</sup>] and  $E$  is the modulus of elasticity of the wire in [N/m].

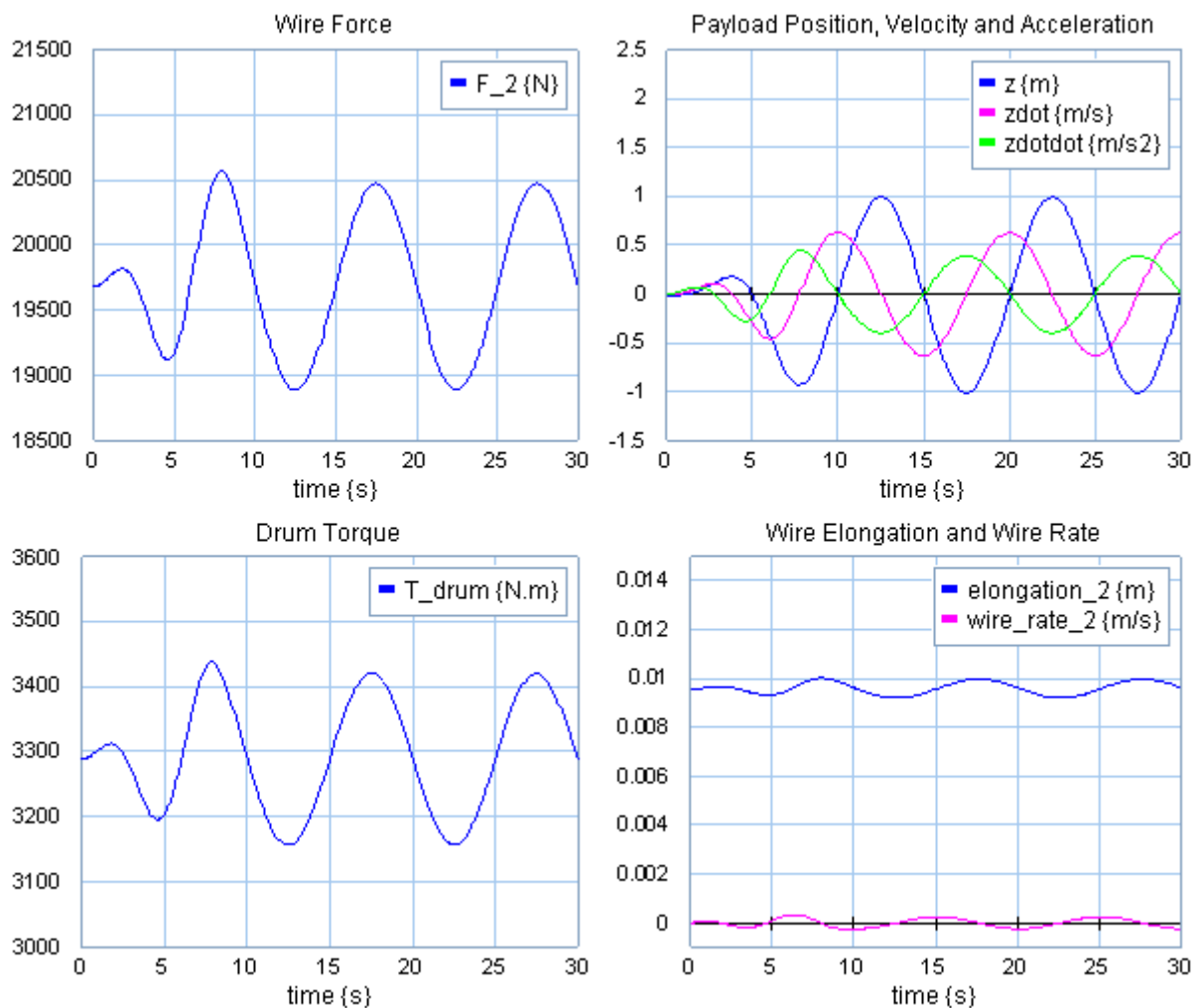


Figure 6.16: Simulation results with heave disturbance

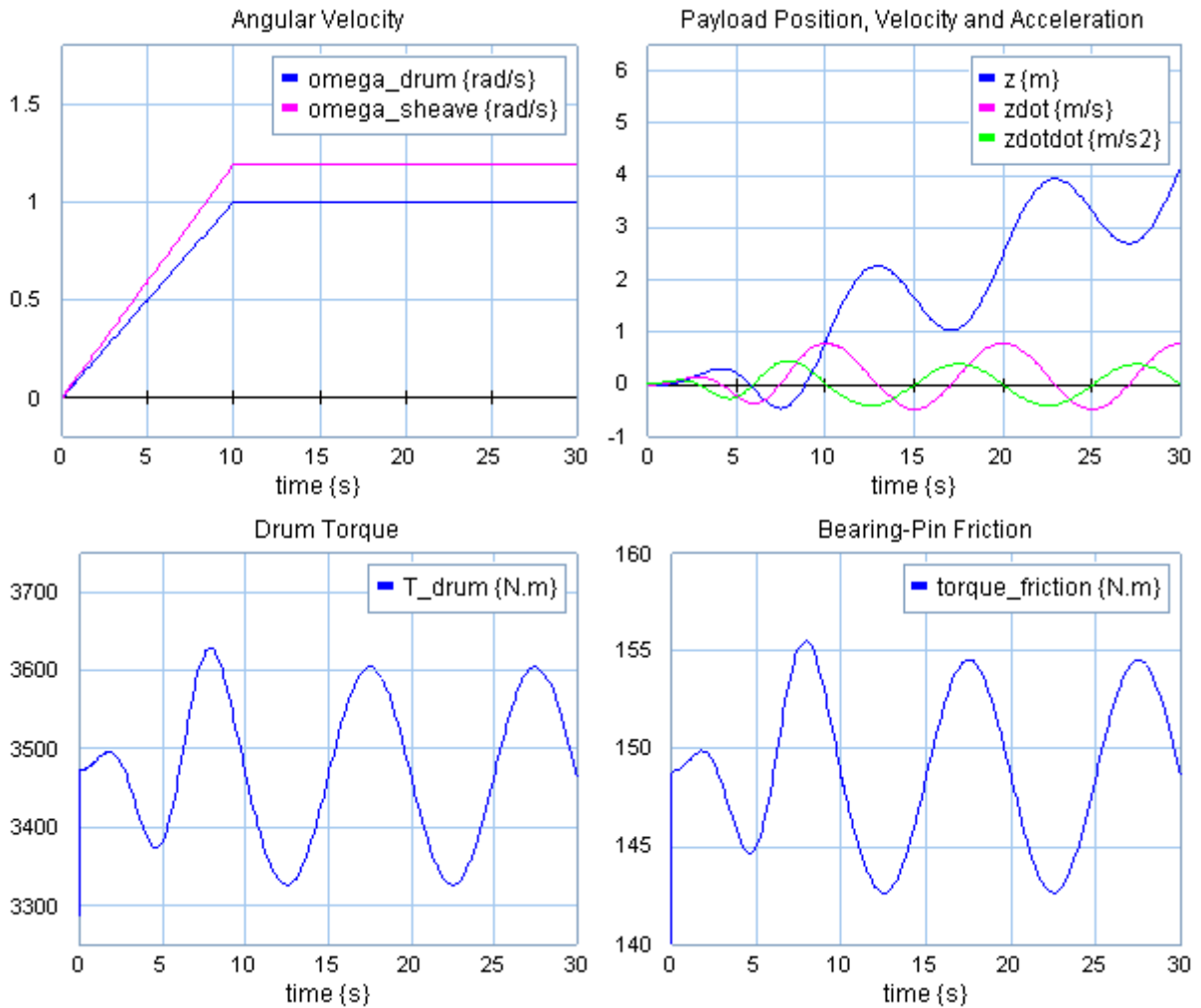


Figure 6.17: Simulation results with angular drum velocity and heave disturbance

Results from a simulation with heave motion are presented in Fig. 6.16. In this simulation the drum is locked, the heave amplitude is set to 1 m and the heave frequency to 0.1 Hz. As expected, the wire force vary as a function of the payload's mass and acceleration. Subsequently the drum torque vary with time. The plots also shows that the heave motion is "ramped up". The ramp-up period is 10 seconds.

Furthermore, simulations were conducted to analyze the system under different velocity inputs. Fig. 6.17 presents simulation results obtained when the velocity input of the drum is set to 1 rad/s (after being "ramped up"). As shown in the plots, the drum and the sheave rotates in the positive defined direction, causing the load to be hoisted. These results are as expected. A plot of the bearing-pin friction is also presented in the figure. As can be seen in figure, the sign of the friction force is positive. This is because the rotational direction of the sheave is positive. As a conclusion, the torque-friction is correctly implemented. Also the drum torque is as expected.

### 6.7.2 Hydro-Mechanical Model

In this section the complete 20-sim model is examined. In order to check that the model gives realistic results, results obtained from the simulation are compared with steady state estimations.

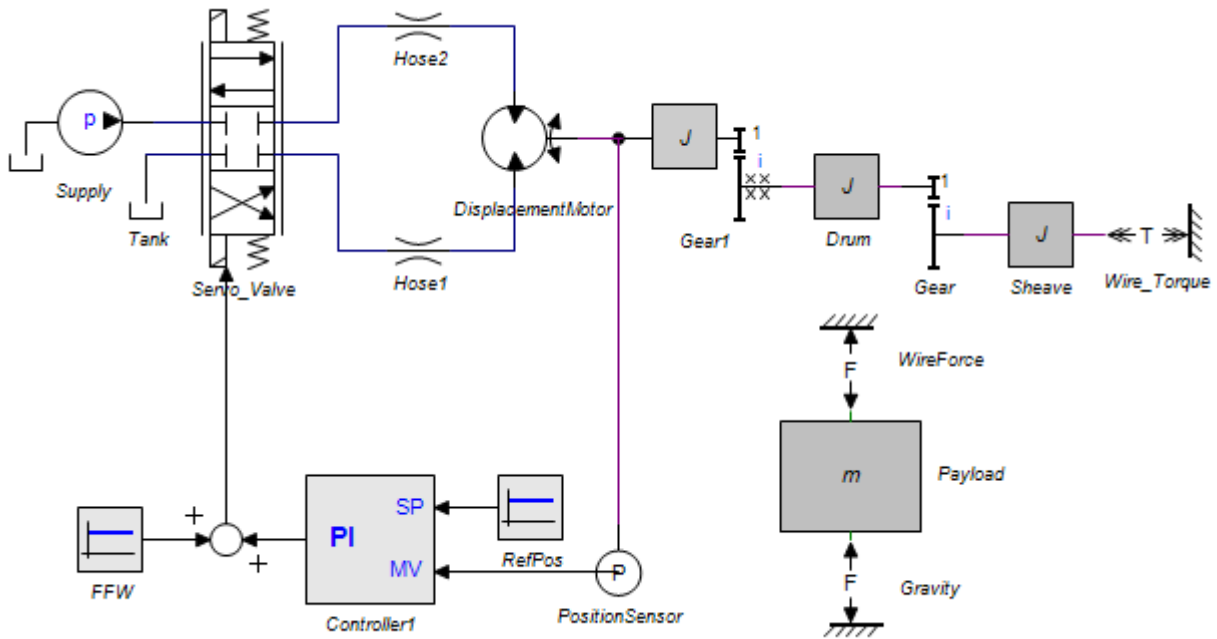


Figure 6.18: 20-sim model of the hydro-mechanical system

The simulation results presented in Fig. 6.19 and Fig. 6.20 are obtained from a simulation with heave compensation in active state. The heave amplitude is set to 1 m and the heave frequency to 0.1 Hz. The controller used consists of a model-based feedforward control and a PI-controller. The control parameters of the feedback controller are:  $K=0.06$  and  $I=2.0s$ .

The simulation results show that the position error is close to zero (less than 0.1 mm). This was realized using a model-based feedforward control with a position feedback PI-controller. This is reasonable since the plant dynamics and disturbances are known in the simulation model.

The average wire forces during movement is simulated to be approximately 19680 N. This value is the same as the value obtained from a simulation with the mechanical model in steady state (as presented in the previous section). This is reasonable, because during heave compensation the payload is held almost at rest. Peak forces are observed during the simulation run. These peaks are present at zero motor velocity-

It can be observed that the motor torque varies with time, as expected. In the static analysis, the drum torque is calculated to 3268.7 Nm. By dividing with the actual gear ratio of 35, the steady state motor torque can be calculated to 93.4 Nm. From the simulation results it can be seen that the motor torque is at its max when the motor is hoisting. It can be read that the motor torque is about 105 Nm during hoisting and around 84 Nm during lowering.

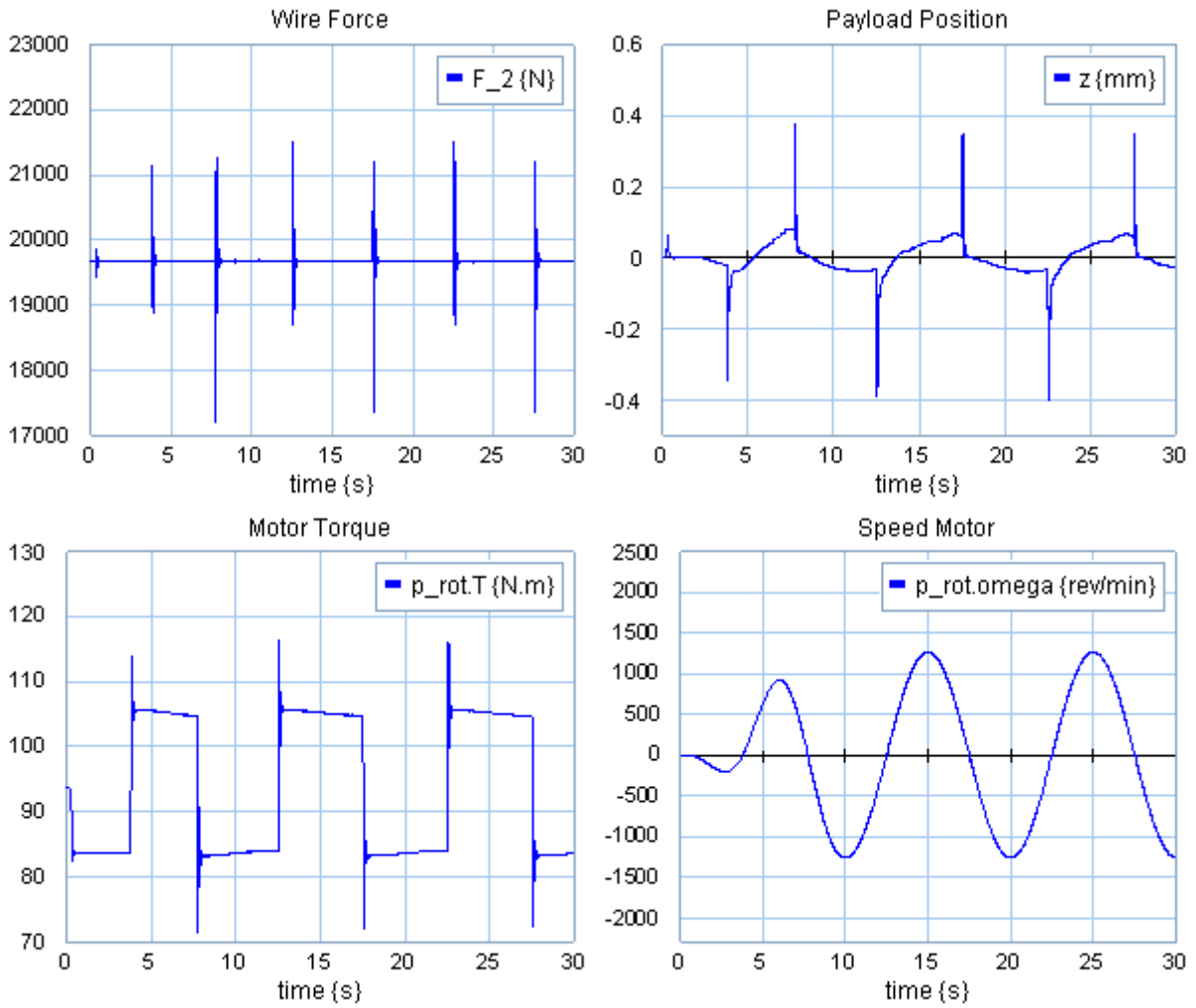


Figure 6.19: Simulation results of active heave compensation

The torque during hoisting is greater than the estimated steady state value, because in this case the motor needs to overcome friction losses. In the lowering case, the friction "helps" the motor, hence the torque is lower, as expected.

Since the system compensate heave motion, the wave profile determines the angular velocity of the winch drum. The maximum expected motor speed with the actual gearing can be calculated to 1260.5 rpm, by using Eq. 6.24. The same maximum value is found from the simulation results.

$$n_{motor,max} = \frac{60 \cdot i_{gear} \cdot \dot{z}_{heave,max}}{\pi \cdot PCD} \quad (6.24)$$

The plot of the spool position shows that the servo valve are not fully utilized. The movement does not reach -1 and 1. The pressure drop across the main spool P-to-A or P-to-B orifices depends on the current spool position. Whenever the motor is hoisting, the oil flows from the P-port to the A-port. In this case, the pressure drop over the spool orifice is simulated to a value of 42 bar. In the case of lowering, the oil flows from P-port to the B-port, a pressure drop of 142 bar is obtained. As expected, the pressure drop is high when lowering.



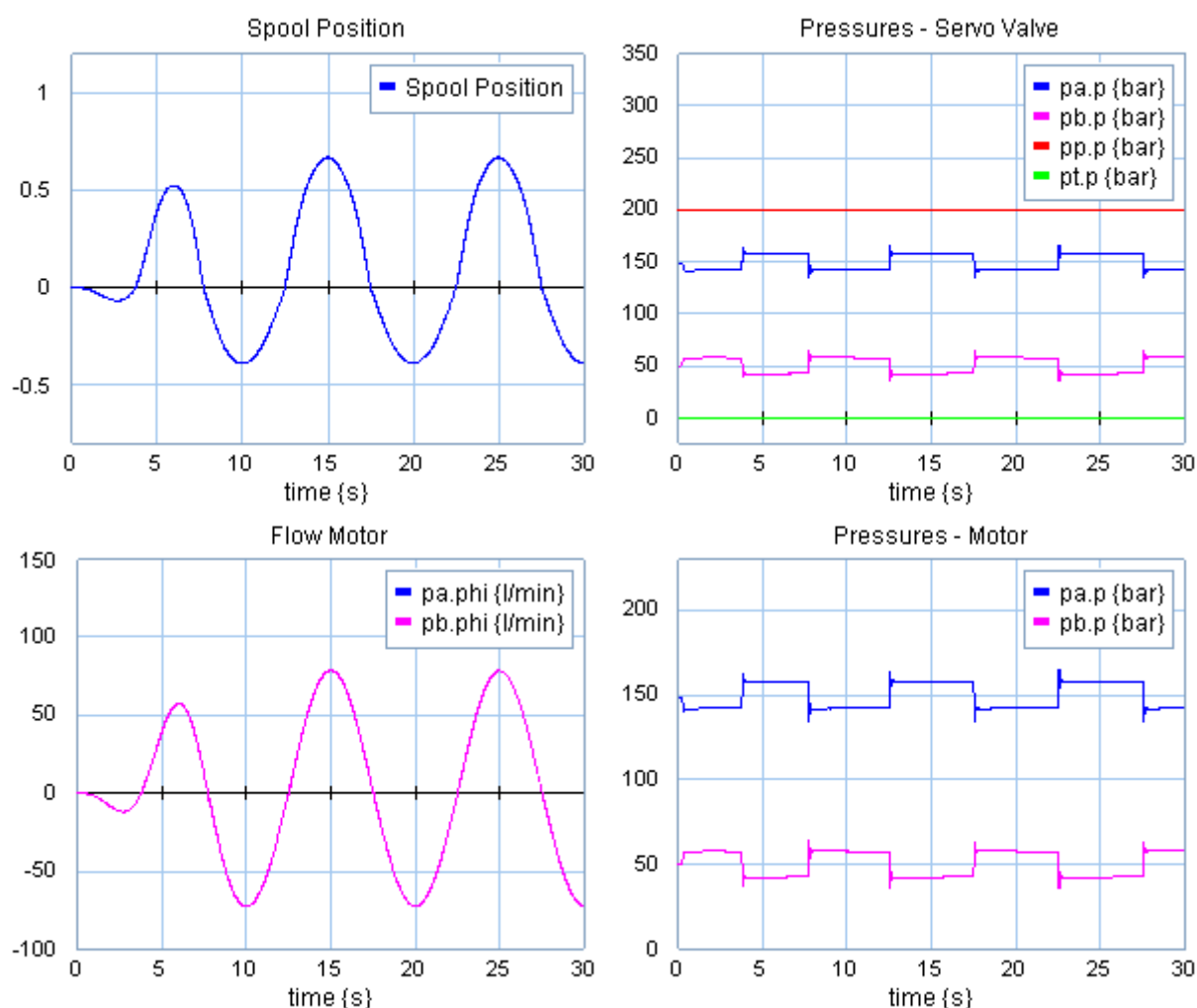


Figure 6.20: Simulation results of active heave compensation

Maximum motor flow and pressure drop across the motor is expected during hoisting. This is verified with the simulation model. From simulation results, a motor flow of 79 l/min and a pressure drop of 115 bar is obtained during hoisting. During lowering, the flow and pressure drop is reduced to 72 l/min and 84 bar.

From the simulation it is clear that a major pressure drop over the servo valve occurs during lowering. With high pressure drops, heat builds up. If including a counterbalance valve/over-center valve, the pressure drops will decrease dramatically during lowering. Keeping the oil temperature at an acceptable level is important to keep the hydraulic system reliable. Overheated oil can result in damaged seals as well as an increase in internal component leakage caused by a drop of viscosity.

In conclusion, the equations were implemented correct. The results correspond well with steady-state calculations. The aim is that the model should represent the real system as best as possible. Hence, the simulation model of the complete system will be updated based on measurements obtained from the experimental work.

# Chapter 7

## Experimental Work

### 7.1 Introduction

The main components of the experimental setup are: winch, gearbox w/brake, hydraulic motor, servo valve, PVG 120, sensors and PLC. The PLC is used to control the AHC winch. It regulates direction and speed of the hydraulic motor through actuation of a control valve. Pictures of the motor, the servo valve and the PVG 120 are given in Fig. 7.1. The experimental setup is shown in Fig. 7.2. In this chapter, information about the electrical instrumentation, the PLC programming and the testing are presented.

### 7.2 Electrical Instrumentation

This part of the work included drawing of electrical loop diagrams and electrical wiring for inputs and outputs from the PLC. The electrical loop diagrams are available in Appendix B.

The main components of the electrical system are:

- Sensors
- Programmable Logic Controller (PLC)
- PR card / Isolation Amplifier
- Joystick

#### 7.2.1 Sensors

Table 7.1 provides an overview of the sensors included in the test setup. Measurement data obtained by these sensors are crucial to validate the dynamic model of the system.

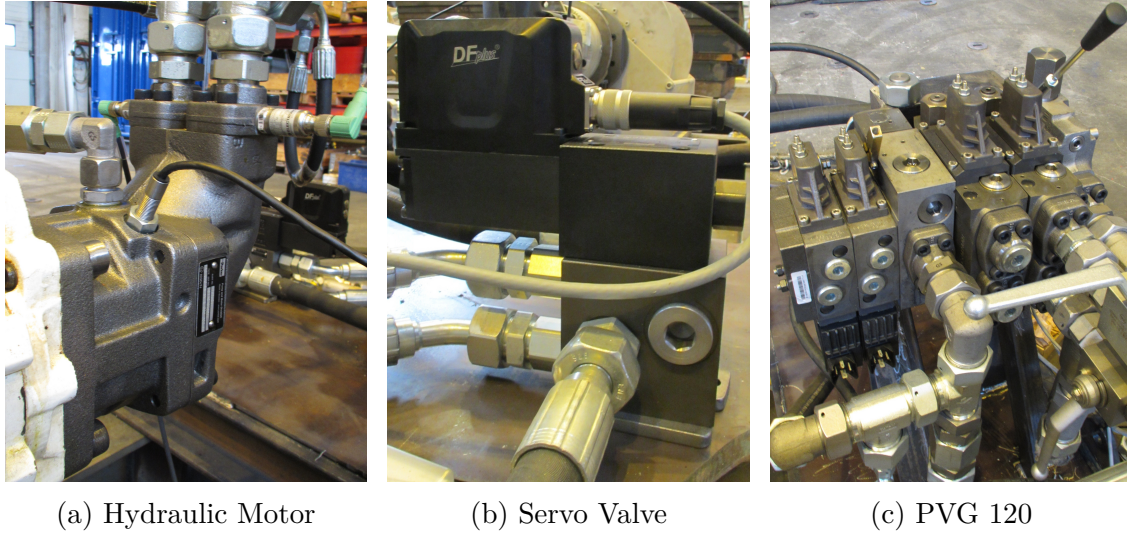


Figure 7.1: System Components

Table 7.1: Sensors

Quantity	Sensor	Description
1	Speed sensor	From Parker Hannifin Manufacturer. Outputs a two-phase shifted square wave signal within a frequency range of 0 Hz to 15 kHz. It detects both speed and direction of rotation. Number of pulses per shaft revolution equals 35.
3	0-400 bar pressure transmitter	In the HDA 4700 series from HYDAC. Pressure range of 0-400 bar, and current range of 4-20 mA.
1	0-60 bar pressure transmitter	In the HDA 4700 series from HYDAC. Pressure range of 0-60 bar, and current range of 4-20 mA.



Figure 7.2: Experimental setup

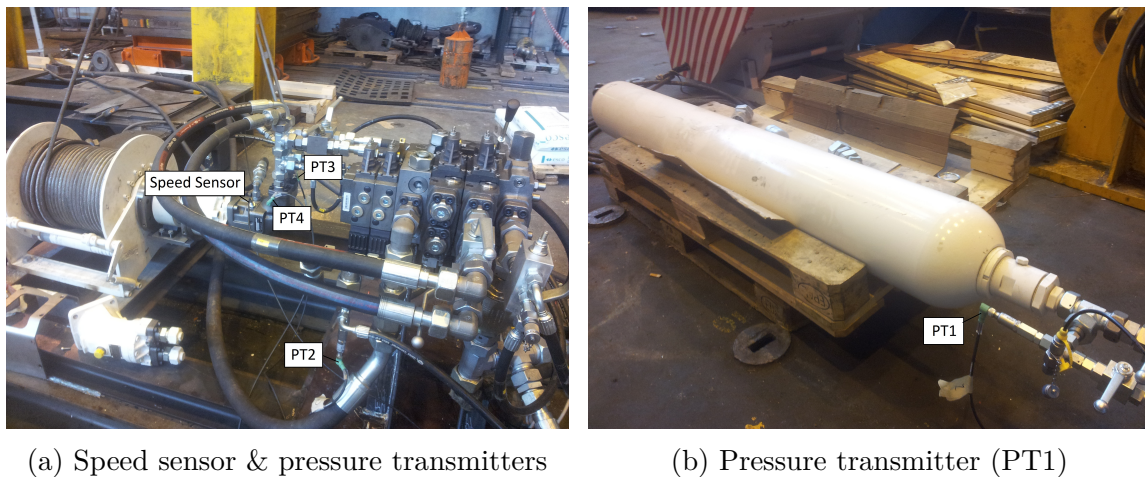


Figure 7.3: Sensors

Fig. 7.3 shows the location of each sensor. The purpose of the sensors are given below:

- Speed sensor: Sense the speed and direction of the rotating motor shaft for closed-loop control.
- PT1: Measure the supply pressure.
- PT2: Measure the pressure at the return line.
- PT3: Measure the pressure at motor port B.
- PT4: Measure the pressure at motor port A.

## 7.2.2 Programmable Logic Controller

The PLC used to control the AHC system is a Siemens S7 modular PLC. The components of the hardware setup are presented in the following table.



Figure 7.4: Siemens S7 modular PLC

Table 7.2: PLC Components

Module	Serial number	Description	Quantity
PSU, DIN RAIL, FLEXIBLE, 3-52V	6EP1353-2BA00	Power supply	1
CPU 317-2 PN/DP	6ES7 317-2EK13-0AB0	SIMATIC S7-300 CPU 317-2 PN/DP	1
AI8x14Bit	6ES7 331-7HF01-0AB0	Analog input module with 8 analog inputs	1
AO8x12Bit	6ES7 332-5HF00-0AB0	Analog output module with 8 analog outputs	1
DO16xDC24V/0.5A	6ES7 322-1BH01-0AA0	Digital output module with 16 channels	1
FM350 COUNTER	6ES7 350-1AH03-0AE0	Counter Module	1

The pressure transmitters were connected to the analog input module, while the Servo Valve and the PVG120 were connected to the analog output module. The PVG120 was connected via a PR card. The on/off valve which controls the brake was connected to the digital output. Furthermore, the speed sensor was connected to the counter module and the joystick was connected with Profibus cable to the PLC. Loop diagrams showing these connections are available in the Appendix.

### 7.2.3 PR-Card / Isolation Amplifier

The PVG120 was connected to the analog output module via a PR-card of type 2284. This PR-card convert the analog output signal from the PLC ( $\pm 10V$ ) into the appropriate control signal. Table 7.3 provides a total overview of the control signal required by the PVES actuation used on the PVG120. The power supply is 24 VDC.

Features of the isolation amplifier:

- Galvanically separated input, output, and supply
- Bipolar current / voltage input
- Signal conversion
- Current and voltage output
- 24 VDC or universally supplied



Figure 7.5: PR card

The PR card was programmed using internal dipswitches.

Table 7.3: Signal voltage - PVES

Function	Signal voltage ( $U_s$ )
Neutral	$U_s = 0.5 \cdot U_{DC}$
Q: P $\rightarrow$ A	$U_s = (0.5 \rightarrow 0.25) \cdot U_{DC}$
Q: P $\rightarrow$ B	$U_s = (0.5 \rightarrow 0.75) \cdot U_{DC}$

### 7.2.4 Joystick

A joystick was included to allow manual operation of the winch. Positive command signals were sent to the control valve by pulling the joystick back. This caused the winch to hoist the payload. In the opposite case, when the joystick was pushed away, negative command signals were sent to the control valve causing the winch to lower the payload. The joystick was also assigned another task. By pressing the red button, the regulator would stop immediately. This function was included for security reasons only.

## 7.3 PLC Programming

A PLC program was created to be used during testing. This program comprises various blocks, listed in Table 7.4. Three of the key blocks are briefly explained in this section. Networks from these blocks and FC95 ("AHC Simulation") are documented in Appendix C. It should be mentioned that the program is based on a crane control program developed by Cargotec.

Table 7.4: PLC Blocks

Block	Name / Description
OB1	Main Program Sweep (Cycle)
FC1	CyclicApplication
FC95	AHC Simulation
FB50	Analog Input
FB51	Analog Output
FB52	Polygon Generator
FB90	True Heave
FB92	sMixer
FB95	Simulate Heave
FB169	Position Monitor
FB170	AHC Regulator
FB194	Encoder Processing
FB285	Joystick Handling
DB98	Param
DB121	HMI Send

*OB1: "Main Program Sweep (Cycle)"*

The operating system of the PLC executes OB1 cyclically. Hence, OB1 is called at the start of every PLC scan. Within this OB, FC1 ("CyclicApplication") and FB194 ("Encoder Processing") are called.

*FC1: "Cyclic Application"*

FC1 calls various FB's and FC's. FB50 ("Analog Input") is called for each instance of analog input (network 8-12). The output of each FB50 is saved in DB121 ("HMI Send"). Furthermore, FB51 ("Analog Output") is called twice (network 6 and network 7), corresponding to number of analog outputs.

Within FC1, it is necessary to determine which control valve to receive the control signal. This is accomplished by enabling one of the two "mixers" in network 3 and 4. A network is also included to enable/disable the brake (network 5).

*FB170: "AHC Regulator"*

FB170 is called by FC95 ("AHC Simulation"). Within this function block the three different feed forward (FFW) strategies are calculated (network 15-18). When enabling one of the FFW's, the two other should be disabled.

Following a I/O table for the PLC is presented.

Table 7.5: I/O table for PLC

Input/output	Address	Comment
Analog Inputs	PIW100	Servo valve feedback
	PIW104	Oil pressure (PT2)
	PIW106	Oil pressure (PT3)
	PIW108	Oil pressure (PT4)
	PIW110	Oil pressure (PT1)
Analog Outputs	PQW100	Servo valve
	PQW108	PVG 120
Digital Out	Q008.0	Brake on/off
Counter Module Inputs	I000.0	Encoder signal A/A*
	I000.2	Encoder signal B/B*

## 7.4 Data Logging in ServiceLab

ServiceLab is a software that has been developed especially for SIMATIC. With this software it is easy to access all the data in the SIMATIC S5 / S7 controller's process image for subsequent analysis, visualization and archiving. Features of ServiceLab includes:

- Monitoring of process over time
- Data logging
- Long-term measurement



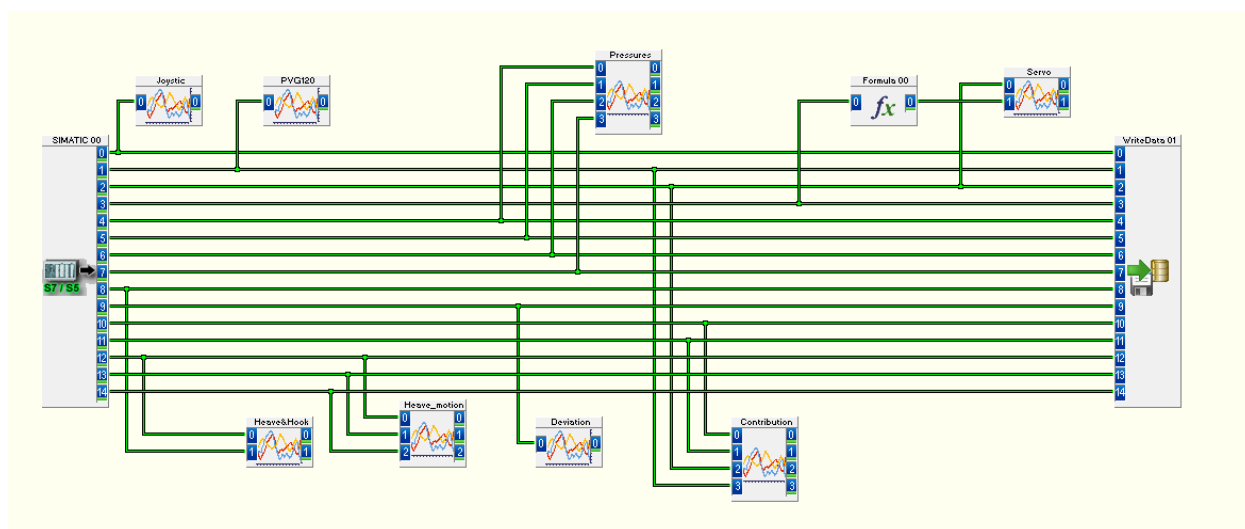


Figure 7.6: ServiceLab worksheet

In the experimental work, ServiceLab was used to monitor and log data. Fig. 7.6 presents the worksheet that was created and used during testing. As shown, a "SIMATIC Read" module was used to read data from the PLC. 15 channels were created to read different process variables/data blocks (see Table 7.6). The process variables were monitored by using multiple "Chart Recorder" modules, and logged by using a "Write Data" module.

Table 7.6: ServiceLab - Process Variables

Channel	Name	Process Variable
0	Joystick	DB121.DBD 374
1	PVG command signal	DB121.DBD 646
2	Servo command signal	DB121.DBD 642
3	Servo feedback	DB121.DBD 416
4	Pressure transmitter 1 (PT1)	DB121.DBD 502
5	Pressure transmitter 2 (PT2)	DB121.DBD 506
6	Pressure transmitter 3 (PT3)	DB121.DBD 542
7	Pressure transmitter 4 (PT4)	DB121.DBD 522
8	Hook position	DB121.DBD 10
9	Deviation	DB121.DBD 106
10	FFW contribution	DB121.DBD 172
11	PID contribution	DB121.DBD 176
12	Heave position	DB41.DBD 6
13	Heave velocity	DB41.DBD 84
14	Heave acceleration	DB41.DBD 72

## 7.5 Testing

This section includes a short description of the experimental tests that have been performed. Different control strategies and heave motions are defined. The test procedure and the pre-startup checklist are also included in this section.

### 7.5.1 Test Cases

Tests have been carried out for the purpose of validating the dynamic 20-sim model. An overview of the various tests conducted during testing follows. The aim of each test was to "actively" compensate for the heave disturbance. Because a sinusoidal heave disturbance was simulated by the PLC, the payload motion was expected to be given by a sinusoidal wave. In the most ideal case the two sinusoidal waves, representing the heave motion and the payload motion, have opposite phase ( $\phi=180$ ), resulting in a deviation of zero.

Two load cases were investigated (500kg and 200kg). In both cases, the system was tested under the influence of different wave conditions. Three control strategies were tested.

Control strategies (velocity feedforward and position feedback):

- Control 1: Constant feed forward gain and position feedback.
- Control 2: Two constant feed forward gains (different gains for lowering and hoisting) and position feedback.
- Control 3: Model-based feed forward and position feedback.

Heave motions (sinusoidal waves):

- Heave 1: Peak-to-peak amplitude: 2 m. Frequency: 0.1 Hz / Period: 10 sec.
- Heave 2: Peak-to-peak amplitude: 1 m. Frequency: 0.1 Hz / Period: 10 sec.

The following tests were conducted (by actuating the servo valve):

Test 1-2: Payload weight: 500 kg  
Control 1  
Heave 1, 2

Test 3-4: Payload weight: 500 kg  
Control 2, 3  
Heave 1

Test 5-6: Payload weight: 200 kg  
Control 1  
Heave 1, 2

Test 7-8: Payload weight: 200 kg  
Control 2, 3  
Heave 1

If time allowed, it was intended to perform tests also with PVG120. However, since no over-center valve was included in the test setup, it was not possible to achieve valid results.

## 7.5.2 Test Procedure and Checklist

The test procedure and the pre-startup checklist are included in this section. These were created prior to testing. The pre-startup checklist was created to ensure that everything was in order before testing.

Table 7.7: Test Procedure

Action #	Description
1	Download the program to the PLC. Enable the required "Mixer" within FC1. Initially the servo valve should receive the control signal.
2	Enable the heave simulator and set the heave parameters.
3	Set the zero hook position and update the parameters. The zero hook position should be set after having hoisted the payload to the top, since positive direction is defined downward.
4	Choose the control strategy, download the block and activate the regulator. Activate the regulator when hook position = 2 m.
5	Enable AHC operation.
6	Tune the regulator.
7	Start testing. Remember to start ServiceLab and log data over time (eg. 1 min per test).

Table 7.8: Pre-Startup Checks

Check #	Description	OK	Checked by
1	Perform a visual inspection of the system. Check all connections and look for damage or errors which can lead to unwanted leakage or danger during startup.	x	SG/TG
2	Check the ball valves. Make sure that the ball valve leading to the Danfoss PVG 120 is open. This valve should always be open, because of the brake. When the servo valve is connected, make sure that the two ball valves leading from the PVG 120 are closed. In the opposite case, make sure that the ball valves leading to and from the servo valve are closed.	x	SG/TG
3	Perform test runs in normal operation to ensure no irregularities. Make sure that the supply pressure is constant within minimum variation.	x	SG/TG
4	Make sure that all measuring instruments are working properly. Verify that the reading/measuring in real time is recorded as planned with a satisfactory frequency.	x	SG/TG
5	Make sure that the position reading is correct. If the reading is incorrect, make corrections: <ol style="list-style-type: none"> <li>1. Set the conversion factor to one.</li> <li>2. Hoist the payload a known distance (eg. 1 m) and register the number of counted pulses.</li> <li>3. Determine the conversion factor by calculating the number of pulses per meter.</li> <li>4. Hoist the payload a know distance to verify that the position reading is correct.</li> </ol>	x	SG/TG

# Chapter 8

## Model Calibration and Validation

### 8.1 Introduction

In this chapter, the simulation model is calibrated and validated by comparing simulated and measured test data. Two load cases are investigated. Model parameters are adjusted so that the model reproduces experimental data to an acceptable accuracy. Results obtained with the calibrated simulation model are presented at the end of this chapter.

In this section the following abbreviations are used:

- "Heave 1": Wave with a amplitude of 1 m and frequency of 0.1 Hz
- "Heave 2": Wave with a amplitude of 1 m and frequency of 0.2 Hz
- PT1: Supply pressure
- PT2: Tank port pressure
- PT3: Pressure at motor port B
- PT4: Pressure at motor port A

### 8.2 Model Inputs

Measurement data were used as inputs to the simulation model, to compare simulated and measured behavior. The following data were included in the model:

- Control signal
- Supply pressure
- Tank port pressure

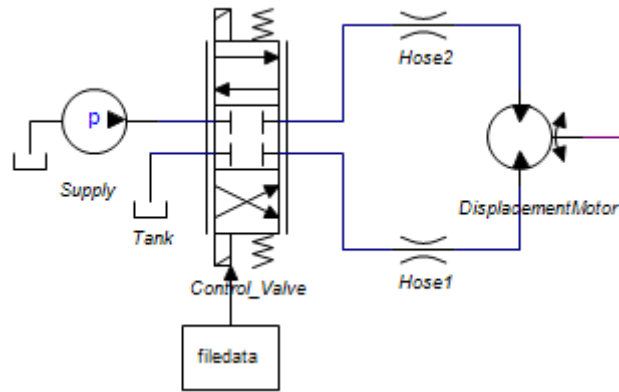


Figure 8.1: Import of data in 20-Sim

Control signals logged during testing were used as inputs to the model. The data were saved in an excel-sheet, and imported to 20-sim with use of the "DataFromFile" block, see Fig. 8.1. The different control signal used are presented in Fig. 8.2 and Fig. 8.3. As illustrated, the control signals vary with load case and heave disturbance. The amplitude and frequency of "Heave1" is 1 m and 0.1 Hz, respectively. The amplitude and frequency of "Heave2" is 1 m and 0.2 Hz, respectively.

The measurements of the supply pressure were used to set the correct value in the simulation model. Fig. 8.4 presents measurement data obtained during one of the tests. As presented, the supply pressure was relative constant during testing (approximately 260 bar).

Measurement data showed that also the tank port pressure was relative constant during a test run. Data is presented in Fig. 8.5. Minor variations are observed. In the simulation model the tank pressure was set to the average measured value (approximately 1 bar).

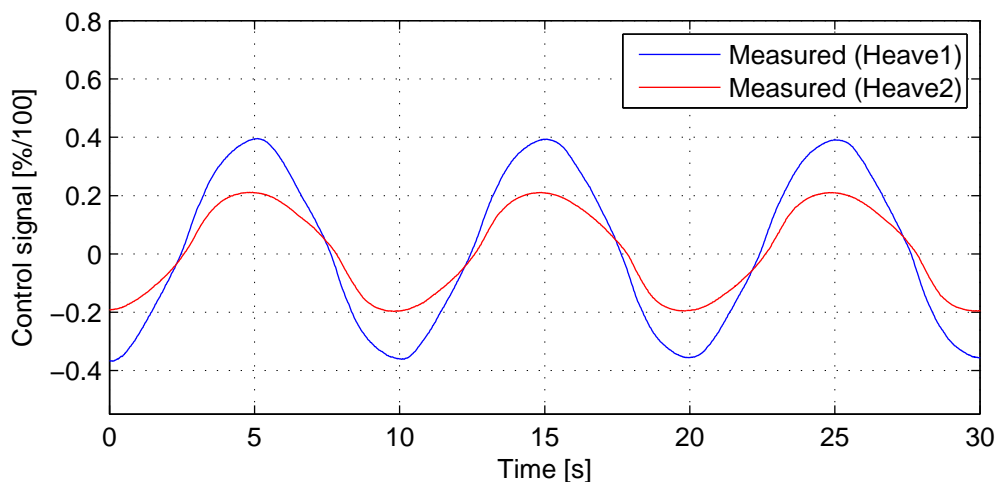


Figure 8.2: Control signals from tests (payload of 500 kg)

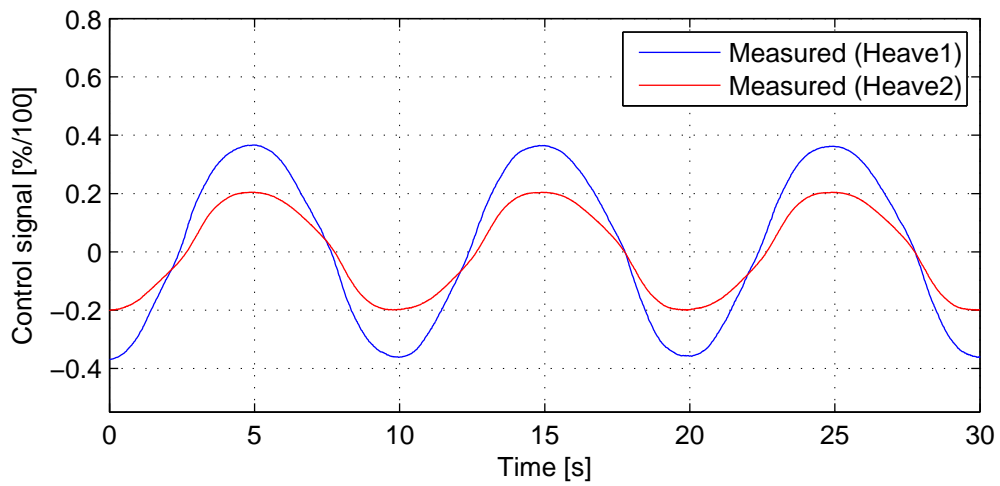


Figure 8.3: Control signals from tests (payload of 200 kg)

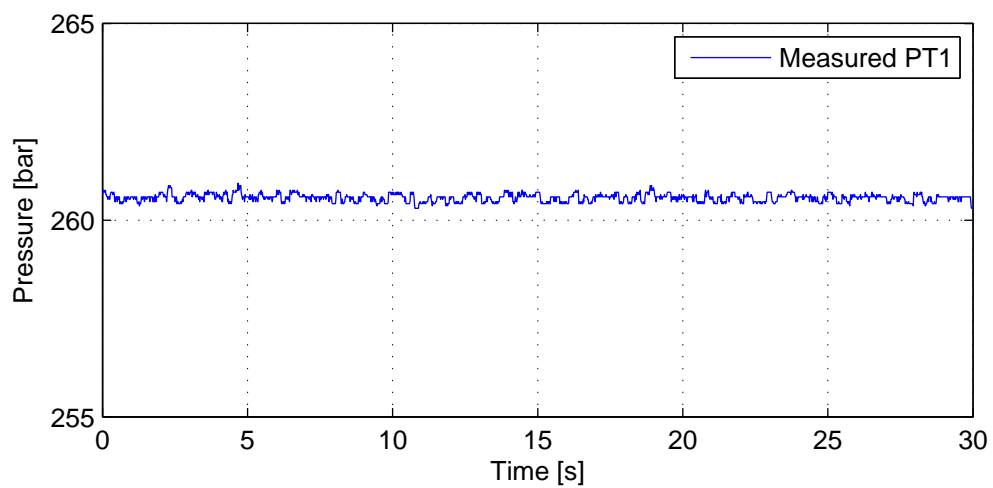


Figure 8.4: Measured supply pressure

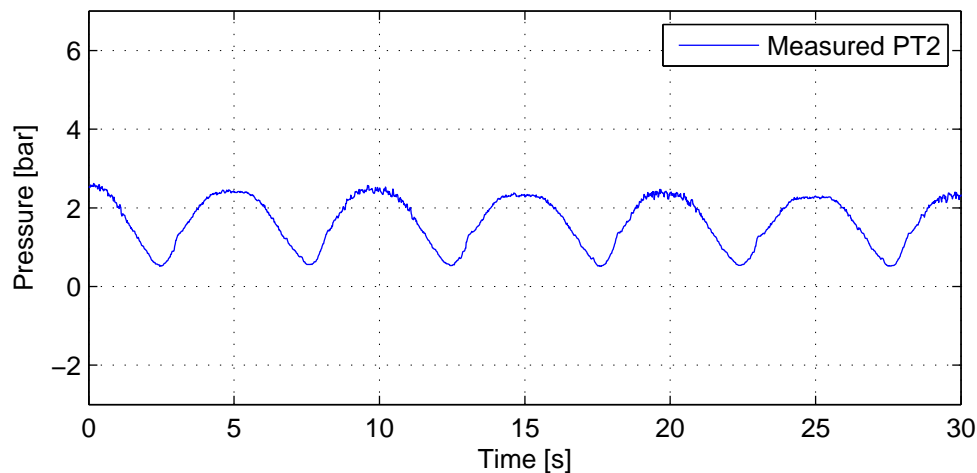


Figure 8.5: Measured tank port pressure

## 8.3 Comparison of Simulated and Measured Test Data

### 8.3.1 Load Case 1

This section presents comparison of simulated and measured test data obtained with a payload of 500 kg. The control parameters were tuned by a trial-and-error approach. The FFW gain and the PI-controller parameters are selected as  $K_{FFW}=60$ ,  $K_p=100$ , and  $T_i=3s$ .

#### Workport Pressures

Fig. 8.6 shows simulated and measured values of the pressures at motor port A and B, obtained with two different heave disturbances. The pressures at port A and B are measured by PT4 and PT3, respectively. Where the greatest pressure difference is observed, the motor is subjected to a positive load (hoisting). In the lowering case, it can be seen that the pressure drop across the motor is approximately 0 bar.



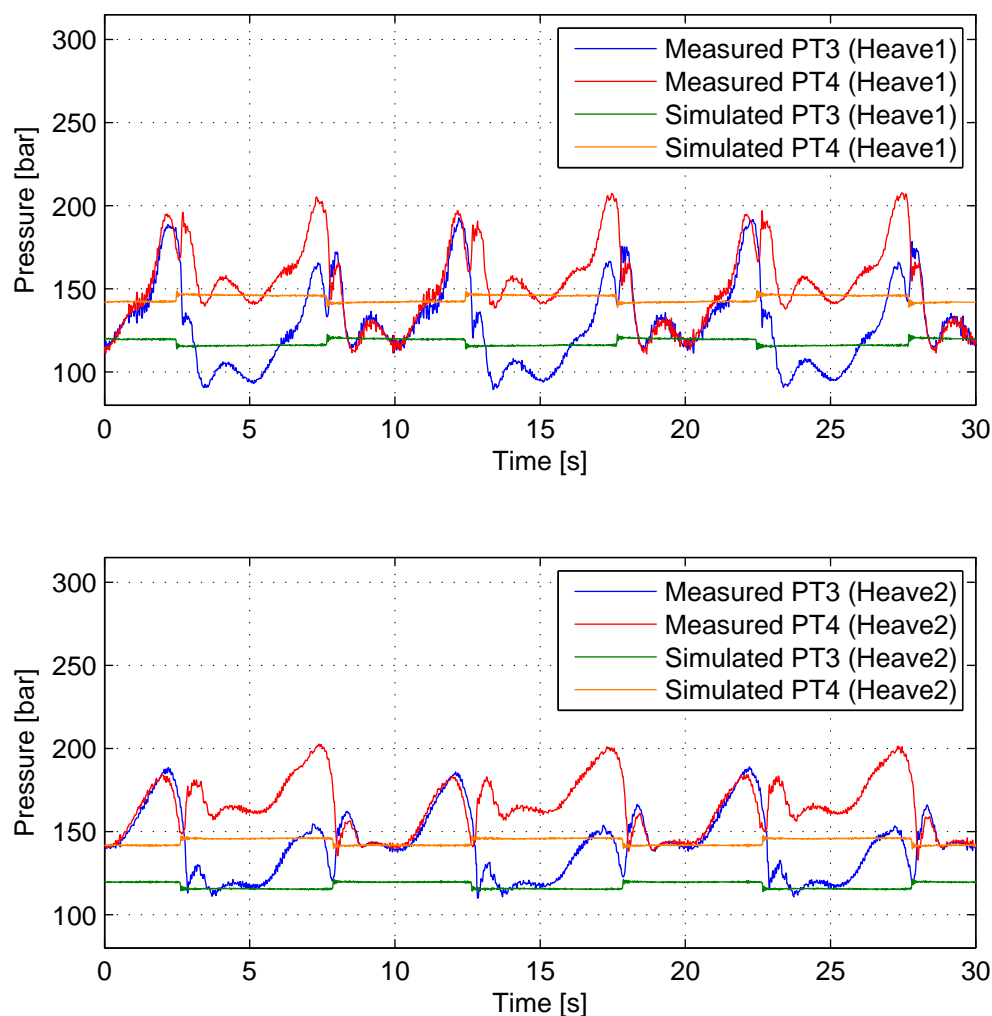


Figure 8.6: Workport pressures with "Heave 1" (Load case1)

Discrepancies between simulated and measured results are observed in the plots of the workport pressures. The simulated pressure drop across the motor (PT4-PT3) proved to be too low during hoisting and too high during lowering, compared to the measurements. This indicates that the motor friction is considerably higher than assumed in the simulation model. The measurements also reveals that significant pressure variations are present in the actual system. Higher pressures occurs at the beginning and end of each hoisting operation. Since both pressures rises at the same time, this is most likely due to valve asymmetry.

In order to make the model fit the measurements, effort was put into determining the actual motor friction and identifying a possible valve asymmetry (see Section 8.4).

## Payload Position

Fig. 8.7 and Fig. 8.8 show the payload movement and the position tracking error obtained with two different heave disturbances. Because the system is not influenced by an actual wave motion, the payload moves up and down during heave compensation. It can be seen from the position-time plots that the motion is sinusoidal. In the simulation, this is achieved by setting the heave motion amplitude to zero.

It can be seen that the simulated motion of the payload is not entirely consistent with the measured motion. The measured position error is within the range of  $\pm 2.5$  cm. The error obtained from simulation is greater, as the model does not match exactly. The discrepancy between simulated and measured payload position is identified and calibrated in Section 8.4.

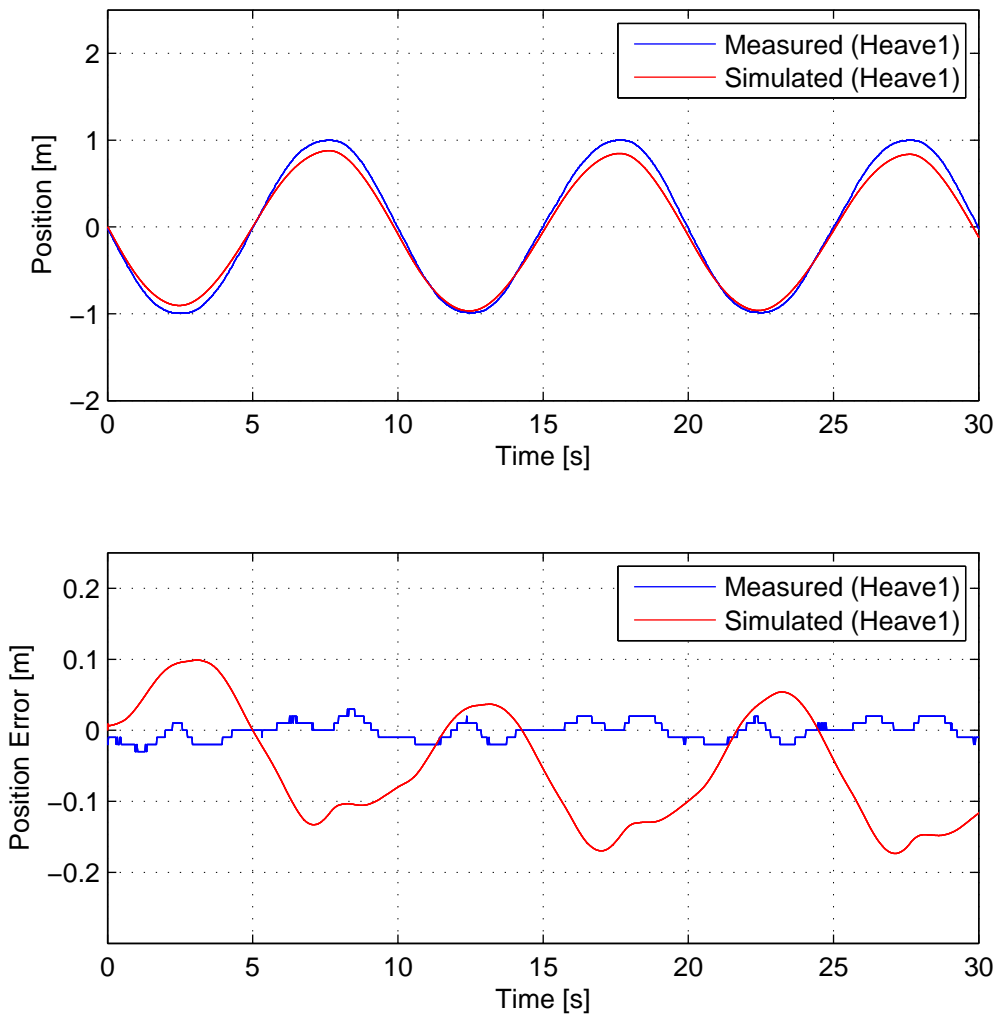


Figure 8.7: Payload position and position error with "Heave1" (Load case 1)

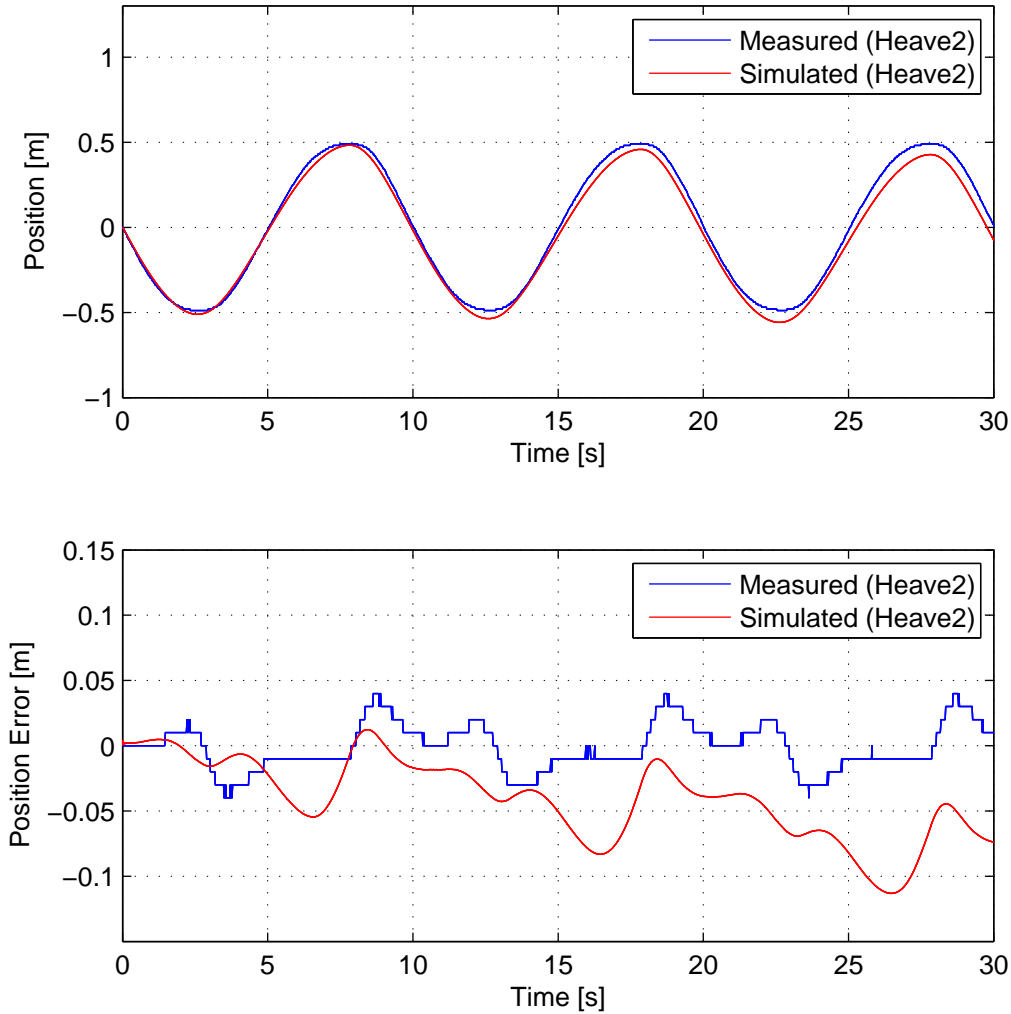


Figure 8.8: Payload position and position error with "Heave2" (Load case 1)

### 8.3.2 Load Case 2

This section presents comparison of simulated and measured test data obtained with a payload of 200 kg. Results obtained with "Heave1" are presented, to show how the system responds with a smaller load. The FFW gain and the PI-controller parameters are selected as  $K_{FFW}=58$ ,  $K_p=100$ , and  $T_i=3s$ .

Fig. 8.9 shows simulated and measured values of the pressures at motor port A and B, measured by PT4 and PT3, respectively. The figure shows discrepancies between the simulated and measured pressure drop across the motor. In addition, the plot shows unexpected pressure variations in the measurements. The same was observed in load case 1.

Fig. 8.10 shows the payload movement and the position tracking error. As shown, the result from the simulation does not match the measurements completely. In the following section, the experimental data are used to calibrate the model.

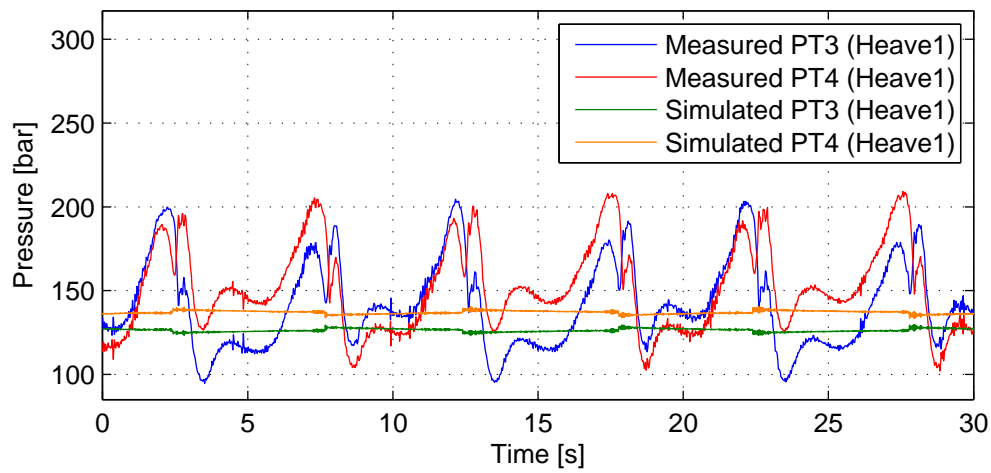


Figure 8.9: Workport pressures with "Heave 1" (Load case 2)

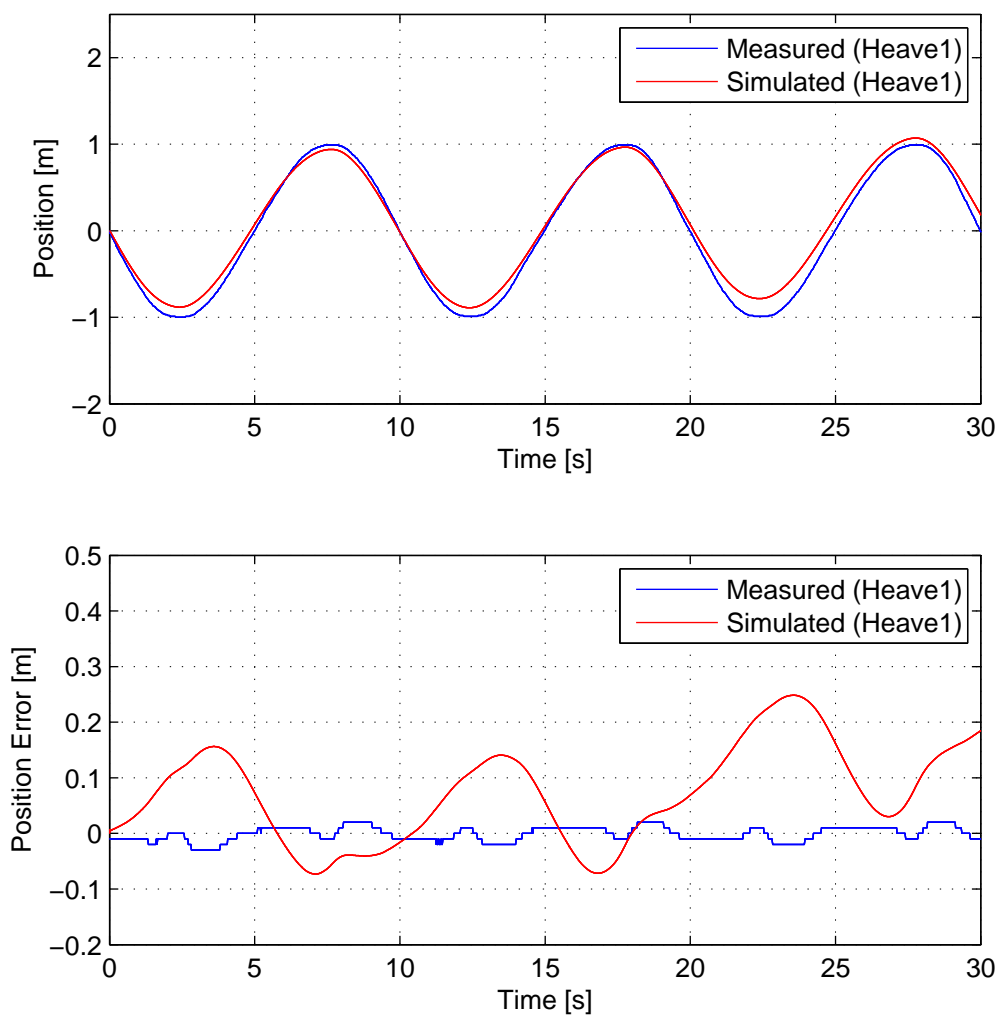


Figure 8.10: Payload position and position error with "Heave1" (Load case 2)

## 8.4 Parameter Identification and Optimization

In this section the measured test data are used to estimate model parameters. The aim of this process is to calibrate the model.

### 8.4.1 Motor Friction

The comparison of simulated and measured data revealed that the motor friction was more significant than anticipated. In order to model the actual friction, it was decided to replace the hydro-mechanical efficiency with a friction model.

#### Friction Model

The proposed friction model consists of a viscous torque friction in combination with a constant torque friction, see Eq. 8.1. The viscous friction coefficient  $B$  is assumed to be proportional to the motor speed  $n$ , while the Coulomb friction torque  $M_C$  is a constant friction contribution.

$$M_{friction} = B \cdot n + M_C \cdot \text{sign}(n) [Nm] \quad (8.1)$$

The two friction losses were determined by analyzing the experimental data. Data from all the tests were considered. The pressure measurements were of particular interest. Fig. 8.11 presents the measured pressure drop across the motor (PT4-PT3), obtained with two different sinusoidal heave disturbances. It can be observed that the pressure drop during hoisting is just below 50 bar, and around 0 bar during lowering. This gives an indication of the total torque loss present in the hydraulic motor. It is clear that the constant friction torque contribution is the dominant one. Small variations in the pressures are observed due to change in motor speed.

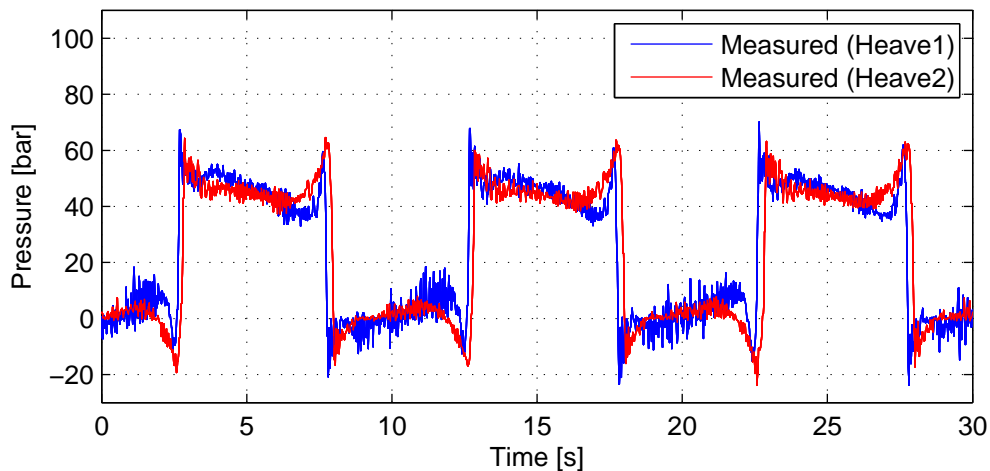


Figure 8.11: Pressure drop across the motor with a payload of 500 kg

The theoretical pressure drop over the motor with a load of 500 kg is calculated to 24.5 bar, using Eq. 8.2 and Eq. 8.3 . This is in accordance with the measurements. Taken into account the gearbox losses, the pressure drop due to the motor friction is considered to be approximately 20 bar. This corresponds to a torque loss of 19 Nm.

$$M_{tM} = \frac{m \cdot g \cdot PCD}{2 \cdot i} [Nm] \quad (8.2)$$

$$\Delta p_M = \frac{2\pi \cdot M_{tM}}{D_M} [Pa] \quad (8.3)$$

In order to determine the friction parameters, tuning was performed. Simulated data were compared with measurement data. The friction parameters were selected as  $B = 0.009$  Nms/rad and  $M_c = 18.3$  Nm.

### 20-sim Implementation

In the calibrated 20-sim model, the hydro-mechanical efficiency is replaced with the developed friction model. Eq. 8.4 is implemented in the friction block inside the motor model. The tanh-function is used in stead of the sign-function.

$$M_{fric} = 0.009 \cdot \omega + 18.3 \cdot \tanh(1e3 \cdot \omega) [Nm] \quad (8.4)$$

Fig. 8.12 presents the measured and simulated pressure drop across the motor. As shown, the results from the simulation and measurements are consistent.

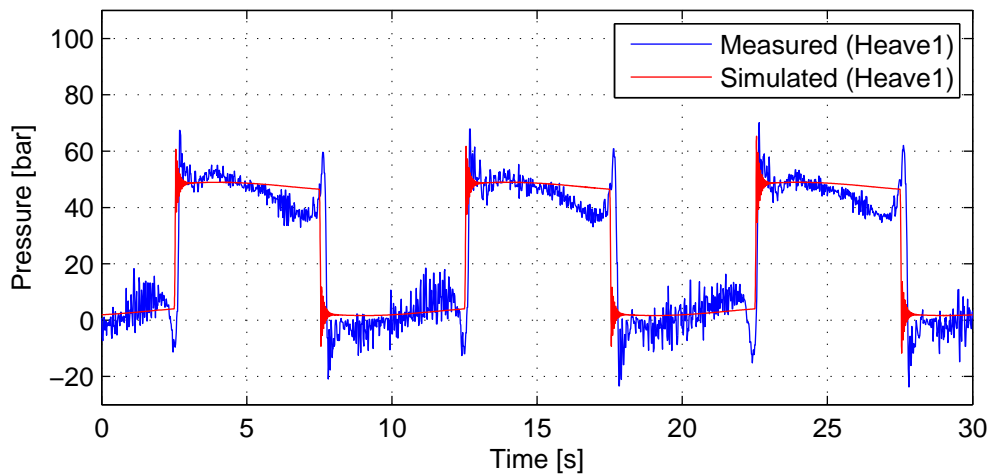


Figure 8.12: Validation of implemented friction model

## 8.4.2 Valve Asymmetry and Leakage

In order to get the simulation model to match the experimental results, it was decided to investigate the pressure variations and find the cause of them.

### Investigation of pressure variations

The experimental data revealed unexpected pressure variations. These variations can be explained by valve asymmetry, i.e. asymmetry between P-A and B-A (or P-B and A-T). This is because the same variation occurs in both pressures simultaneously. The pressures analyzed were measured at the inlet and outlet line of the motor.

In the simulation model perfectly symmetrical laps were assumed. However, in real life, asymmetrical laps occur because of normal manufacturing tolerances. Fig. 8.13 displays the mean value of the measured pressures of the A and B port. The red curve represents the theoretical middle value of the load pressure, i.e. 50% of the supply test pressure. It can be seen that the measured mean value is well above the ideal value of 130 bar, especially at the beginning and end of a hoisting operation. The cause of the higher pressures is the return land B-T. It is more closed than its associated metering edge (P-A). Consequently, the pressure drop across the return land B-T is higher than the pressure drop across P-A.

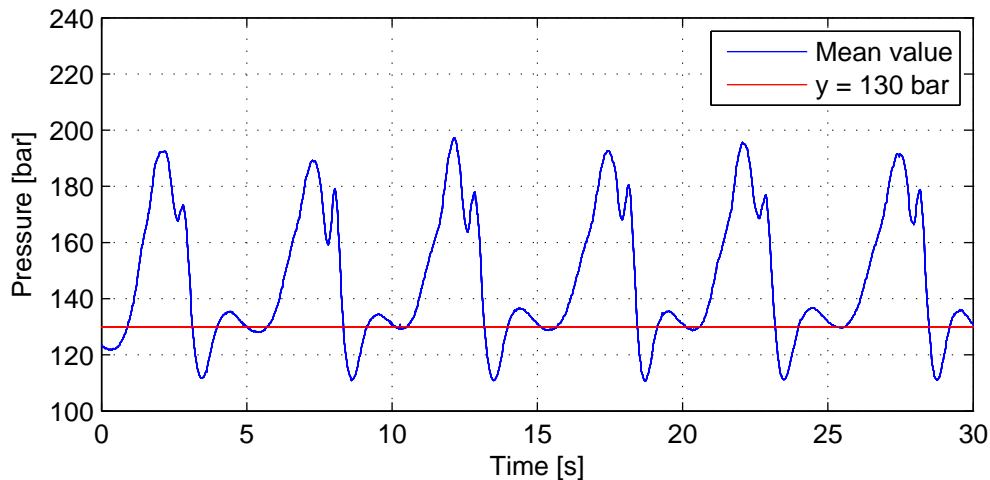


Figure 8.13: Measured and ideal mean value of PT4 and PT3

### 20-sim Implementation

Due to asymmetry the discharge areas are not the same function of the spool travel. It was decided to model the metering-in area (P-A and P-B) according to the catalog as described earlier. This was achieved by implementing a look-up table (see Section 6.5.4). The metering-out area (A-T and B-T) follow the second order polynomial  $a$ :

$$a = C_3 \cdot qpp^2 + C_2 \cdot qpp + C_1 \quad (8.5)$$

where  $qpp$  [%/100] is the factor which defines the relation between control input and delivered flow. The coefficients  $C_1$ ,  $C_2$  and  $C_3$  needed to be determined. After several iterations, the following coefficients were found:  $C_1=0.4$ ,  $C_2=2.17$  and  $C_3=-1.02$ . Fig. 8.14 displays the polynomial curve implemented. It should be stressed that the  $qpp$  factor, during the simulation run, is in the range of around  $\pm 0.4$ . The area outside this range has not been investigated in this thesis.

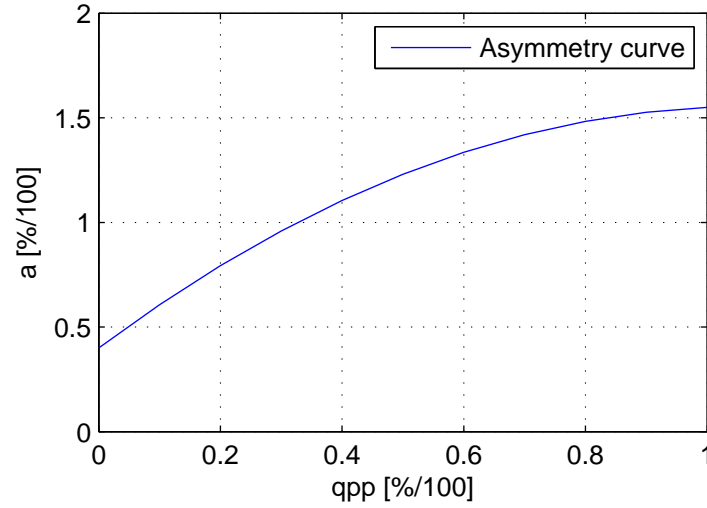


Figure 8.14: Asymmetry curve

In 20-sim the asymmetry (function  $a$ ) was implemented in the B-T and A-T flow equations, with the following equation:

$$Q = C_D \cdot qpp \cdot a \cdot A_{max} \cdot \sqrt{\frac{2}{\rho} \cdot |\Delta p|} \cdot \text{sign}(\Delta p) \quad (8.6)$$

Fig. 8.16 verifies that much of the pressure variations can be captured by implementing asymmetry. The effect of including external leakage flows at the motor ports (using laminar resistance blocks) was also looked at. By adjusting the leakage coefficients, it was possible to get the simulated values to fit better with the measurements. Fig. 8.16 shows how well the simulated values of the pressures fit the measured values, after including asymmetry and external leakage in the model.



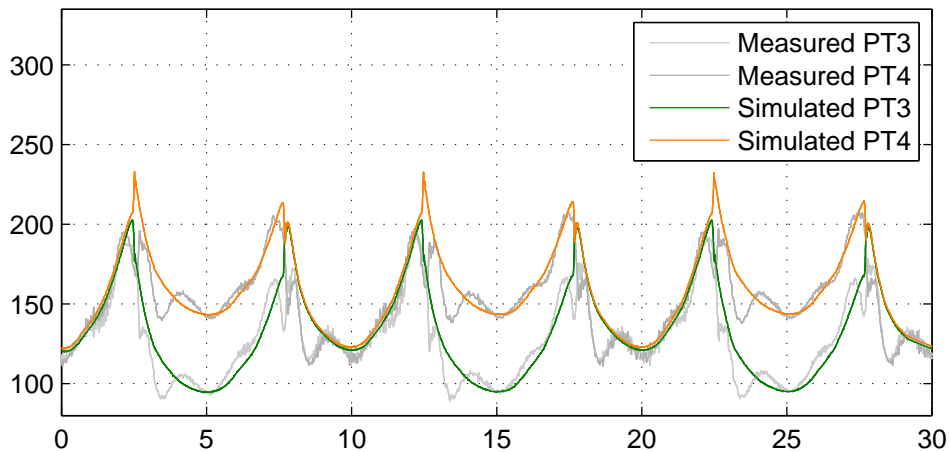


Figure 8.15: Pressures as a result of asymmetry

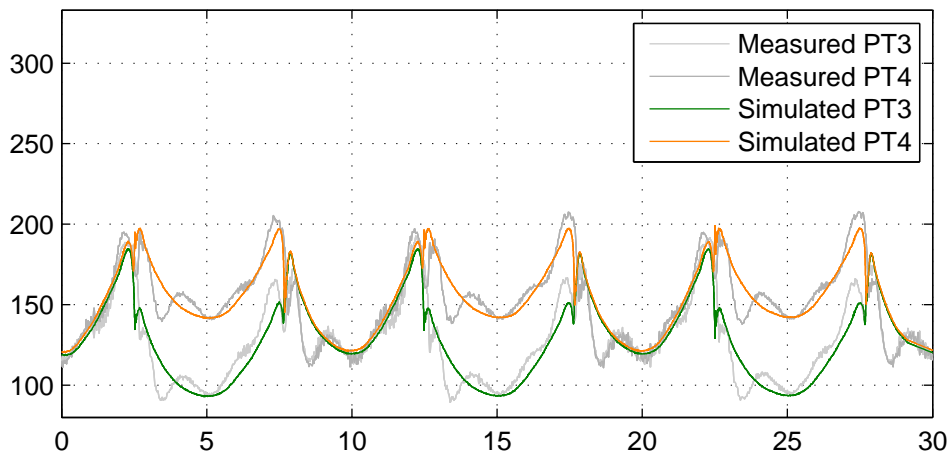


Figure 8.16: Pressures as a result of asymmetry and external motor leakage

### 8.4.3 Valve Area-Opening Relationship

Comparison of simulated and experimental test data revealed that the simulated motion of the payload was not entirely consistent with the measured motion. To get the simulated data to match better, the signal-flow relationship in the valve model was changed. It was discovered that by making small amendments in the flow characteristic of the valve, the simulated and the measured values matched to a greater extent.

#### 20-sim Implementation

In the simulation model a look-up table is included to define the servo valve's flow characteristic. Tuning of the flow characteristic was achieved by adding a constant to each of the values in the look-up table. Fig. 8.17 shows the difference between the old and the new flow

characteristic. Furthermore, Fig. 8.18 depicts the simulated motor flow, before and after tuning. As shown, the flow increased by implementing the new characteristic. Consequently the position error was reduced, as wanted.

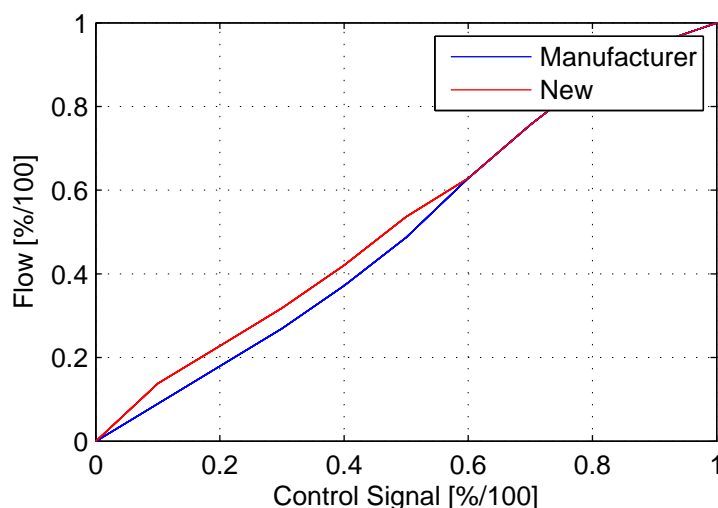


Figure 8.17: Flow characteristics of servo valve

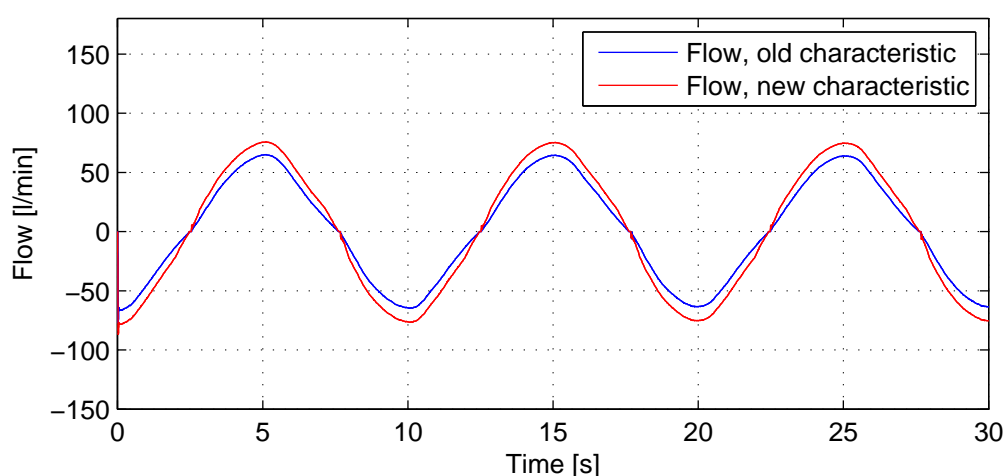


Figure 8.18: Motor flow with different flow characteristics

#### 8.4.4 Valve Dynamics

In the simulation the valve's dynamics are described with a second order transfer function. The undamped natural frequency and damping ratio are determined from the frequency characteristic provided by the manufacturer. However, a review of the frequency response clearly points out the existence of non-linearities.

The servo valve feedback signal was logged during testing. Initially it was intended to use this information, together with the input signal, to evaluate the actual dynamics of the valve and calibrate the valve model. Measurements of the control signal and the feedback signal

were compared. However, the results obtained from the comparison were not as expected. An offset of approximately 750 ms can be observed. This offset is shown in Fig. 8.19. It seems to be a time delay present. This is because the difference is too large for it to be a result of how fast the valve responds. For comparison, the difference is 230 ms, assuming a valve bandwidth of 1 Hz. This value was identified by means of simulation.

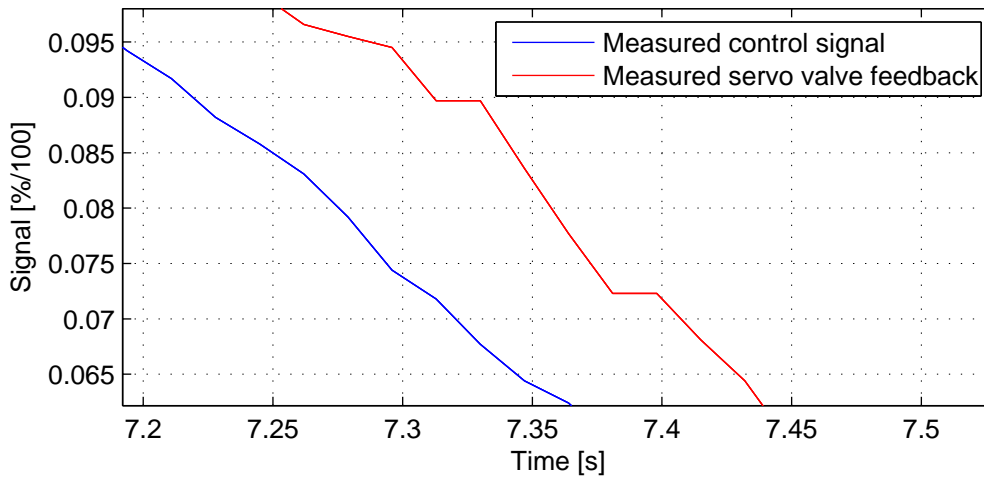


Figure 8.19: Measured input signal versus valve feedback signal

## 8.5 Key findings

Simulated and measured data have been compared to get a calibrated model and gain experience in what parameters that must be adjusted. In the calibration phase, the following needed to be added/adjusted:

- friction loss in the motor
- valve asymmetry
- external motor leakage
- flow characteristic
- volumetric efficiency

It was found that the friction loss in the motor needed to be adjusted. The leakage losses also needed to be modified. The volumetric efficiency was increased, while external leakage at the motor ports were included.

This study has shown that a servo valve cannot be modeled just from catalogue data if the aim is to create a model to come close to real data. Both asymmetry and flow characteristic (flow vs. spool position) needed to be implemented.

The calibrated simulation model was found to represent the real system in a good way. Thus, it could be used to study the system behavior further.

## 8.6 Using the Calibrated Model

The calibrated simulation model has been used to evaluate the control strategies. In addition, the importance of valve bandwidth has been explored by means of simulation.

### 8.6.1 Evaluation of Control Strategies

In this section, the proposed control strategies are analyzed. Both simulation and experimental results are presented. In the proposed control system, the PI-controller complements the feedforward control. Three different feedforward control strategies were investigated (as presented in Chapter 5):

1. One constant feedforward gain
2. Two constant feedforward gains (one for lowering and one for hoisting)
3. Model-based feedforward (with pressure measurements)

The basic idea of the feedforward control is to continuously compute the control valve input based on knowledge of the system. The disturbance of which the system is exposed to is a known sine wave. According to the theory, by included just one feedforward gain, the control effort from the PI-controller is greater during hoisting than lowering. By implementing two gains (one for hoisting and one for lowering), the feedforward gains can be tuned such that the control output of the PI-controller is quite similar during hoisting and lowering. This may lead to a improved tracking performance. The third feedforward strategy being explored, is the model-based prediction of input. This feedforward is given by:

$$K_h = \frac{i \cdot D_M}{\eta_{vM} \cdot 2\pi \cdot r_{drum} \cdot Q_{Nom.} \cdot \sqrt{\frac{(p_p - p_b)}{\Delta p_{Nom.}}}} \quad (8.7)$$

$$K_l = \frac{\eta_{vM} \cdot i \cdot D_M}{2\pi \cdot r_{drum} \cdot Q_{Nom.} \cdot \sqrt{\frac{(p_p - p_a)}{\Delta p_{Nom.}}}} \quad (8.8)$$

where  $K_h$  is the feedforward gain when the motor is hoisting and  $K_l$  the feedforward gain when the motor is lowering.

A comparison of the three different control strategies are given in Fig. 8.20. The presented experimental results are obtained with a payload of 500 kg, a heave amplitude of 1 m and a heave frequency of 0.1 Hz ("Heave1"). The control parameters of the PI-controller was selected to  $K_p=100$  and  $T_i=3.0$ . The measurements have been scaled with a factor of 100. In the plots, the value 1 correspond to the maximum control valve input.

The experimental testing revealed that active heave compensation was performed with satisfactory results. Small deviations were achieved with all the regulators (approximately  $\pm$

2.5 cm). It can be observed that the feedforward counts for most of the control effort (approximately 96% of the total control effort). Fig. 8.21 presents the PI-controller contribution during the test runs. As shown, the control efforts are in the same range.

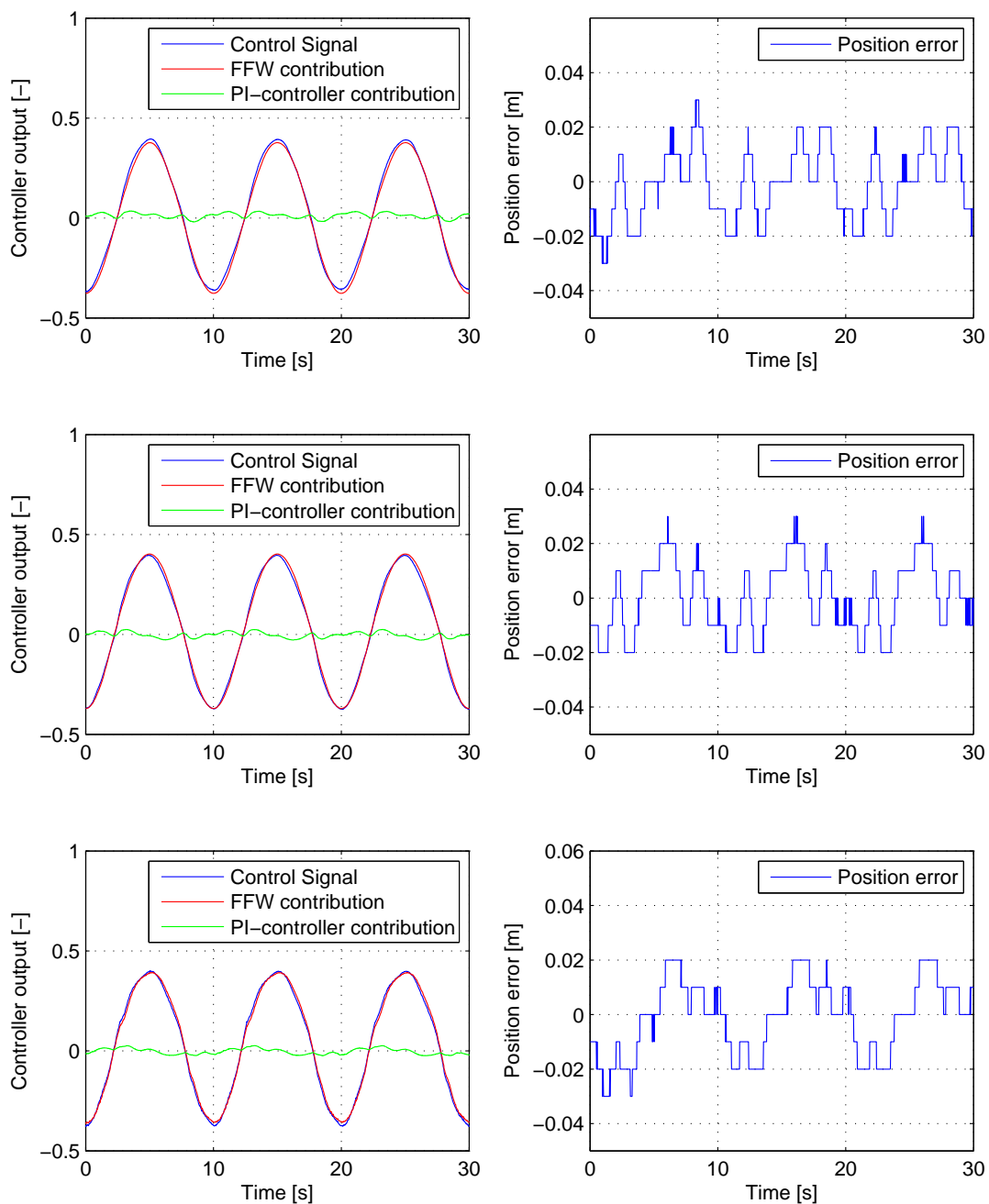


Figure 8.20: Logged control effort and deviation obtained from tests with a load of 500 kg. Control strategy 1 (top), control strategy 2 (middle) and control strategy 3 (bottom)

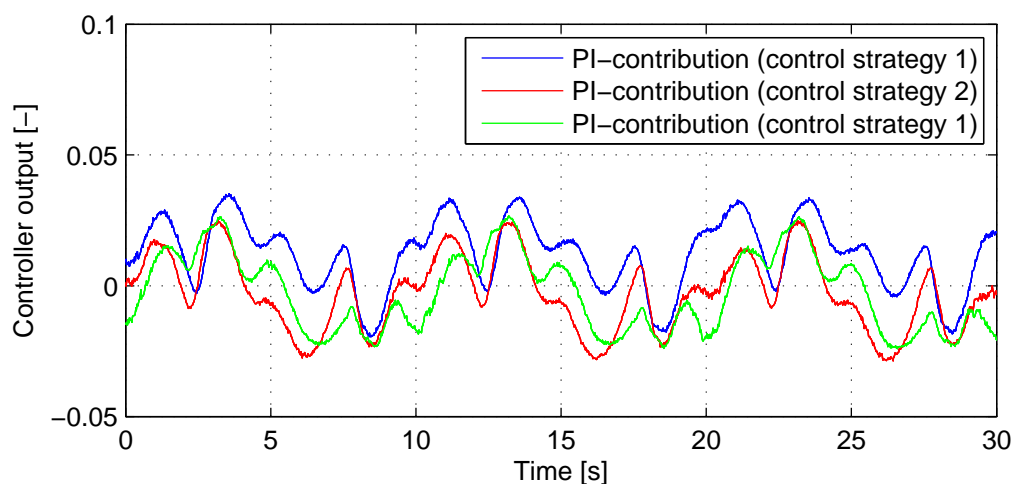


Figure 8.21: Measured feedback control

The controllers were tested for various load cases. The effect of including two feedforward gains proved to be minimal, when having small loads. The feedforward strategy with just one gain proved to give the same result. One advantage of the model-based feedforward is that no tuning is needed. It automatically adjusts the control effort based on the systems pressure variations. Fig. 8.22 shows simulation results obtained with the model-based controller with a load of 2000 kg. As expected, the feedforward control predicts the system input well.

Both simulation and test results have revealed that model-based feedforward in combination with a feedback controller, is a good control strategy. It is found that this controller is more robust, as it adapts to load changes.

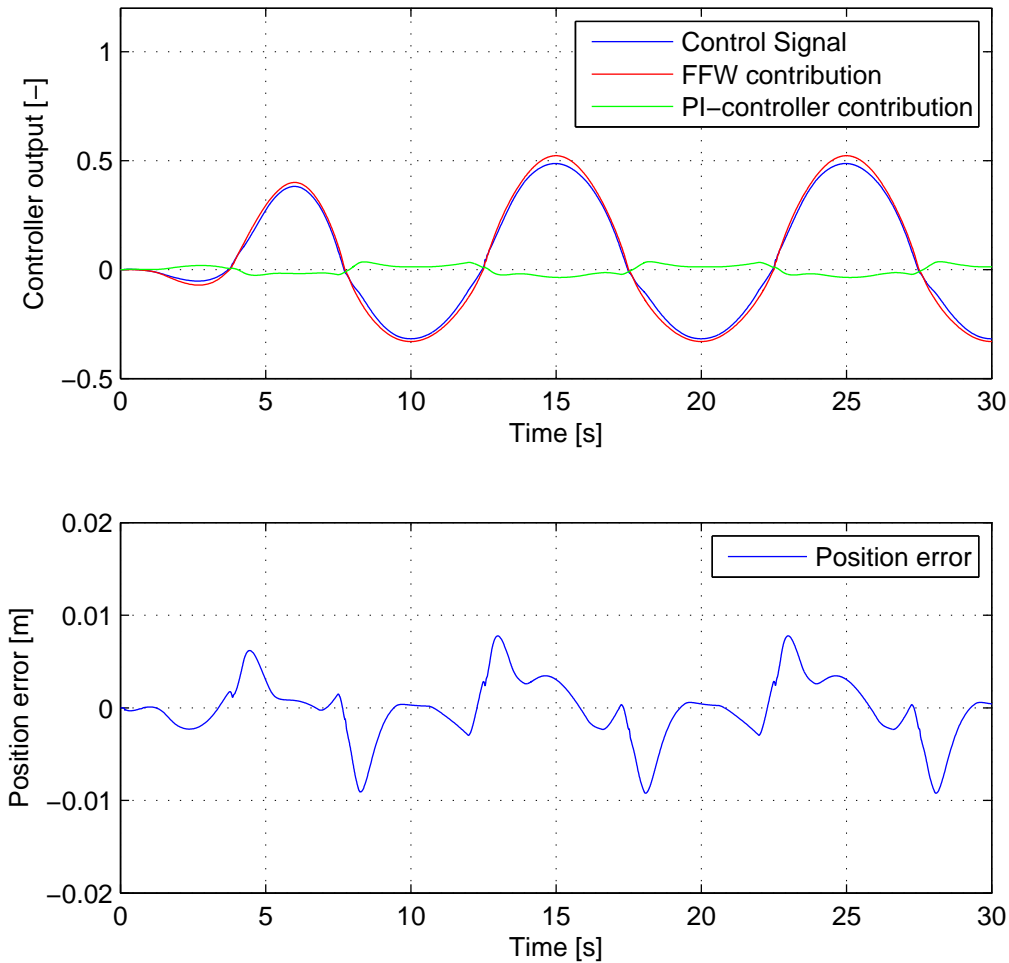


Figure 8.22: Simulated. Load 200kg.

### 8.6.2 Importance of valve bandwidth

The choice of control valve is an important consideration in any hydraulic control application. Usually this choice is a compromise between the control requirements and the cost. Best control performance is normally offered by servo valves. This is mainly due to their good linear flow characteristic and their high bandwidth characteristic. In this section the importance of valve bandwidth is looked into. This is achieved by using the calibrated model.

In the 20-sim model, the spool dynamics is modelled by a second order transfer function. This transfer function is characterized by the bandwidth frequency ( $\omega_0$  [rad/s]) and the damping coefficient ( $\zeta$  [-]):

$$G(s) = \frac{\omega_0^2}{s^2 + 2\zeta\omega_0 s + \omega_0^2} \quad (8.9)$$

Therefore, by adjusting  $\omega_0$  it is possible to get an idea of the importance of valve band-

width. Different valve bandwidths were tested by simulating the system. By decreasing the valve bandwidth, the valve becomes slower. By reducing the valve bandwidth to 1 Hz, a time delay of 230 ms was observed. The actuation system managed to compensate without large delays in the system. The results of the simulation study indicate that it is possible to achieve good compensation with slower valves. However, this was not further discussed, due to time limitations and increased focus on validating the dynamic 20-sim model.



# Chapter 9

## Conclusion and Further Work

The main objective of the project was to analyze and model an active heave compensation winch system provided by Cargotec. The test setup is a scale model of a real system. The overall accomplishment of the project was the dynamic modeling with the use of 20-sim.

The dynamic model was calibrated and validated by comparing simulation and experimental results. Part of the calibration process included modifying the friction loss in the hydraulic motor. Initially this loss was assumed to be less than that observed. The valve's flow characteristic was also modified to enhance the dynamic model. It was found that the flow characteristic provided by the manufacturer was not consistent with the experimental results. The experimental results also indicated valve asymmetry. A function was derived and implemented to compensate for this.

Three different feedforward control strategies were tested and evaluated. All strategies proved to work well. Especially the model-based feedforward was analyzed. Through simulation it was proven that the developed feedforward adapts to load changes, and is therefore more robust.

The importance of valve bandwidth was studied by using the created simulation model. By reducing the valve bandwidth to 1 Hz, a time delay of 230 ms was observed. The actuation system managed to compensate without large delays in the system. The results of the simulation study indicate that it is possible to achieve good compensation with slower valves. A further study investigating the possibility of active heave compensation with slower control valves would be very interesting. By including an over-center valve in the test-setup, the PVG120 can be used for this purpose. Due to time limitations this has not been a part of this project.

As a conclusion, the modeling of an active heave compensation winch system using 20-sim was proven to be feasible.

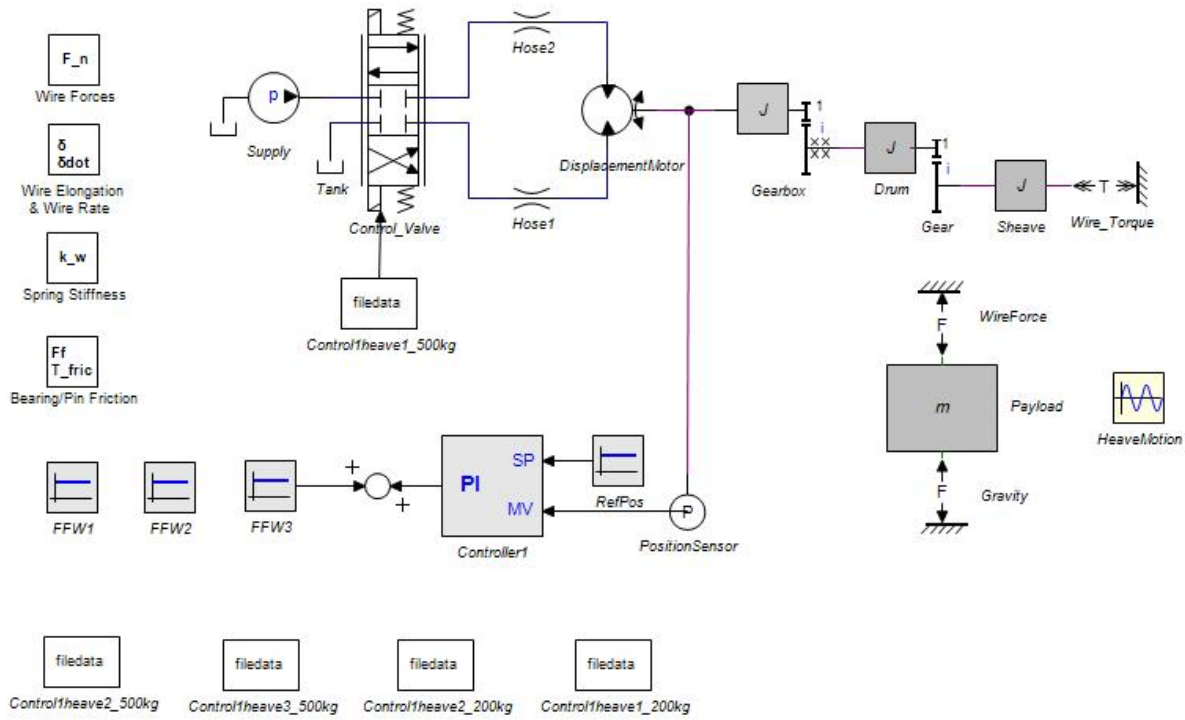
# Bibliography

- [1] DNV, “Modelling and Analysis of Marine Operations,” [http://www.stalforbund.com/\\_member/rp-h103\\_2011-04.pdf](http://www.stalforbund.com/_member/rp-h103_2011-04.pdf), accessed: 22/02/2013.
- [2] Huisman, “Heave Compensation,” [http://www.huismanequipment.com/en/products/heave\\_compensation/heave\\_compensation\\_product](http://www.huismanequipment.com/en/products/heave_compensation/heave_compensation_product), accessed: 22/02/2013.
- [3] M. Jelali and A. Kroll, *Hydraulic Servo-systems: Modelling, Identification and Control*. Springer-Verlag, 2003.
- [4] D. DeRose, “Proportional and Servo Valve Technology,” *Fluid Power Journal*, March/April 2003.
- [5] Parker Hannifin, “Press Report DF plus,” <http://www.parker.com/literature/Hydraulic%20Controls%20Europe/Press%20Reports/HY11-3324UK.pdf>, accessed: 04/03/2013.
- [6] H. E. Merritt, *Hydraulic Control Systems*. John Wiley and Sons, Inc, 1967.
- [7] M. R. Hansen and T. O. Andersen, *Hydraulic Components and Systems*, 2009.
- [8] A. Maria, “Introduction to Modeling and Simulation,” *Proceedings of the 1997 Winter Simulation Conference*, 1997.
- [9] I. C. Kleijn and I. M. A. Groothuis, *Getting Started with 20-sim 4.3*, Controllab Products B.V, 2013.

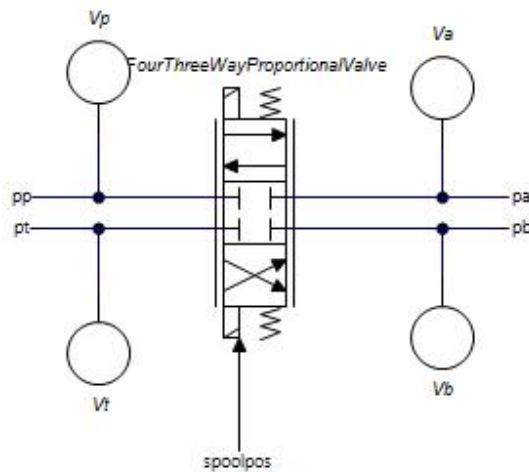
# Appendix A

## 20-sim Model

# Hydro-mechanical 20-sim model



## Servo Valve (Parker D3FP Valve)



### parameters

```

real p_vapour = -99900.0 {Pa};           // vapour presure
real rho = 865.0 {kg/m3};               // mass density
real GLeak = 0;                         // conductance of laminar leakage flow
real GLeak_Ret = 0;                     // conductance of laminar leakage flow
real overlap = 0.0 {};                  // valve overlap as percentage of full stroke: -1 < overlap < 1
real Cd = 0.6 {};                       // discharge coefficient;
real f = 100.0 {Hz};                   // natural frequency [Hz],read from -90 degree phase lag
real d = 0.7 {};                        // relative damping []
real global pr = 35e5 {Pa};
real global Qr = 100{l/min}; //0.0075 {m3/s}
real PRet_1 = 0.4; //Assymetry @ 0% opening
real PRet_2 = 1.23; //Assymetry @ 50% opening
real PRet_3 = 1.55; //Assymetry @ 100% opening

```

### //Lookup table

```

real spTab[11]= [0;0.1;0.2;0.3;0.4;0.5;0.6;0.7;0.8;0.9;1];
real QpTab[11]= [0;0.08974;0.1795;0.2692;0.3718;0.4872;0.6282;0.7564;0.8718;0.9487;1];

```

### //Parameters used to tune the flow characteristic

```

real c1 = 0.048;
real c2 = 0.048;
real c3 = 0.049;
real c4 = 0.049;
real c5 = 0.049;

```

### variables

```

real pp_lim, pt_lim,pa_lim, pb_lim;
real global Ax_pos, Ax_neg;
real global Ax_pos_Ret, Ax_neg_Ret;

```

```

real global dp_p_a, dp_p_b, dp_a_t, dp_b_t;
real p_p_a_phi, p_p_b_phi, p_a_t_phi, p_b_t_phi;
real Amax;
real hidden rate1,rate2, state1;
real sp;
real omega;

```

```

real global flow_curve;
real global flowcurve_pos;
real global flowcurve_neg;
real global flowcurve_pos_Ret;
real global flowcurve_neg_Ret;
real spp;
real qpp;
real CRet_1;
real CRet_2;
real CRet_3;

```

#### initialequations

```

omega = f * 2 * pi;
Amax = Qr / (Cd * (2/rho * pr)^0.5); // Maximum valve opening area
CRet_1 = PRet_1;
CRet_3 = (PRet_3-2*PRet_2+PRet_1)/0.5;
CRet_2 = PRet_3-CRet_3-PRet_1;

```

#### equations

```
// second order spool dynamics
```

```

sp = int(rate2);
rate1 = (spoolpos - sp) * omega;
state1 = int(rate1);
rate2 = (state1 - 2*d*sp) * omega;

```

```
// Linear interpolation
```

```
//  $y_2 = (x_2 - x_1) * (y_3 - y_1) / (x_3 - x_1) + y_1$ , here  $y_2 = spp$  and  $x_2 = spp$ 
```

```

spp = abs(sp);
if spp <= 0.1 then
    qpp = ((spp-0) * (0.08974+c1-0)) / (0.1-0) + 0;
else
if spp <= 0.2 then
    qpp = ((spp-0.1) * (0.1795+c2-(0.08974+c1))) / (0.2-0.1) + 0.08974+c1;
else
if spp <= 0.3 then
    qpp = ((spp-0.2) * (0.2692+c3-(0.1795+c2))) / (0.3-0.2) + 0.1795+c2;
else
if spp <= 0.4 then
    qpp = ((spp-0.3) * (0.3718+c4-(0.2692+c3))) / (0.4-0.3) + 0.2692+c3;
else
if spp <= 0.5 then

```

```

        qpp=((spp-0.4)*(0.4872+c5-(0.3718+c4)))/(0.5-0.4)+0.3718+c4;
else
    if spp<=0.6 then
        qpp=((spp-0.5)*(0.6282-(0.4872+c5)))/(0.6-0.5)+0.4872+c5;
    if spp<=0.7 then
        qpp=((spp-0.6)*(0.7564-(0.6282)))/(0.7-0.6)+0.6282;
    else
        if spp<=0.8 then
            qpp=((spp-0.7)*(0.8718-0.7564))/(0.8-0.7)+0.7564;
        else
            if spp<=0.9 then
                qpp=((spp-0.8)*(0.9487-0.8718))/(0.9-0.8)+0.8718;
            else
                if spp<=1 then
                    qpp=((spp-0.9)*(1-0.9487))/(1-0.9)+0.9487;
                    end;
                    end;
                    end;
                    end;
                    end;
                    end;
end;
        end;
        end;
    end;

    if sp>0 then
        flowcurve_pos = qpp;
        flowcurve_pos_Ret = qpp*(CRet_1+CRet_2*qpp+CRet_3*qpp^2);
        flowcurve_neg = 0;
        flowcurve_neg_Ret = 0;
    else
        flowcurve_pos = 0;
        flowcurve_pos_Ret = 0;
        flowcurve_neg = qpp;
        flowcurve_neg_Ret = qpp*(CRet_1+CRet_2*qpp+CRet_3*qpp^2);
    end;

    pp_lim = if pp.p < p_vapour then p_vapour else pp.p end;
    pt_lim = if pt.p < p_vapour then p_vapour else pt.p end;
    pa_lim = if pa.p < p_vapour then p_vapour else pa.p end;
    pb_lim = if pb.p < p_vapour then p_vapour else pb.p end;

    // Ax_pos = limit(((sp-overlap)/(1-overlap))*Amax,0,Amax);
    // Ax_neg = limit(((sp-overlap)/(1-overlap))*Amax,0,Amax);

```

```

Ax_pos = limit(flowcurve_pos*Amax,0,Amax);
Ax_pos_Ret = limit(flowcurve_pos_Ret*Amax,0,Amax);
Ax_neg = limit(flowcurve_neg*Amax,0,Amax);
Ax_neg_Ret = limit(flowcurve_neg_Ret*Amax,0,Amax);

dp_p_a = pp_lim - pa_lim;
p_p_a_phi = sign(dp_p_a) * Cd * abs(Ax_pos) * sqrt( (2/rho) * abs(dp_p_a) ) + GLeak * dp_p_a;

dp_b_t = pb_lim - pt_lim;
p_b_t_phi = sign(dp_b_t) * Cd * abs(Ax_pos_Ret) * sqrt( (2/rho) * abs(dp_b_t) ) + GLeak_Ret *
dp_b_t;

dp_p_b = pp_lim - pb_lim;
p_p_b_phi = sign(dp_p_b) * Cd * abs(Ax_neg) * sqrt( (2/rho) * abs(dp_p_b) ) + GLeak * dp_p_b;

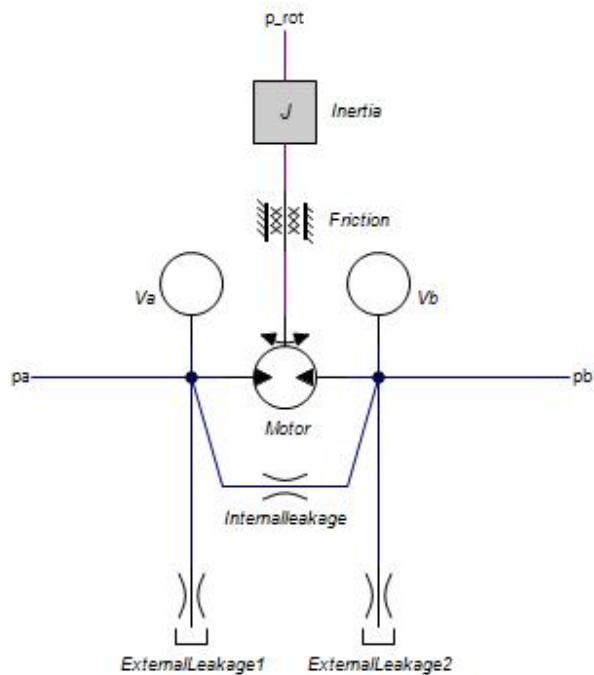
dp_a_t = pa_lim - pt_lim;
p_a_t_phi = sign(dp_a_t) * Cd * abs(Ax_neg_Ret) * sqrt( (2/rho) * abs(dp_a_t) ) + GLeak_Ret *
dp_a_t;

//Flow:
pp.phi = p_p_a_phi + p_p_b_phi;
pt.phi = p_b_t_phi + p_a_t_phi;
pa.phi = p_p_a_phi - p_a_t_phi;
pb.phi = p_b_t_phi - p_p_b_phi;

```



## Hydraulic Motor (Parker F12-60)



Motor block:

### parameters

```

real p_vapour = -99900.0 {Pa};           // vapour pressure
real global Dmot = 5.98e-5 {m3};        // displacement per revolution
real vol_eff = 0.975;

```

### variables

```

real hidden pa_s {};                    // uniform pressure from 0 (pa = p_vapour) to 1 (pa = 0)
real hidden pb_s {};                    // uniform pressure from 0 (pa = p_vapour) to 1 (pa = 0)
real hidden factor {};                  // varies from 0 (p < p_vapour) to 1 (p = 0)

```

```

real global z_heave;
real global zdot_heave;
real eff1;

```

### equations

```

eff1 = vol_eff + (1/2*tanh(1e3*p_rot.omega) + 1/2)*(1/vol_eff-vol_eff);
pa.phi = eff1* factor * Dmot / (2*pi) * p_rot.omega;
pb.phi = pa.phi;
p_rot.T = factor * Dmot / (2*pi)*(pa.p - pb.p);

```

```

// factor goes fluently from 0 to 1 from p = p_vapour to p = 0
pa_s = 1 - pa.p/p_vapour;
pb_s = 1 - pb.p/p_vapour;

```

```

factor = if (p_rot.omega > 0 and pa_s < 0) then
    0
else
    if (p_rot.omega > 0 and pa_s < 1) then
        if pa_s < 0.5 then
            2*pa_s^2
        else
            4 * pa_s - 2*pa_s^2 - 1
        end
    else
        if (p_rot.omega < 0 and pb_s < 0) then
            0
        else
            if (p_rot.omega < 0 and pb_s < 1) then
                if pb_s < 0.5 then
                    2*pb_s^2
                else
                    4 * pb_s - 2*pb_s^2 - 1
                end
            else
                1
            end
        end
    end
end
end;

```

Friction block:

**equations**

```
p.T = 0.009*p.omega+18.3*tanh(1e3*p.omega);
```

## Gearbox

### parameters

```
real global i {}; // gearbox ratio
real eff = 0.9409 {}; // gearbox efficiency (0 < eff <= 1) , 3% loss per stage (2 stages)
real J = 0.00001 {kg.m2/rad}; // rotational inertia
```

### variables

```
real p_in_T;
real global z_0 {m};
real global zdot_heave;
real u_0;
```

### equations

```
p_in.omega = (1/J)*int(p_in.T - p_in_T);
u_0 = 1/eff + (1/2*tanh(1e3*p_in.omega) + 1/2)*(eff-1/eff);
p_out.T = p_in_T*i*u_0;
p_out.omega = p_in.omega/i;
```

## Hose1

### parameters

```
real p_vapour = -0.999e5 {Pa}; //vapour pressure
real viscosity = 32e-6; //kinematic viscosity, [m^2/s] (equals 30cSt)
real density = 865; //[kg/m^3]
real length = 1.2; //[m]
real diameter = 0.01905; //[m], equals 3/4 tommes
real Re_crit = 2300; //Reynolds number
```

### variables

```
real dp {Pa}; // differential pressure
real pa_lim {Pa}; // pa.p with a minimum equal to vapour pressure
real pb_lim {Pa}; // pb.p with a minimum equal to vapour pressure
real global volume1 {m3};
real global Flow_motor;
real v_avg;
real Re;
```

### equations

```
pa_lim = if pa.p < p_vapour then p_vapour else pa.p end;
pb_lim = if pb.p < p_vapour then p_vapour else pb.p end;
dp = pa_lim - pb_lim;
pa.phi = (pi*diameter^4)/(128*viscosity*density*length)*dp;
pb.phi = pa.phi;
volume1=pi/4*diameter^2*length;
v_avg= pa.phi/(pi/4*diameter^2);
Re= (v_avg*diameter)/viscosity;
```

## Payload

### parameters

```
real global gravity {m/s2};
real global mass_wire {kg/m};
real global length_wire2 {m};
real global m_payload {kg};
```

### variables

```
real interesting z {m};
real global z_err {m};
real a {m/s2};
real global m_payload_comb {kg};
real global k_w2 {N/m};
real global z_0 {m};
real global v_0 {m/s};
real global z_payload {m};
real global zdot_payload {m/s};
real global zdotdot_payload {m/s2};
real global deviation_sim {m};
```

### initialequations

```
m_payload_comb = m_payload + mass_wire * (length_wire2 / 2);
z_0 = -gravity * m_payload_comb / k_w2;
v_0 = 0;
```

### equations

```
a = p.F / m_payload_comb;
p.v = int(a) + v_0;
z = int(p.v) + z_0;
z_payload = z;
zdot_payload = p.v;
zdotdot_payload = a;
z_err = z - z_0;
deviation_sim = 1 * sin(2 * pi * 0.1 * time) + z_err;
```

## Drum

### parameters

```
real global outer_diameter_drum {m};
real global width_drum {m};
real global thickness_drum {m};
real global diameter_end_disk {m};
real global thickness_end_disk {m};
real global density_steel_drum {kg/m3};
real global mass_wire {kg/m};
```

### variables

```
real interesting phi {rad};
real alpha {rad/s2};
real inner_radius_drum {m};
real volum_drum {m3};
real mass_drum {kg};
real volum_end_disk {m3};
real mass_end_disk {kg};
real J {kg.m2/rad};
real global outer_radius_drum {m};
real global alpha_drum {rad/s2} ;
real global omega_drum {rad/s};
real global phi_drum {rad};
```

### initialequations

```
outer_radius_drum = outer_diameter_drum / 2;
inner_radius_drum = outer_radius_drum - thickness_drum;
volum_drum = pi * width_drum * (outer_radius_drum^2 - inner_radius_drum^2);
mass_drum = volum_drum * density_steel_drum + 82.3*mass_wire; //3 layers of wire: L_tot=82.3m
volum_end_disk = pi * (diameter_end_disk/2)^2 * thickness_end_disk;
mass_end_disk = volum_end_disk * density_steel_drum;
J = (1/2)*mass_drum*(inner_radius_drum^2 + outer_radius_drum^2) +
(mass_end_disk*((diameter_end_disk/2)^2)); //Drum inertia
```

### equations

```
alpha = p.T / J;
p.omega = int (alpha);
phi = int (p.omega);
alpha_drum=alpha;
omega_drum=p.omega;
phi_drum=phi;
```

## Sheave

### parameters

```
real global mass_sheave {kg};
real global outer_radius_sheave {m};
real global inner_radius_sheave {m};
```

### variables

```
real interesting phi {rad};
real alpha {rad/s2};
real J {kg.m2/rad};
real global alpha_sheave {rad/s2};
real global omega_sheave {rad/s};
real global phi_sheave {rad};
```

### equations

```
J = (1/2)*mass_sheave*(inner_radius_sheave^2 + outer_radius_sheave^2); //Sheave inertia
alpha = p.T / J;
p.omega = int (alpha);
phi = int (p.omega);
alpha_sheave=alpha;
omega_sheave=p.omega;
phi_sheave = phi;
```

## Gear

### parameters

```
real global outer_radius_sheave {m};
```

### variables

```
real global outer_radius_drum {m};
```

### equations

```
p_out.T = p_in.T*outer_radius_sheave/outer_radius_drum;
p_out.omega = p_in.omega*outer_radius_drum/outer_radius_sheave;
```

## Wire\_Torque

### parameters

```
real global outer_radius_sheave {m};
```

### variables

```
real hidden omega {rad/s};
real global F_2 {N};
real global G_w2 {N};
real global torque_friction {N.m};
```

### equations

```
p.T = (-F_2-G_w2)*outer_radius_sheave-torque_friction;
omega = p.omega;
```

## Heave Motion

```
parameters
    real amplitude = 1{m};           // heave amplitude
    real f = 0.1 {Hz};              // heave frequency
variables
    real global z_heave {m};
    real global zdot_heave {m/s};
    real global zdotdot_heave {m/s2};
    real RampUp {};
    real RampUpDot {};
    real RampUpDotDot {};
    real tRamp {s};
initialequations
    tRamp = 1/f;
equations
    if time<tRamp then
        RampUp = 1/tRamp*(time-tRamp/(2*pi)*cos(2*pi/tRamp*time-pi/2));
        RampUpDot = 1/tRamp*(1+sin(2*pi/tRamp*time-pi/2));
        RampUpDotDot = 2*pi/tRamp^2*cos(2*pi/tRamp*time-pi/2);
    else
        RampUp = 1;
        RampUpDot = 0;
        RampUpDotDot = 0;
    end;
    output = RampUp * amplitude * sin(2*pi*f*time);
    z_heave = output;
    zdot_heave = 2*pi*f*RampUp*amplitude*cos(2*pi*f*time)+RampUpDot*amplitude*sin(2*pi*f*time);
    zdotdot_heave = -4*pi^2*f^2*RampUp*amplitude*sin(2*pi*f*time)+
    2*pi*f*RampUpDot*amplitude*cos(2*pi*f*time)+RampUpDotDot*amplitude*sin(2*pi*f*time);
```

## Wire Forces

```
parameters
    real global damping_wire {N.s/m};
variables
    real global F_1 {N};
    real global F_2 {N};
    real global k_w1 {N/m};
    real global k_w2 {N/m};
    real global elongation_1 {m};
    real global elongation_2 {m};
    real global wire_rate_1 {m/s};
    real global wire_rate_2 {m/s};
equations
    F_1 = k_w1*elongation_1+damping_wire*wire_rate_1;
    F_2 = k_w2*elongation_2+damping_wire*wire_rate_2;
```

## Wire Elongation & Wire Rate

### parameters

```
real global outer_radius_sheave {m};
```

### variables

```
real global outer_radius_drum {m}; //ie. PCD
real global phi_drum {rad};
real global omega_drum {rad/s};
real global phi_sheave {rad};
real global omega_sheave {rad/s};
real global z_heave {m};
real global zdot_heave {m/s};
real global z_payload {m};
real global zdot_payload {m/s};
real global elongation_1 {m};
real global wire_rate_1 {m/s};
real global elongation_2 {m};
real global wire_rate_2 {m/s};
```

### equations

```
elongation_1 = phi_drum*outer_radius_drum-phi_sheave*outer_radius_sheave;
wire_rate_1 = omega_drum*outer_radius_drum-omega_sheave*outer_radius_sheave;
elongation_2 = phi_sheave*outer_radius_sheave+z_heave-z_payload;
wire_rate_2 = omega_sheave*outer_radius_sheave+zdot_heave-zdot_payload;
```

## Spring Stiffness

### parameters

```
real global length_wire1 {m};
real global length_wire2 {m};
real global E_w {N/m2};
real global A_w {m2};
```

### variables

```
real global k_w1 {N/m}; // Spring stiffness wire1
real global k_w2 {N/m}; // Spring stiffness wire2
```

### initialequations

```
k_w1 = (E_w*A_w)/length_wire1; //k=(E*A)/l
k_w2 = (E_w*A_w)/length_wire2;
```



## Bearing/Pin Friction

### parameters

```
real global mass_wire {kg/m};
real global length_wire2 {m};
real global angle_wire1 {deg};
real global mass_sheave {kg};
real global u_sh {-};
real global gravity {m/s2};
real global inner_radius_sheave {m};
```

### variables

```
real global F_2 {N};
real global G_w2 {N};
real global F_f {N};
real global phi_sheave {rad};
real global torque_friction {N.m};
```

### equations

```
G_w2 = (length_wire2 * mass_wire)/2*gravity; //Wire weight upper section
```

```
\\ Bearing/Pin Friction: F_f=abs(u_sh*N)
```

```
F_f = abs(u_sh*(2*(F_2+G_w2)+(gravity*mass_sheave)));
```

```
torque_friction = F_f*inner_radius_sheave*tanh(1e3*phi_sheave);
```

## Global Relations

### parameters

```
//Wire parameters (test_setup) - 16mm wire
  real global mass_wire = 1.24 {kg/m};
  real global length_wire1 = 10 {m};
  real global length_wire2 = 10 {m};
  real global angle_wire1 = 45 {deg};
  real global damping_wire = 272000 {N.s/m};
  real global E_w = 1.36e11 {N/m2}; //Effective modulus of a steel cable
  real global A_w = 1.51e-4 {m2}; //Effective area of a steel cable
  //16mm wire

//Drum parameters (from GA-drawings)
  real global outer_diameter_drum = 0.3332 {m}; //PCD3! d_D=0.266
  real global width_drum = 0.4335 {m};
  real global thickness_drum = 0.04 {m};
  real global diameter_end_disk = 0.47244 {m};
  real global thickness_end_disk = 0.013 {m};

//Sheave parameters
  real global mass_sheave = 15 {kg};
  real global outer_radius_sheave = 0.14 {m};
  real global inner_radius_sheave = 0.0375 {m};
  real global u_sh = 0.1 {}; //Friction coeff. between bearing and pin

//Payload parameters
  real global m_payload = 500{kg};

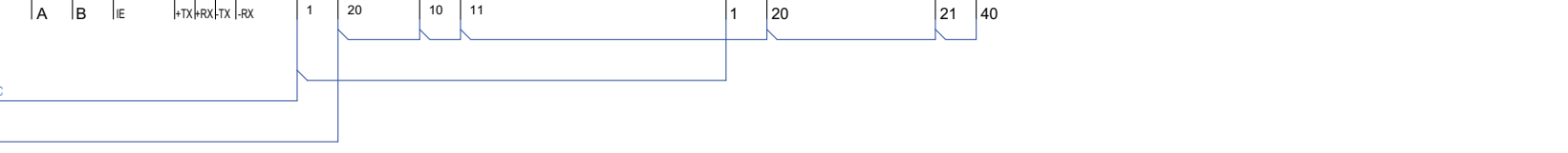
//Others
  real global gravity = 9.81 {m/s2};
  real global i = 35 {}; //Gearbox efficiency
  real global B = 800e6 {Pa}; //Effective bulk modulus
```

# Appendix B

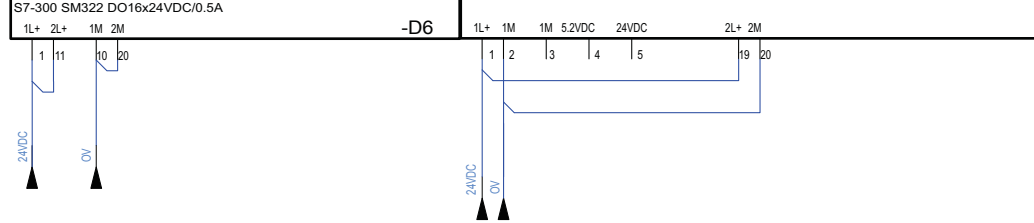
## Electrical Loop Diagrams



-D1					S7-300 CPU 317					-D4					-D5					
Pin	Addr	Ref	PLC Comment 1	Comment 2	Pin	Addr	Ref	PLC Comment 1	Comment 2	Pin	Addr	Ref	PLC Comment 1	Comment 2	Pin	Addr	Ref	PLC Comment 1	Comment 2	
2	PIW100	/502.B6	Servo valve feedback		2	PQW100	/502.A5	Servo valve / AHC ctrl valve 1		22	PQW108	/502.A8	PVG 120 / AHC ctrl valve 2		23					
3					3					24					24					
4	PIW102				4					25					25					
5					5					26					26					
6	PIW104	/502.E2	Oil Pressure	-PT2	6					27					27					
7					7					28					28					
8	PIW106	/502.E3	Oil Pressure	-PT3	8	PQW102				29					29					
9					9					30					30					
10					10					31					31					
11					11					32					32					
12	PIW108	/502.E4	Oil Pressure	-PT4	12	PQW104				33					33					
13					13					34					34					
14	PIW110	/502.E1	Oil Pressure	-PT1	14					35					35					
15					15					36					36					
16	PIW112				16					37					37					
17					17					38					38					
18	PIW114				18	PQW106				39					39					
19					19															



Pin	Addr	Ref	PLC Comment 1	Comment 2
0	Q008.0	/504.A2	Brake on/off	
3	Q008.1			
4	Q008.2			
5	Q008.3			
6	Q008.4			
7	Q008.5			
8	Q008.6			
9	Q008.7			
12	Q009.0			
13	Q009.1			
14	Q009.2			
15	Q009.3			
16	Q009.4			
17	Q009.5			
18	Q009.6			
19	Q009.7			
6	I000.0	/503.F2	Encoder signal A / A*	-ZT1
7	I000.1	/503.F2	Spare	
8	I000.2	/503.F3	Encoder signal B / B*	-ZT1
9	I000.3	/503.F4	Spare	
10	I000.4	/503.F5	Spare	
11	I000.5	/503.F6	Spare	
12	I000.6	/503.F6	Spare	
14	I000.7	/503.F7	Spare	
15	I001.0	/503.F8	Spare	
17	I001.1			
18	I001.2			



Rev.	Description	Date	Modified by	Approved
0	Issued for production	08.04.2013	SG	TG
A	Issued for Discipline Control	05.04.2013	SG	TG

Gunvaldsen & Gunvaldsen  
Master Thesis  
UiA

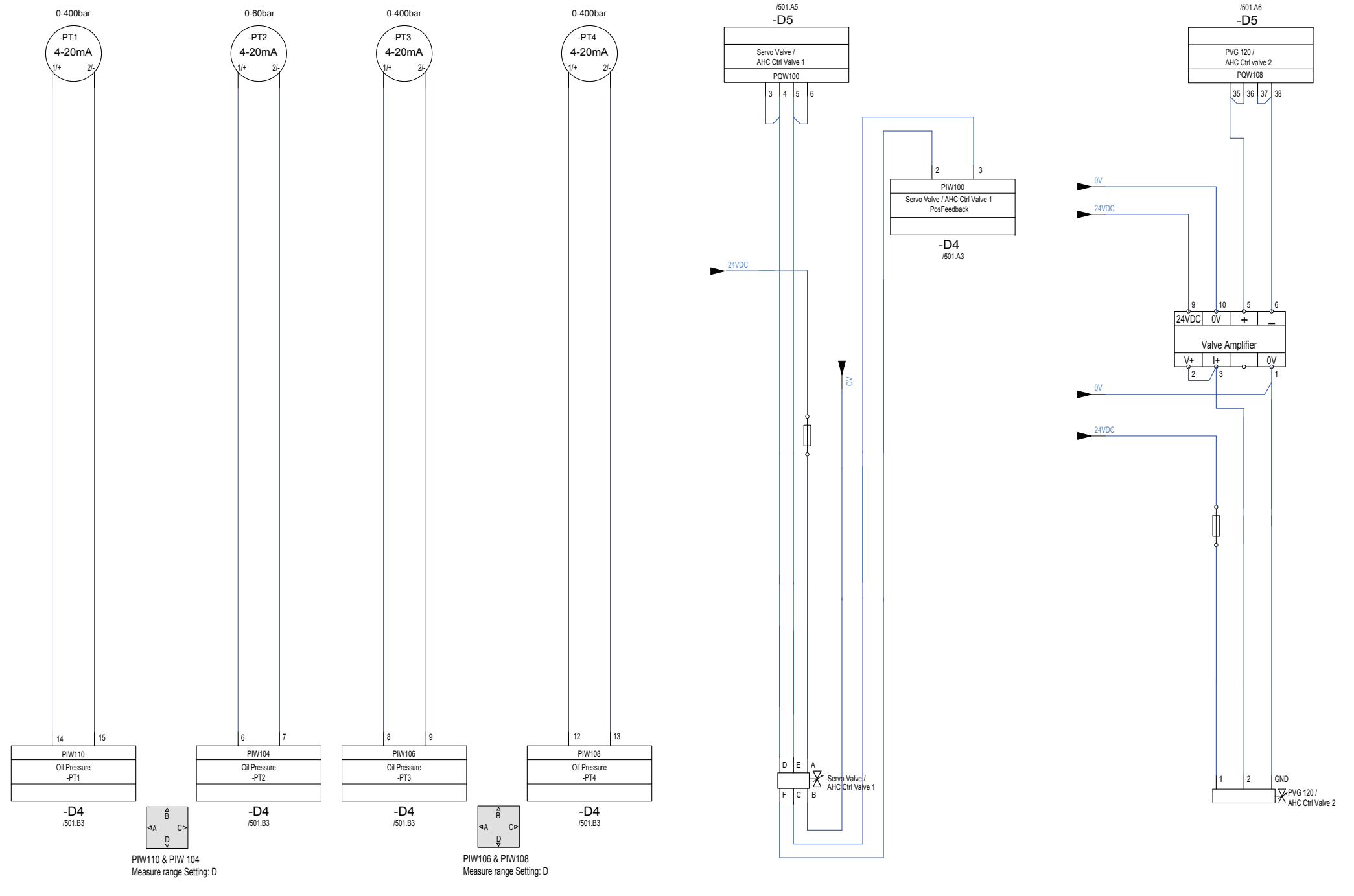
Drawn by	SG
Date	05.04.2013
Project rev.	0



Loop diagram  
PLC Configuration

Dwg. No.	Master Thesis - UiA 2013		501
HLA:	Current rev.	0	Next sheet
Loc:			502

Not to be used for design purposes. This drawing is for information only. It is not intended for use in the design of any system. It is not intended to be used as a basis for any design. It is not intended to be used as a basis for any design. © 2013 Macgregor AS



Rev.	Description	Date	Modified by	Approved
0	Issued for production	08.04.2013	SG	TG
A	Issued for Discipline Control	05.04.2013	SG	TG

**Gunvaldsen & Gunvaldsen**  
 Master Thesis  
 UiA

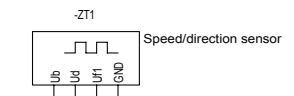
Drawn by	SG
Date	05.04.2013
Project rev.	0



Loop diagram  
 Analog In/Output signals

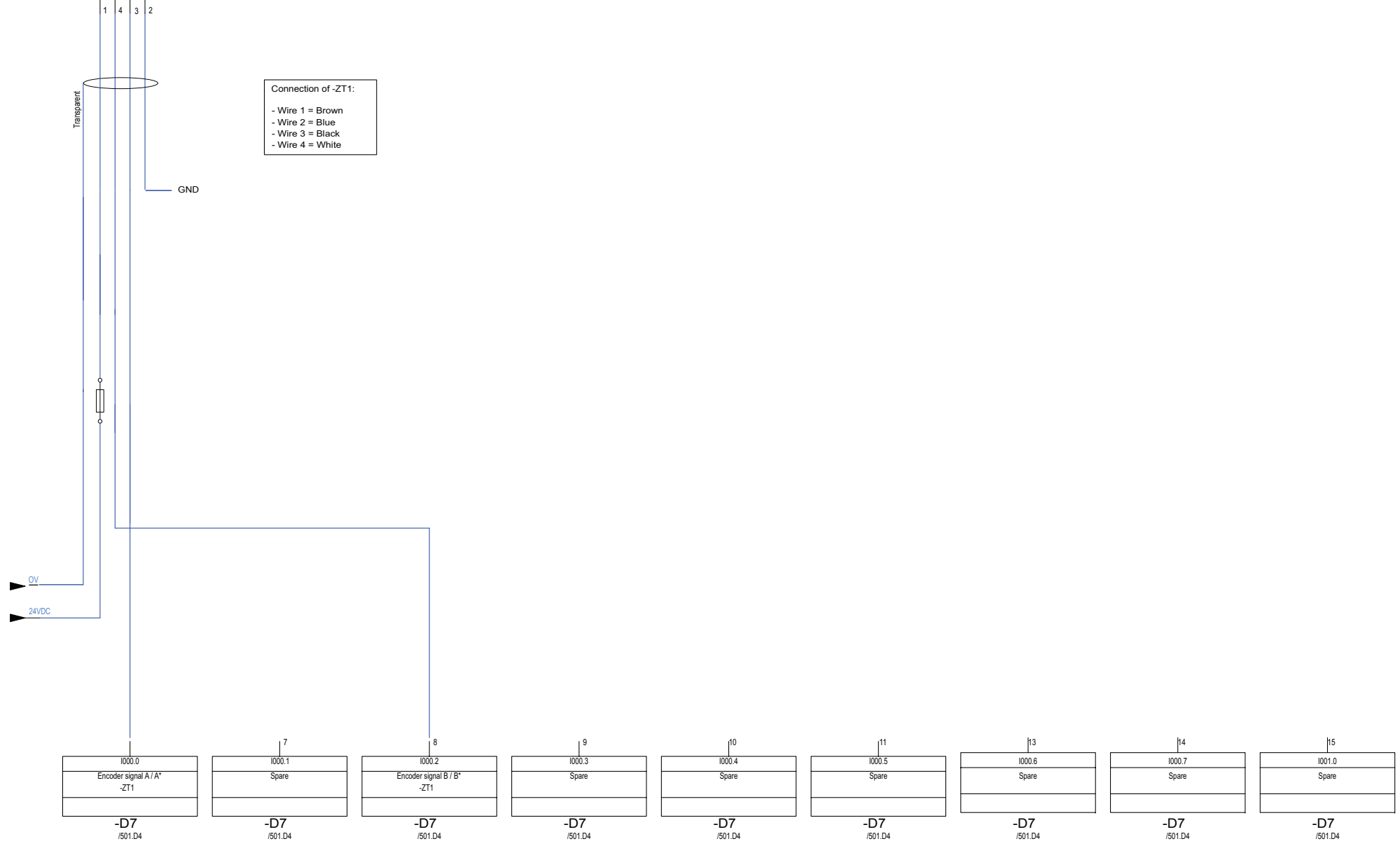
Dwg. No.	Master Thesis - UiA 2013		502
HLA:	Current rev.	0	Next sheet
Loc:			503

This document is the property of Macgregor PLC. It is not to be distributed, copied, reproduced, or otherwise used without the express authority of Macgregor PLC.  
 © Macgregor PLC 2013



Connection of -ZT1:

- Wire 1 = Brown
- Wire 2 = Blue
- Wire 3 = Black
- Wire 4 = White



Rev.	Description	Date	Modified by	Approved
0	Issued for production	08.04.2013	SG	TG
A	Issued for Discipline Control	05.04.2013	SG	TG

Gunvaldsen & Gunvaldsen  
 Master Thesis  
 UiA

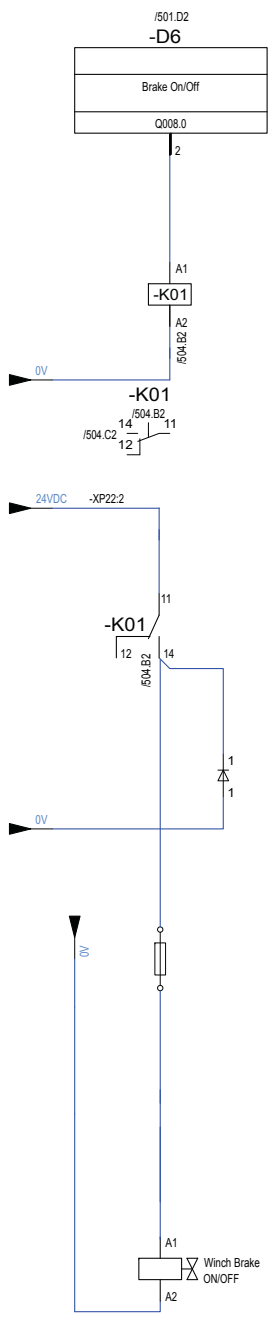
Drawn by	SG
Date	05.04.2013
Project rev.	0



Loop diagram  
 Counter module

Dwg. No.		Master Thesis - UiA 2013		503
HLA:		Current rev.		Next sheet
Loc:		0		504

This document is the property of Macgregor & Co. Ltd. It is not to be distributed outside the company without the written consent of the Director. © Macgregor & Co. Ltd.



Rev.	Description	Date	Modified by	Approved
0	Issued for production	08.04.2013	SG	TG
A	Issued for Discipline Control	05.04.2013	SG	TG

Gunvaldsen & Gunvaldsen  
 Master Thesis  
 UiA

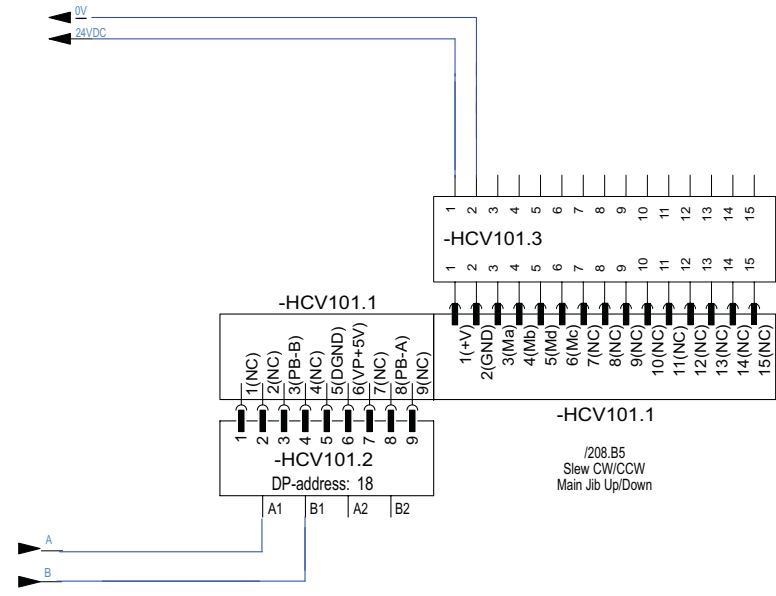
Drawn by	SG
Date	05.04.2013
Project rev.	0



Loop diagram  
 Digital output signals

Dwg. No.	Master Thesis - UiA 2013		504
HLA:	Current rev.	Next sheet	
Loc:	0	505	

This document is the property of Macgregor AS.  
 It is intended for use only by the person to whom it is issued.  
 No part of this document may be reproduced, stored in a retrieval system,  
 or transmitted in any form or by any means, electronic, mechanical,  
 photocopying, recording, or by any information storage and retrieval system,  
 without the prior written permission of Macgregor AS.  
 © Macgregor AS



Rev.	Description	Date	Modified by	Approved
0	Issued for production	08.04.2013	SG	TG
A	Issued for Discipline Control	05.04.2013	SG	TG

Gunvaldsen & Gunvaldsen  
 Master Thesis  
 UiA

Drawn by	SG
Date	05.04.2013
Project rev.	0



Loop diagramDigital  
 Profibus Joystick

Dwg. No.	Master Thesis - UiA 2013		505
HLA:	Current rev.	0	
Loc:	Next sheet		



# Appendix C

## PLC Program

**FC1 - <offline>**

"CyclicApplication"

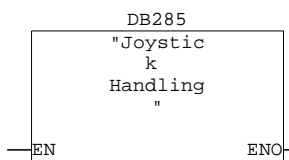
**Name:**  
**Author:**  
**Time stamp Code:**  
**Interface:**  
**Lengths (block/logic/data):**

**Family:**  
**Version:** 0.1  
**Block version:** 2  
 05/09/2013 11:25:50 AM  
 03/19/2013 01:37:53 PM  
 01232 01106 00010

Name	Data Type	Address	Comment
IN		0.0	
OUT		0.0	
IN_OUT		0.0	
TEMP		0.0	
Temp1	Real	0.0	
RETURN		0.0	
RET_VAL		0.0	

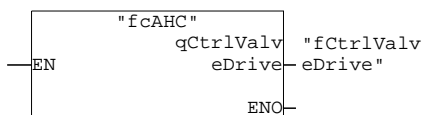
**Block: FC1**

Network: 1 Joystick handling

**Symbol information**

FB285 Joystick Handling

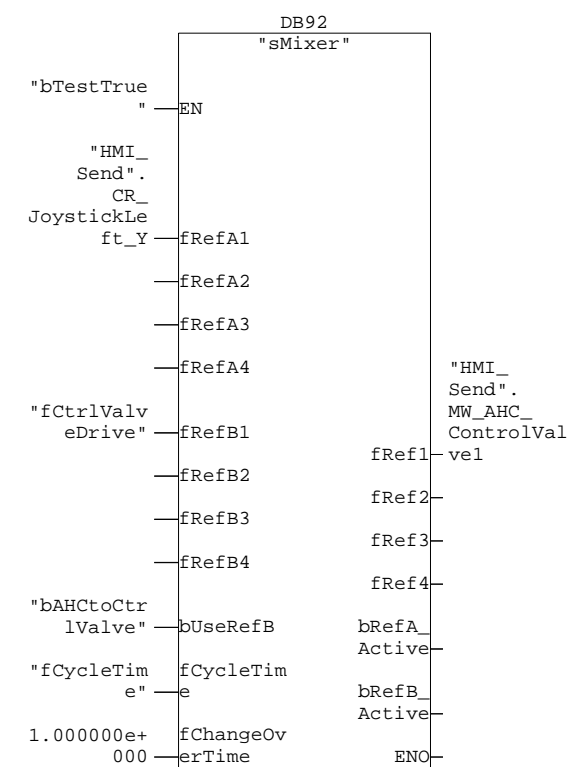
Network: 2 AHC controller

**Symbol information**

FC95 fcAHC  
 MD544 fCtrlValveDrive AHC control valve

Network: 3 Send command signal to servo valve

fRefA1 = Joystick signal  
 fRefB1 = AHC signal  
 bUseRefB = 0 ved joystick operasjon og 1 ved AHC operasjon av vinsjen

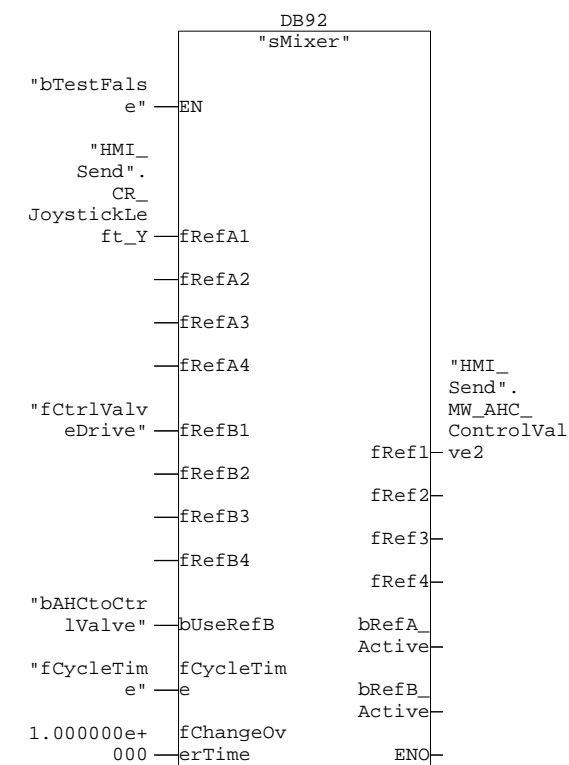


#### Symbol information

FB92	sMixer	
M10.1	bTestTrue	Always 1 for test purposes
DB121.DBD374	"HMI_Send".CR_JoystickLeft_Y	Joystick Left - Y Axis
MD544	fCtrlValveDrive	AHC control valve
M100.5	bAHCtoCtrlValve	Select AHC output to control valve
MD26	fCycleTime	OB1 cycle time (Sec)
DB121.DBD642	"HMI_Send".MW_AHC_ControlValve1	Main Winch AHC Control Valve 1

Network: 4 Send command signal to PVG120

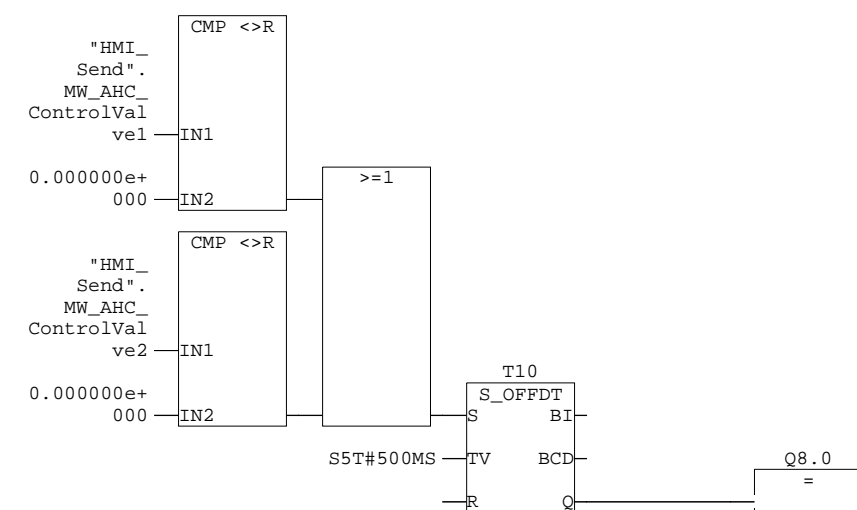
fRefA1 = Joystick signal  
 fRefB1 = AHC signal  
 bUseRefB = 0 ved joystick operasjon og 1 ved AHC operasjon av vinsjen



#### Symbol information

FB92	sMixer	
M10.0	bTestFalse	Always 0 for test purposes
DB121.DBD374	"HMI_Send".CR_JoystickLeft_Y	Joystick Left - Y Axis
MD544	fCtrlValveDrive	AHC control valve
M100.5	bAHCtoCtrlValve	Select AHC output to control valve
MD26	fCycleTime	OB1 cycle time (Sec)
DB121.DBD646	"HMI_Send".MW_AHC_ControlValve2	Main Winch AHC Control Valve 2

Network: 5 Enable Brake

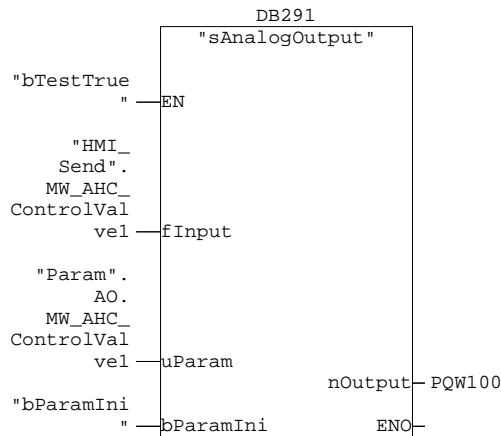


**Symbol information**

DB121.DBD642 "HMI\_Send".MW\_AHC\_ControlValve1 Main Winch AHC Control Valve 1  
 DB121.DBD646 "HMI\_Send".MW\_AHC\_ControlValve2 Main Winch AHC Control Valve 2

Network: 6 Valve control (servo valve)

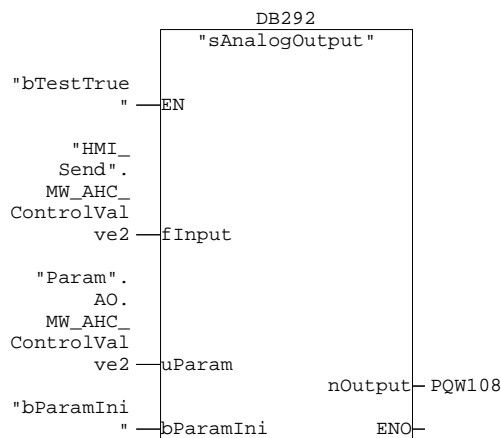
Dødbånd er satt slik at startverdi i positiv retning er 0 (til 27648) og i negativ retning 0 (til -27648). Verdiene finnes i DB98 fra DW1596.  
 Les av pådragsverdi (PQW100) som skal til før vinsjen begynner å bevege seg og legg inn disse verdiene som startverdier opp/ned i DB98.DBW1612 og DBW1614.  
 Ved endring må "bParamIni" aktiveres for at nye verdier skal overtas.  
 PQW100 er den første utgangen på analogmodulen i hardwarekonfigurasjonen.

**Symbol information**

FB51 sAnalogOutput  
 M10.1 bTestTrue Always 1 for test purposes  
 DB121.DBD642 "HMI\_Send".MW\_AHC\_ControlValve1 Main Winch AHC Control Valve 1  
 P#DB98.DBX1596.0 "Param".AO.MW\_AHC\_ControlValve1 Main Winch AHC Control Valve 1  
 M15.2 bParamIni Initialize Parameters

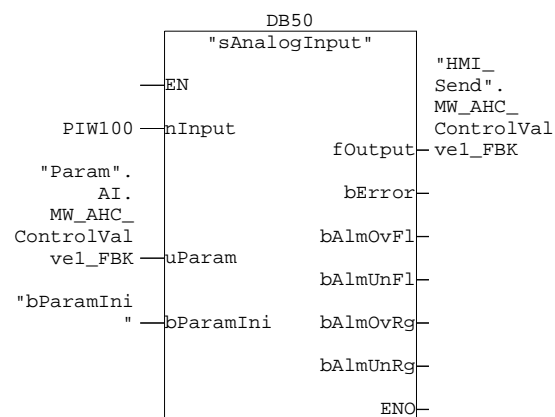
Network: 7 Valve control (PVGI20)

Dødbånd er satt slik at startverdi i positiv retning er 0 (til 27648) og i negativ retning 0 (til -27648). Verdiene finnes i DB98 fra DW1618.  
 Les av pådragsverdi (PQW108) som skal til før vinsjen begynner å bevege seg og legg inn disse verdiene som startverdier opp/ned i DB98.  
 Ved endring må "bParamIni" aktiveres for at nye verdier skal overtas.

**Symbol information**

FB51 sAnalogOutput  
 M10.1 bTestTrue Always 1 for test purposes  
 DB121.DBD646 "HMI\_Send".MW\_AHC\_ControlValve2 Main Winch AHC Control Valve 2  
 P#DB98.DBX1618.0 "Param".AO.MW\_AHC\_ControlValve2 Main Winch AHC Control Valve 2  
 M15.2 bParamIni Initialize Parameters

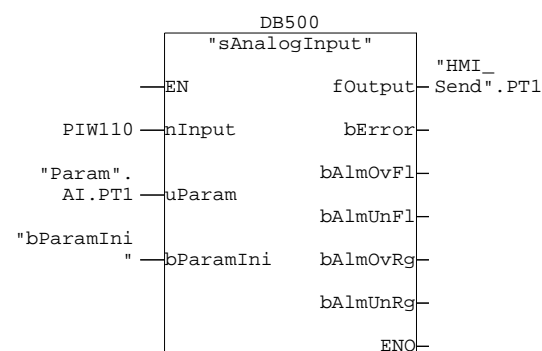
Network: 8 Read Control valve feedback



#### Symbol information

FB50 sAnalogInput  
 P#DB98.DBX946.0 "Param".AI.MW\_AHC\_ControlVal.vel\_FBK Main Winch AHC control valve 1 - Feedback  
 M15.2 bParamIni Initialize Parameters  
 DB121.DBD416 "HMI\_Send".MW\_AHC\_ControlVal.vel\_FBK Main Winch AHC Control Valve 1 feedback

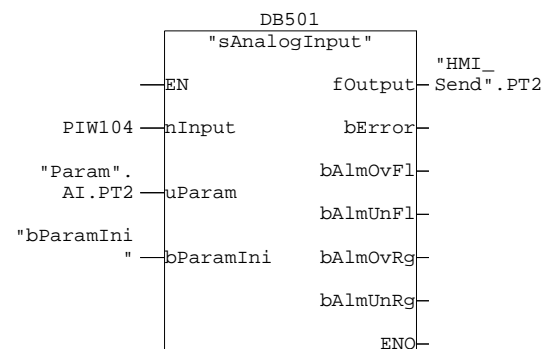
Network: 9 Read PT1



#### Symbol information

FB50 sAnalogInput  
 P#DB98.DBX1186.0 "Param".AI.PT1 Pressure Transmitter 1, Accumulator  
 M15.2 bParamIni Initialize Parameters  
 DB121.DBD502 "HMI\_Send".PT1 Pressure Transmitter 1

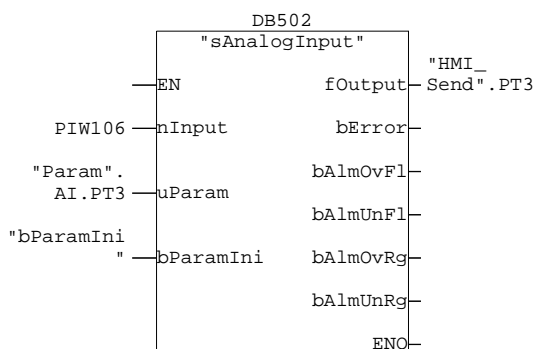
Network: 10 Read PT2



**Symbol information**

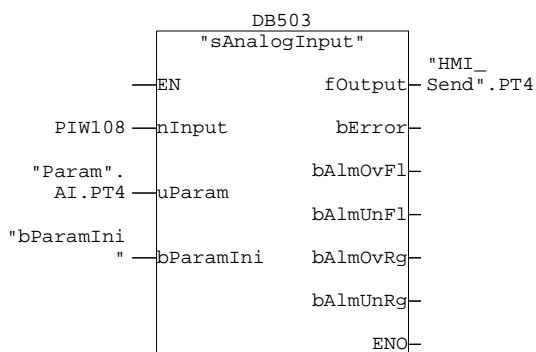
FB50	sAnalogInput	
P#DB98.DBX1216.0	"Param".AI.PT2	Pressure Transmitter 2, Tank
M15.2	bParamIni	Initialize Parameters
DB121.DBD506	"HMI_Send".PT2	Pressure Transmitter 2

Network: 11	Read PT3
-------------	----------

**Symbol information**

FB50	sAnalogInput	
P#DB98.DBX1276.0	"Param".AI.PT3	Pressure Transmitter 3, B-side Motor
M15.2	bParamIni	Initialize Parameters
DB121.DBD542	"HMI_Send".PT3	Pressure Transmitter 3

Network: 12	Read PT4
-------------	----------

**Symbol information**

FB50	sAnalogInput	
P#DB98.DBX736.0	"Param".AI.PT4	Pressure Transmitter 4, A-side Motor
M15.2	bParamIni	Initialize Parameters
DB121.DBD522	"HMI_Send".PT4	Pressure Transmitter 4

**FC95 - <offline>**

"fcAHC"

**Name:**  
**Author:**  
**Time stamp Code:**  
**Interface:**  
**Lengths (block/logic/data):**

**Family:**  
**Version:** 0.1  
**Block version:** 2

04/15/2013 01:10:36 PM

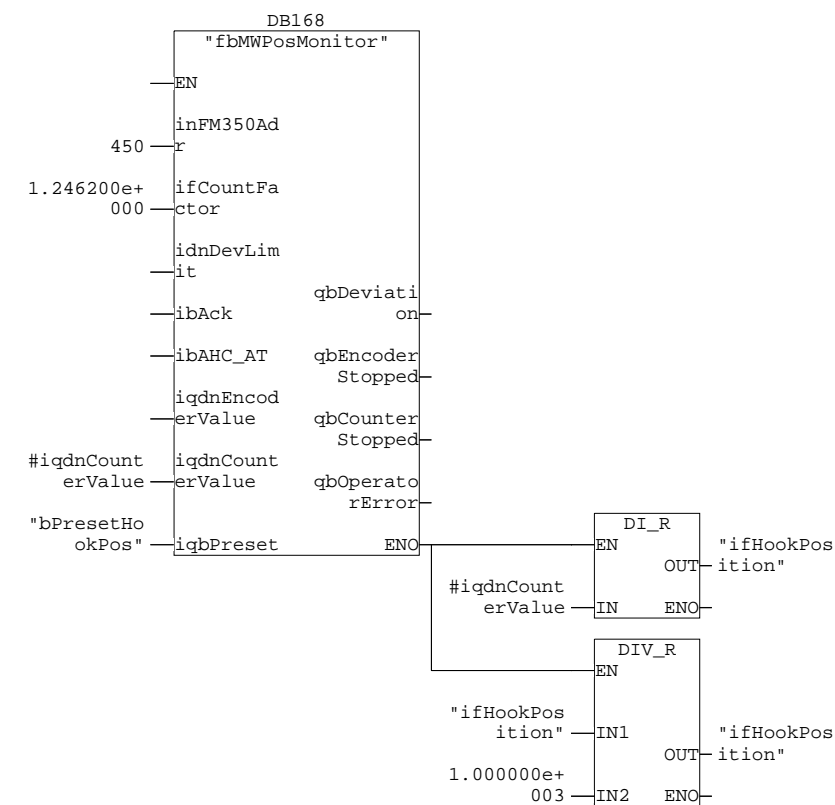
03/26/2013 10:46:47 AM

01106 00980 00042

Name	Data Type	Address	Comment
IN		0.0	
OUT		0.0	
qCtrlValveDrive	Real	0.0	AHC/AT Output to controlvalve
IN_OUT		0.0	
TEMP		0.0	
fAHCDrive	Real	0.0	AHC/AT regulator output drive signal
fCtrlValveDrive	Real	4.0	AHC/AT control valve drive signal
iqdnCounterValue	DInt	8.0	Countervalue
RETURN		0.0	
RET_VAL		0.0	

**Block: FC95 AHC Simulation**

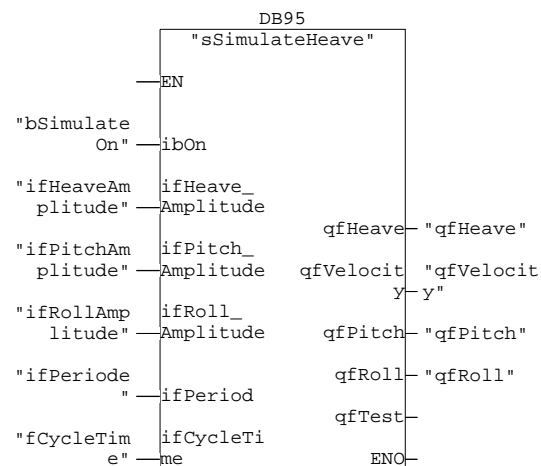
**Network: 1 Winch position**

**Symbol information**

FB169	fbMWPosMonitor	Main Winch Position Monitoring
#iqdnCounterValue	#iqdnCounterValue	Countervalue
M100.4	bPresetHookPos	Preset Hook pos in FM350-1
MD576	ifHookPosition	Scaled Hook position from FM350-1 counter module



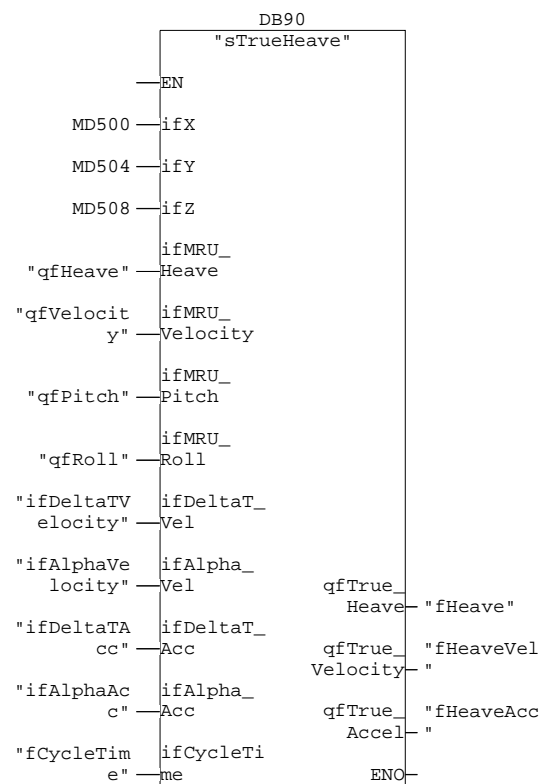
Network: 2 Heave simulation



### Symbol information

FB95	sSimulateHeave	
M100.3	bSimulateOn	AHC simulator On
MD560	ifHeaveAmplitude	Simulator input Heave amplitude
MD564	ifPitchAmplitude	Simulator input Pitch amplitude
MD568	ifRollAmplitude	Simulator input Roll amplitude
MD572	ifPeriode	Simulator input Periode
MD26	fCycleTime	Obl cycle time (Sec)
MD512	qfHeave	Simulator output Heave
MD516	qfVelocity	Simulator output Velocity
MD520	qfPitch	Simulator output Pitch
MD524	qfRoll	Simulator output Roll

Network: 3 Heave calculations

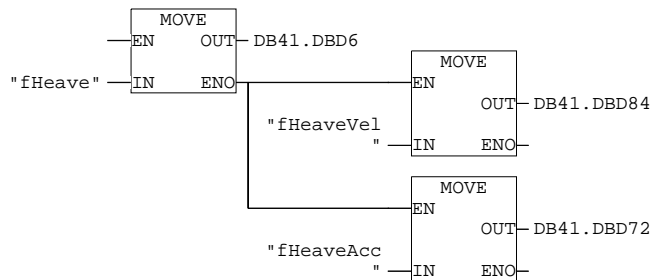


**Symbol information**

FB90	sTrueHeave	
MD512	qfHeave	Simulator output Heave
MD516	qfVelocity	Simulator output Velocity
MD520	qfPitch	Simulator output Pitch
MD524	qfRoll	Simulator output Roll
MD528	ifDeltaTVelocity	Heave calculation input Delta T velocity
MD532	ifAlphaVelocity	Heave calculation input Alpha (filter factor) velocity
MD536	ifDeltaTAcc	Heave calculation input Delta T acceleration
MD540	ifAlphaAcc	Heave calculation input Alpha (filter factor) acceleration
MD26	fCycleTime	OB1 cycle time (Sec)
MD548	fHeave	Heave
MD552	fHeaveVel	Heave velocity
MD556	fHeaveAcc	Heave acceleration

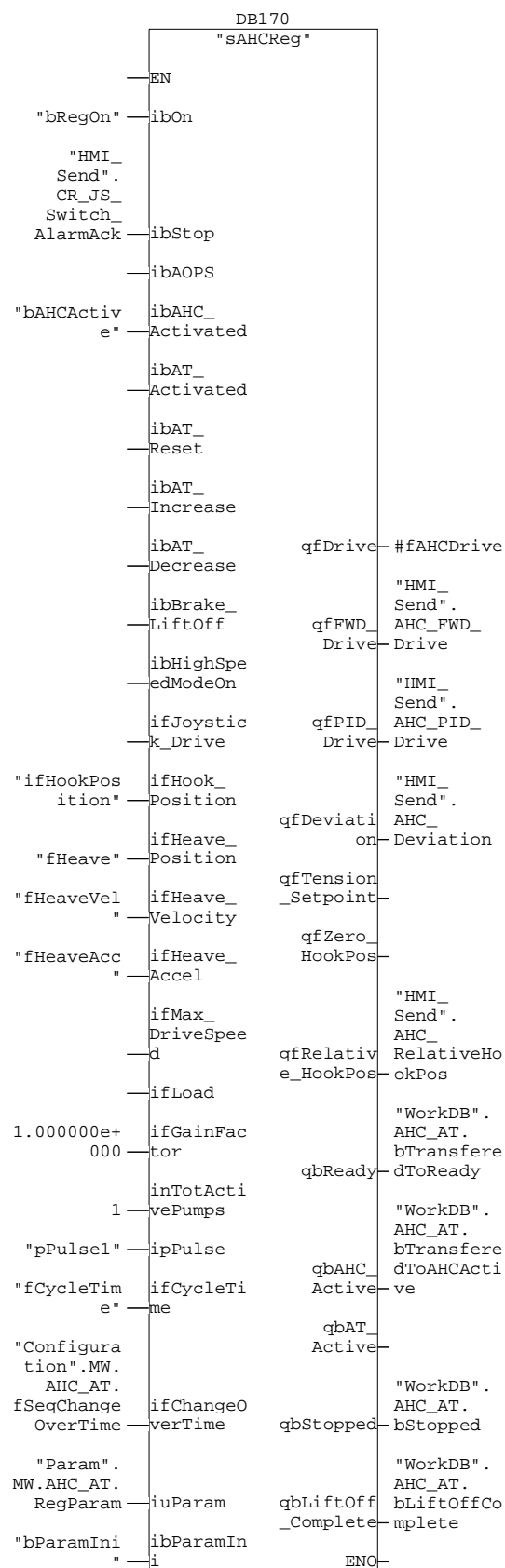
Network: 4      Presentasjon av trend i PID Control

DB41.DBD6 = Setpoint value  
 DB41.DBD84 = Integral action  
 DB41.DBD72 = Manipulated variable

**Symbol information**

MD548	fHeave	Heave
MD552	fHeaveVel	Heave velocity
MD556	fHeaveAcc	Heave acceleration

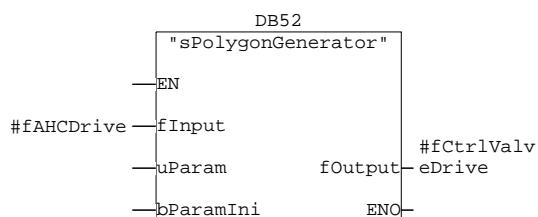
Network: 5	AHC/AT controller
------------	-------------------



**Symbol information**

FB170	sAHCReg	Regulator enable
M100.0	bRegOn	Joystick switch Alarm acknowledge
DB121.DBX362.1	"HMI_Send".CR_JS_Switch_AlarmAck	AHC activate
M100.2	bAHCActive	Scaled Hook position from FM350-1 counter module
MD576	ifHookPosition	Heave
MD548	fHeave	Heave velocity
MD552	fHeaveVel	Heave acceleration
MD556	fHeaveAcc	Pulse every 0,1s ('1' in one PLC cycle)
M12.0	pPulse1	OB1 cycle time (Sec)
MD26	fCycleTime	AHC/AT sequence mode to mode transfer time
DB97.DBD140	"Configuration".MW.AHC_AT.fSeqChangeOverTime	Initialize Parameters
P#DB98.DBX2880.0	"Param".MW.AHC_AT.RegParam	AHC/AT regulator output drive signal
M15.2	bParamIni	MW AHC regulator feed forward contribution
#fAHCDrive	#fAHCDrive	MW AHC regulator PID contribution
DB121.DBD172	"HMI_Send".AHC_FWD_Drive	Active Heave Deviation
DB121.DBD176	"HMI_Send".AHC_PID_Drive	Hook pos. relative to zero position
DB121.DBD106	"HMI_Send".AHC_Deviation	AHC Controller is transferred to standby mode (ready)
DB121.DBD118	"HMI_Send".AHC_RelativeHookPos	AHC Controller is using heave as reference (active)
DB9.DBX34.1	"WorkDB".AHC_AT.bTransferredToReady	AHC/AT controller has ramped output to zero
DB9.DBX34.2	"WorkDB".AHC_AT.bTransferredToAHCActive	AHC/AT liftoff for brake release complete
DB9.DBX46.0	"WorkDB".AHC_AT.bStopped	
DB9.DBX46.2	"WorkDB".AHC_AT.bLiftOffComplete	

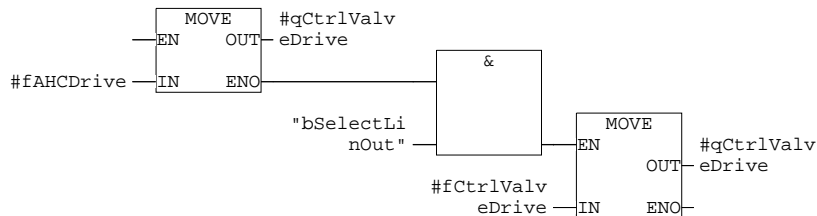
Network: 6 AHC/AT Valve Linearization

**Symbol information**

FB52	sPolygonGenerator	
#fAHCDrive	#fAHCDrive	AHC/AT regulator output drive signal
#fCtrlValveDrive	#fCtrlValveDrive	AHC/AT control valve drive signal

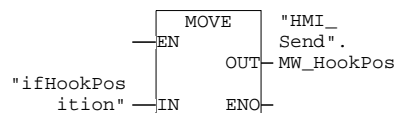
Network: 7 Output to control valve

Default = direkte output til ventil  
 Ved M100.6 = 1, er det linearisert verdi fra FB52 som blir sendt til ventil

**Symbol information**

#fAHCDrive	#fAHCDrive	AHC/AT regulator output drive signal
#qCtrlValveDrive	#qCtrlValveDrive	AHC/AT Output to controlvalve
M100.6	bSelectLinOut	Select between direct =0 or linearized =1 control valve output
#fCtrlValveDrive	#fCtrlValveDrive	AHC/AT control valve drive signal

Network: 8

**Symbol information**

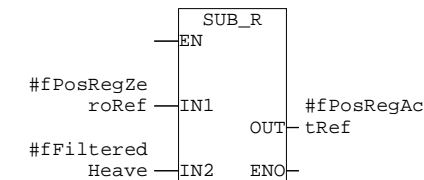
MD576	ifHookPosition	Scaled Hook position from FM350-1 counter module
DB121.DBD10	"HMI_Send".MW_HookPos	Main Winch Hook Position

**Symbol information**

#ipPulse	#ipPulse	Pulse every 0,1s (high in one scan)
#ifJoystick_Drive	#ifJoystick_Drive	Joystick drive signal
#ifMax_DriveSpeed	#ifMax_DriveSpeed	Maximum speed from joystick drive
#fTemp	#fTemp	Temporary REAL
#fPosRegZeroRef	#fPosRegZeroRef	Position regulator zero reference

Network: 14 Position Reference in AHC Active Mode

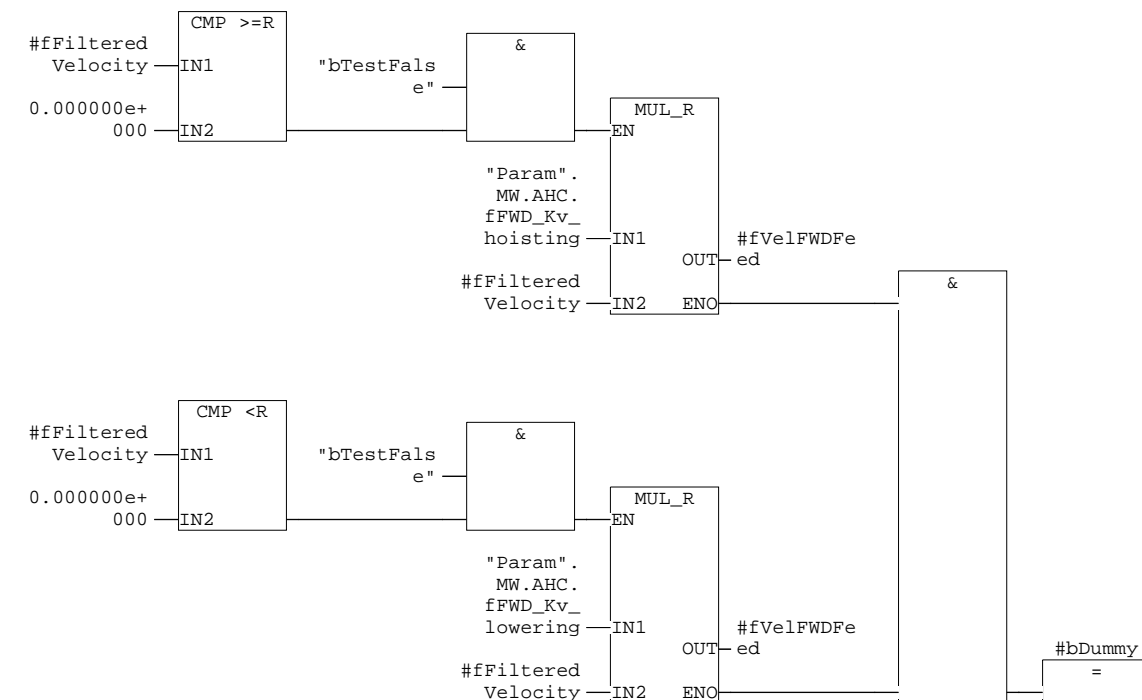
Add heave signal to the zero position reference for active mode.

**Symbol information**

#fPosRegZeroRef	#fPosRegZeroRef	Position regulator zero reference
#fFilteredHeave	#fFilteredHeave	Filtered heave position
#fPosRegActRef	#fPosRegActRef	Position regulator reference in AHC active mode

Network: 15 Velocity Feed Forward S&T

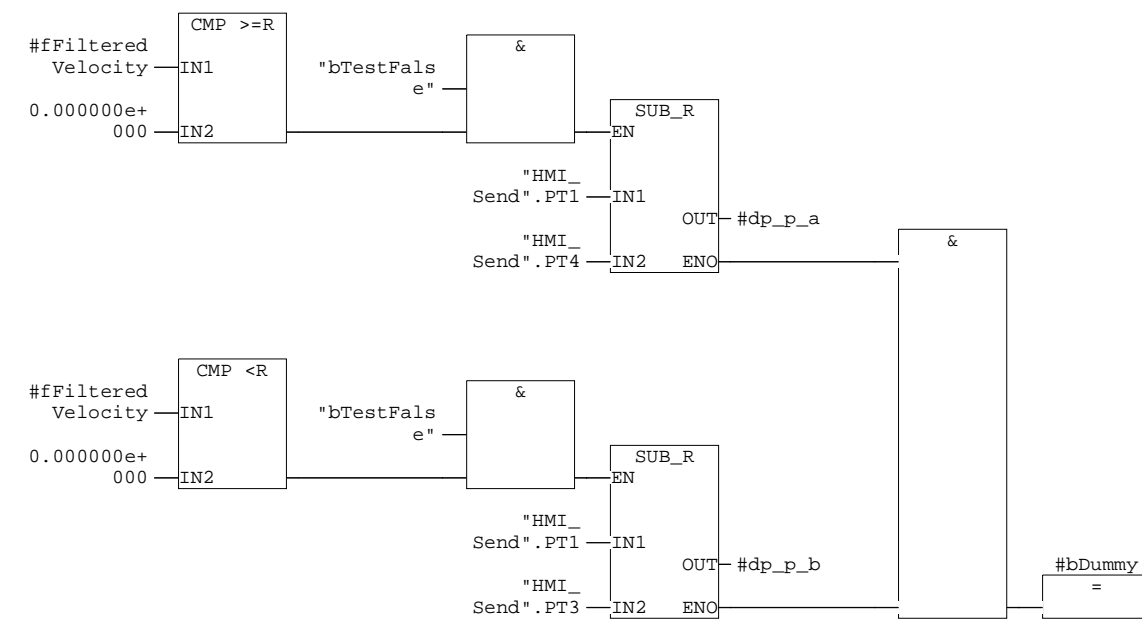
Two Feed-Forward Gains. Heave velocity <0 then lowering, else hoisting.

**Symbol information**

#fFilteredVelocity	#fFilteredVelocity	Filtered heave velocity
M10.0	bTestFalse	Always 0 for test purposes
DB98.DBD3128	"Param".MW.AHC.fFWD_Kv_hoisting	Main Winch Displacement Valve 1 Regulator Gain
#fVelFWDFeed	#fVelFWDFeed	Velocity FWD feed
DB98.DBD3296	"Param".MW.AHC.fFWD_Kv_lowering	Main Winch Displacement Valve 2 Regulator Gain
#bDummy	#bDummy	Dummy bit

Network: 16 Model Based Feed Forward Part 1 S&T

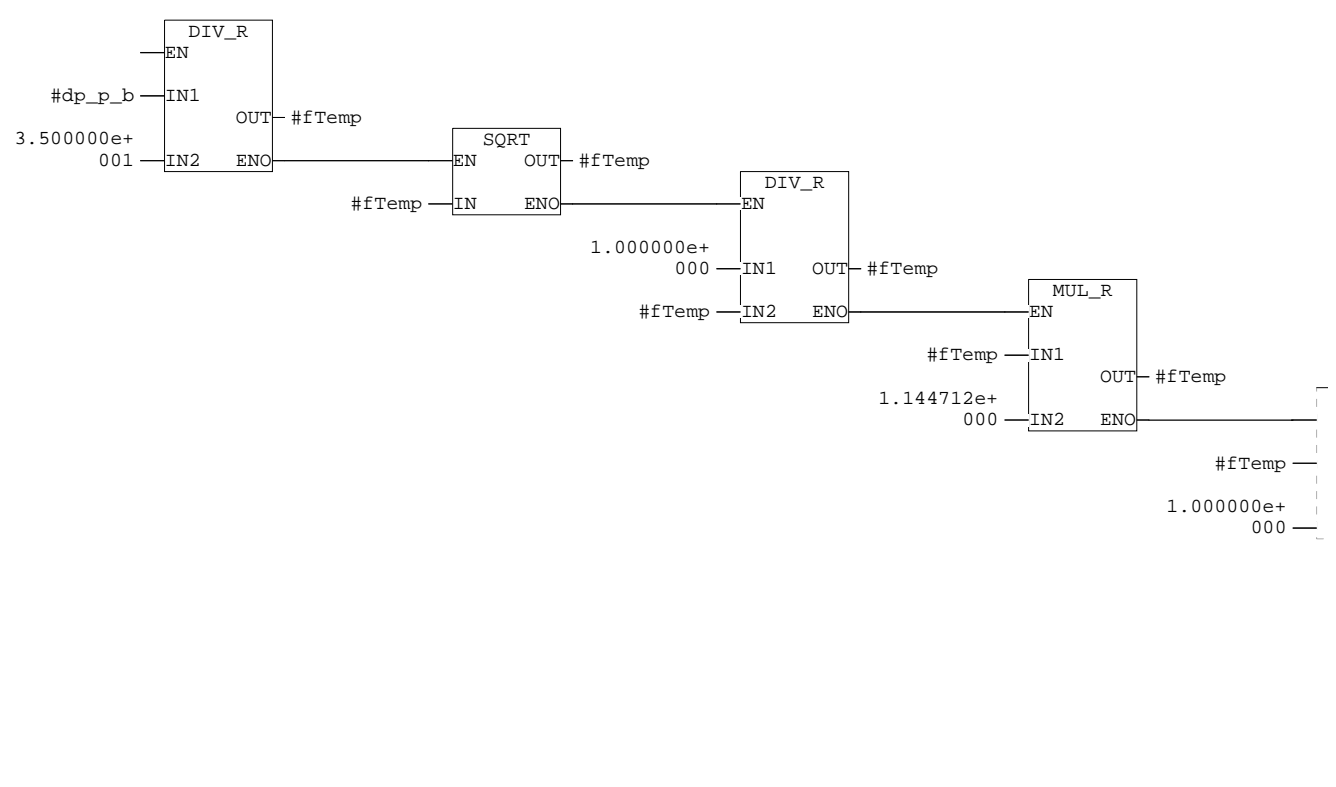
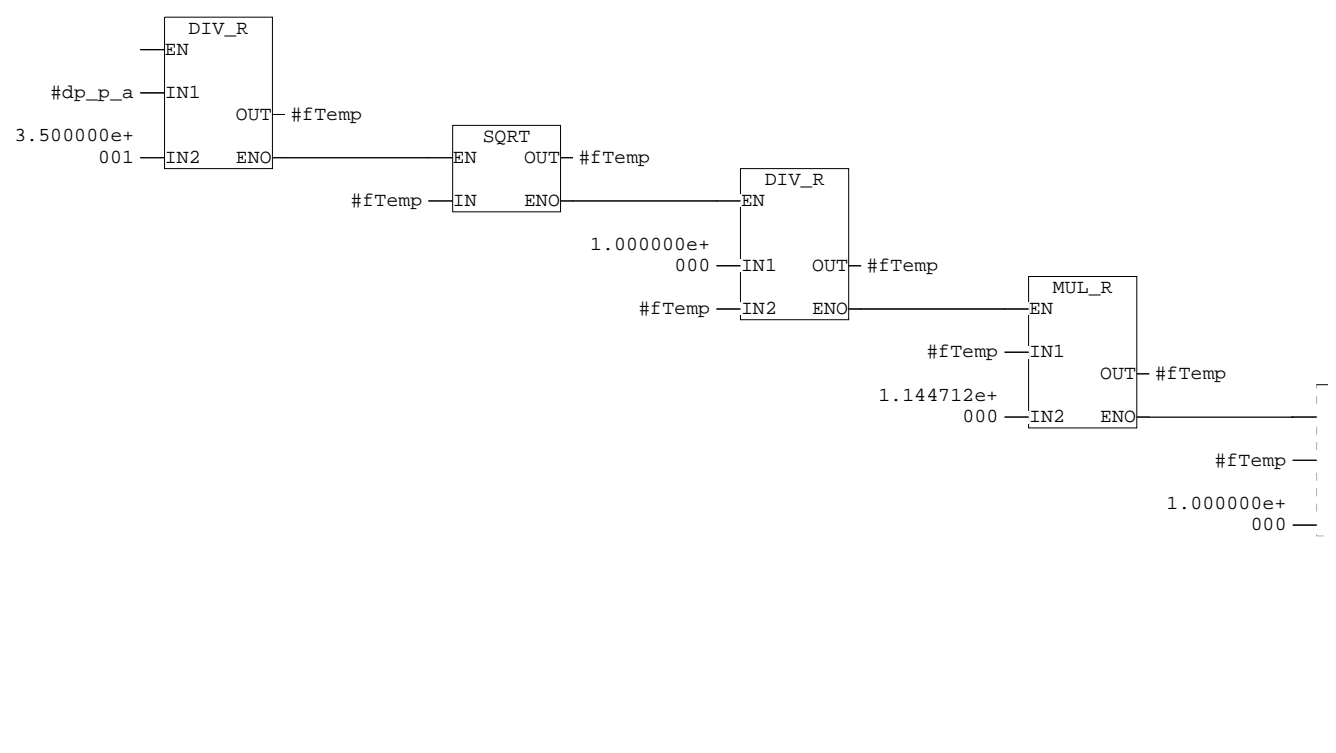
Compute pressure drop over servo to use in model based feed forward



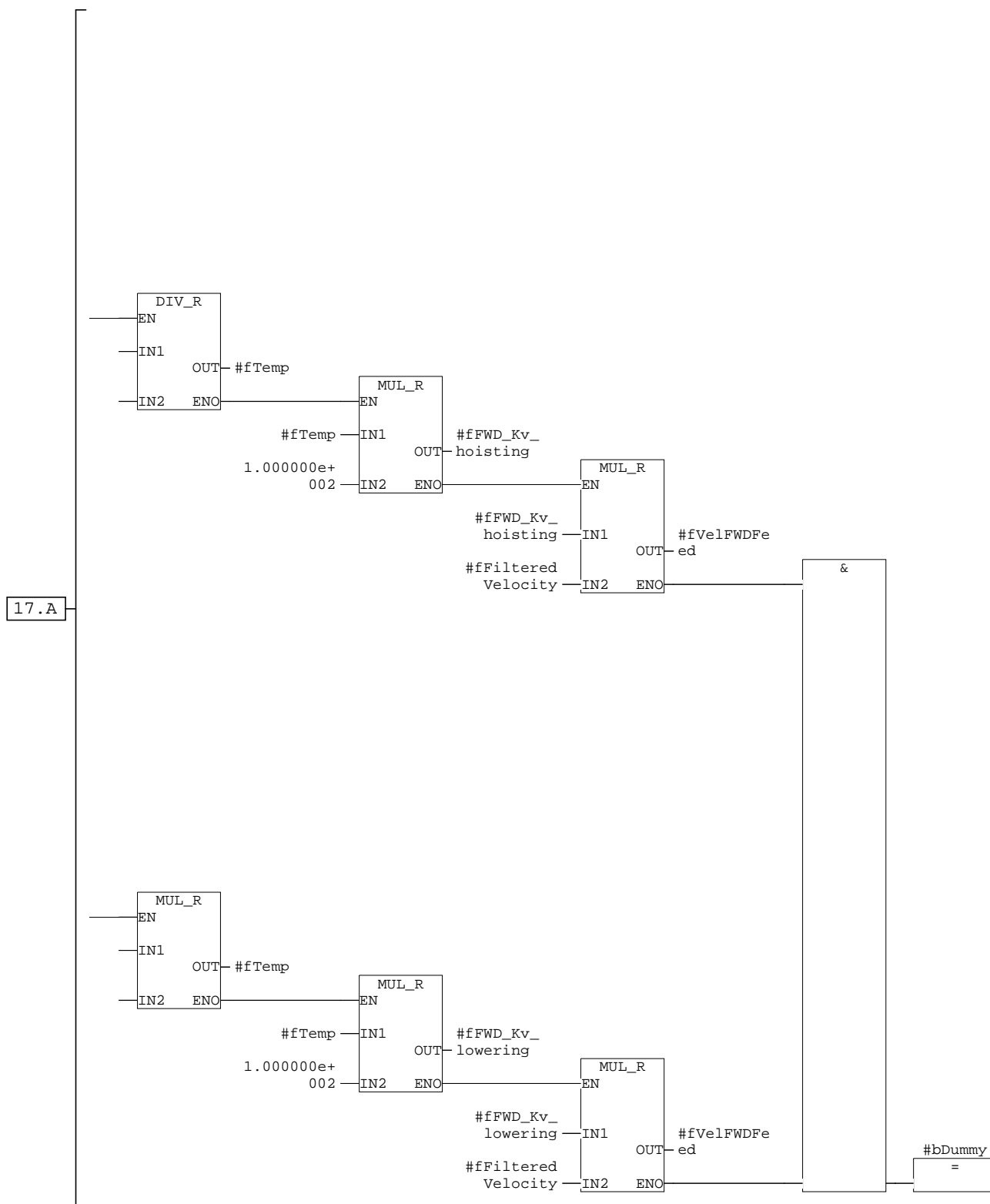
#### Symbol information

Symbol	Symbol	Description
#FilteredVelocity	#FilteredVelocity	Filtered heave velocity
M10.0	bTestFalse	Always 0 for test purposes
DB121.DBD502	"HMI_Send".PT1	Pressure Transmitter 1
DB121.DBD522	"HMI_Send".PT4	Pressure Transmitter 4
#dp_p_a	#dp_p_a	Pressure drop p to a
DB121.DBD542	"HMI_Send".PT3	Pressure Transmitter 3
#dp_p_b	#dp_p_b	Pressure drop p to b
#bDummy	#bDummy	Dummy bit

Network: 17 Model Based Feed Forward Part 2 S&T  
Compute velocity feed forward.



17.A

**Symbol information**

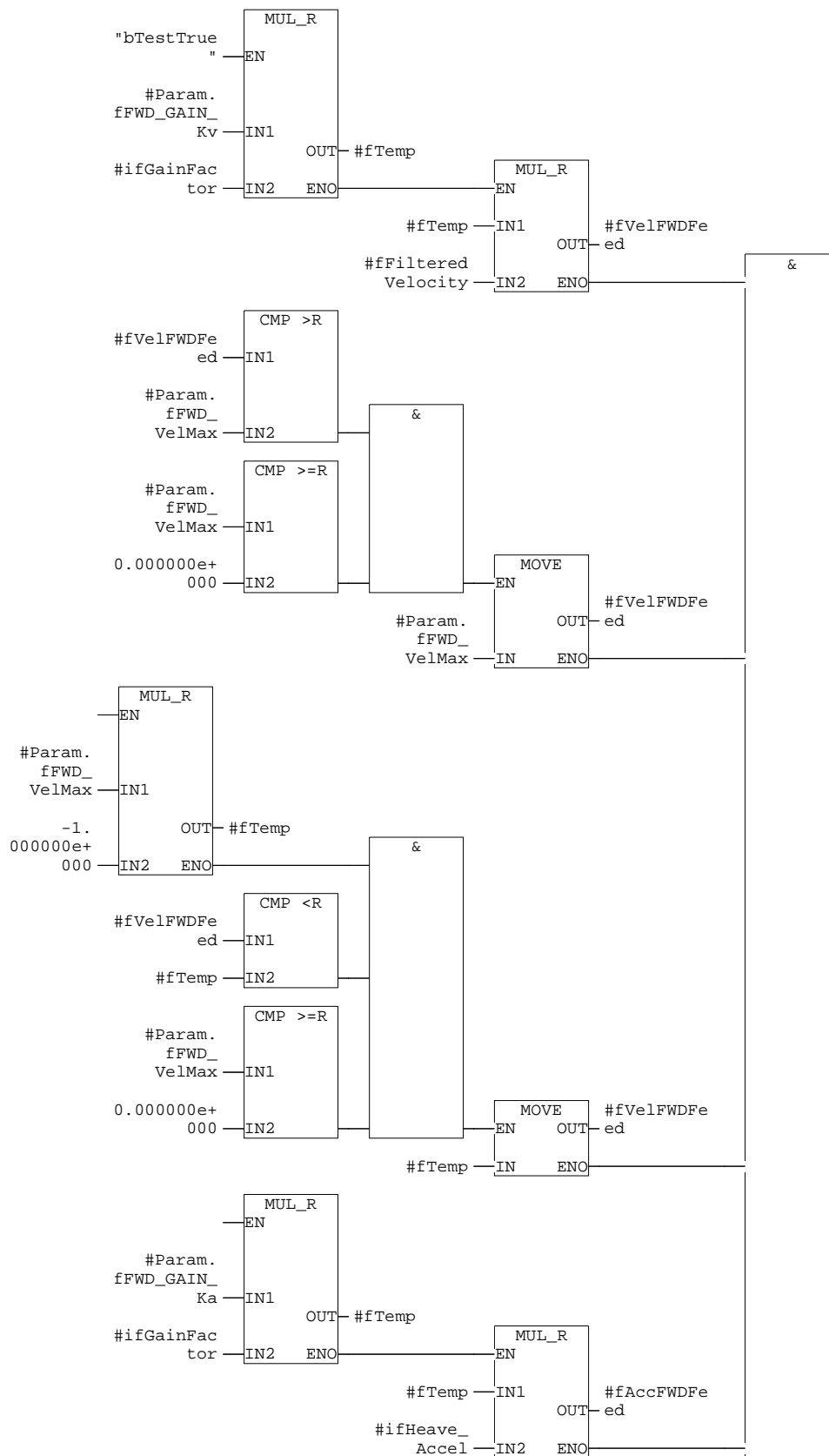
#dp_p_a	#dp_p_a	Pressure drop p to a
#fTemp	#fTemp	Temporary REAL
#fFWD_Kv_hoisting	#fFWD_Kv_hoisting	Model based feed forward
#fFilteredVelocity	#fFilteredVelocity	Filtered heave velocity
#fVelFWDFeed	#fVelFWDFeed	Velocity FWD feed
#dp_p_b	#dp_p_b	Pressure drop p to b
#fFWD_Kv_lowering	#fFWD_Kv_lowering	Model based feed forward
#bDummy	#bDummy	Dummy bit

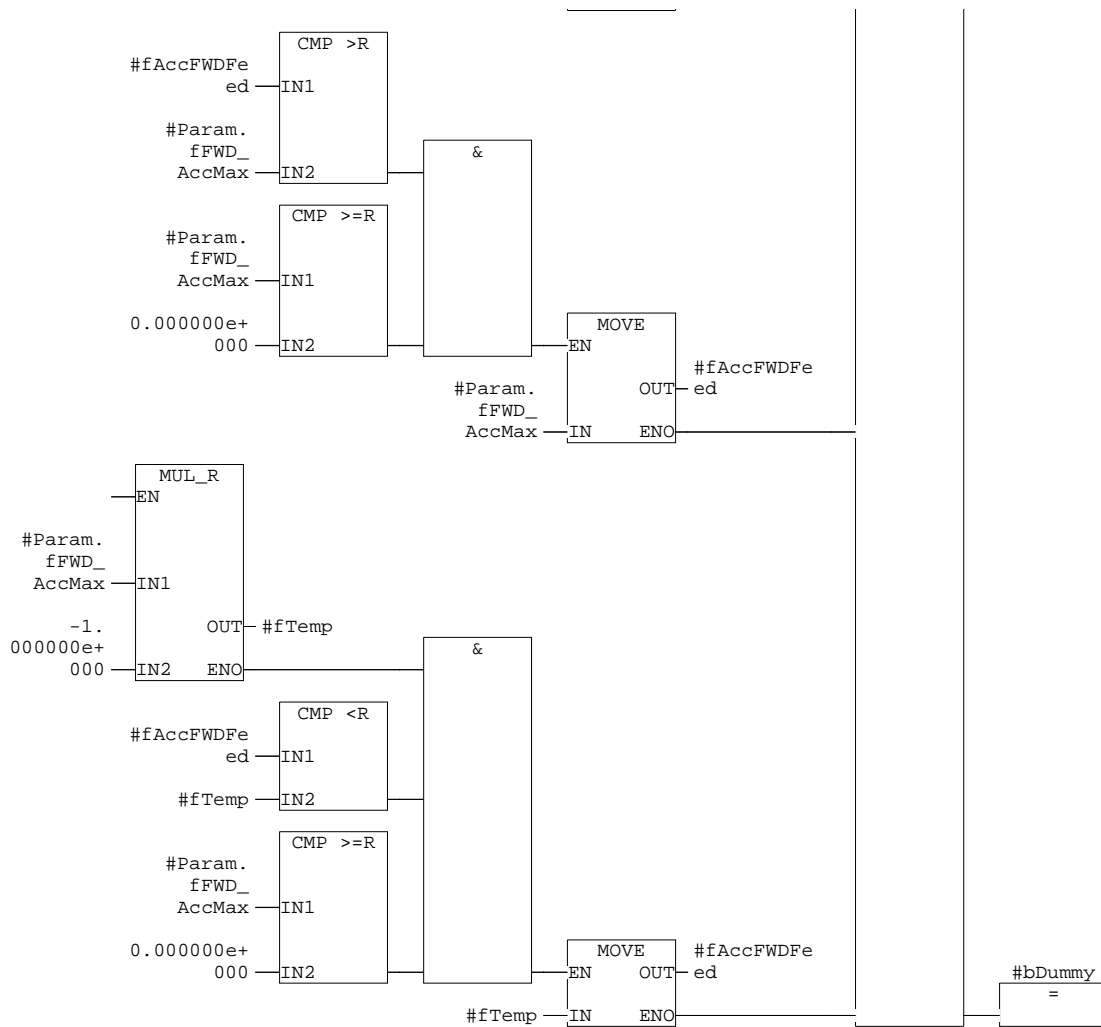


## Network: 18 Velocity and Acceleration Forward Feed

The velocity and acceleration forward feeds are given by applying gain factors to the heave velocity and acceleration inputs.

The acceleration flow contribution is limited by the fMaxAccelFWD parameter.

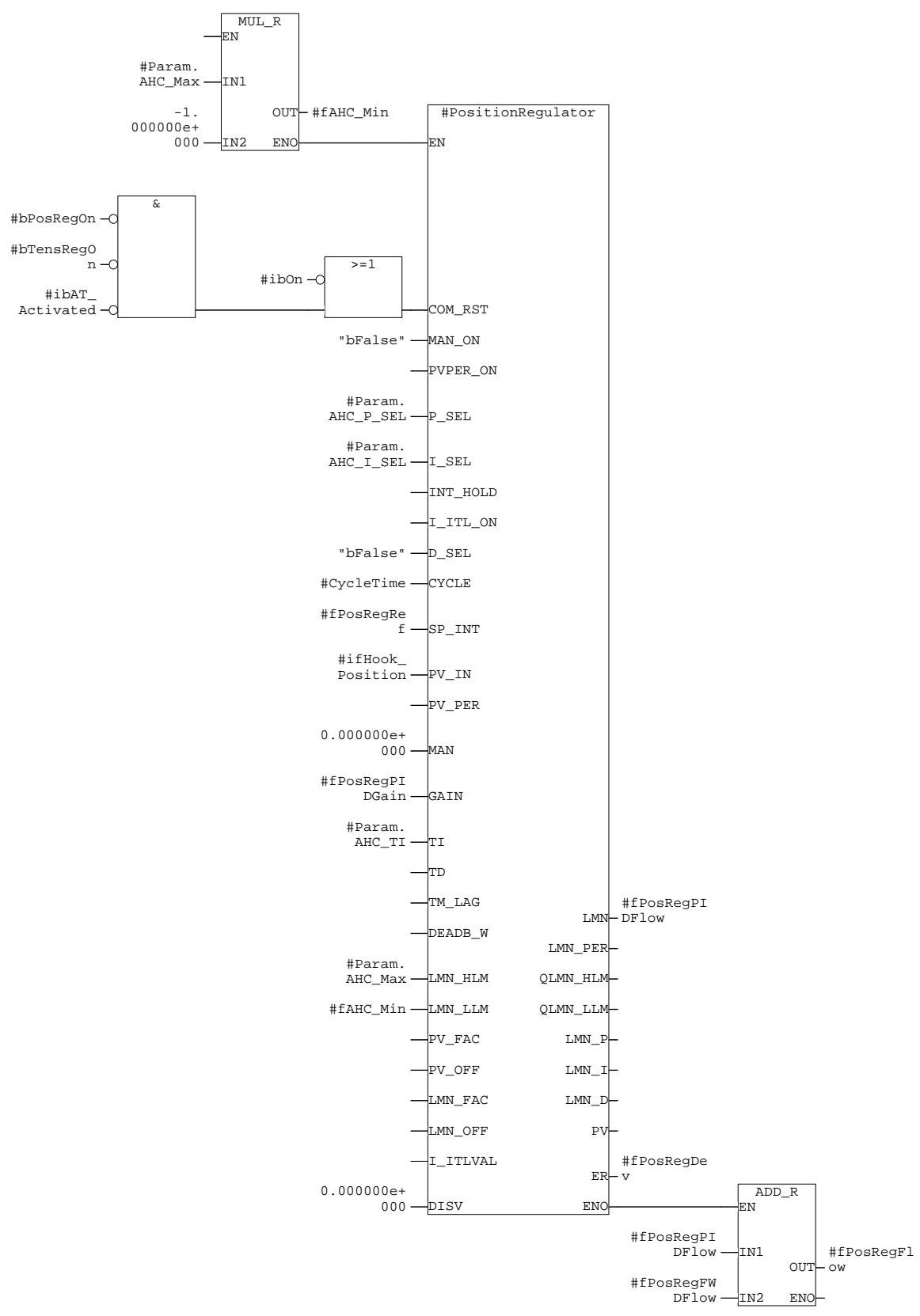


**Symbol information**

M10.1	bTestTrue	Always 1 for test purposes
#Param.fFWD_GAIN_Kv	#Param.fFWD_GAIN_Kv	Velocity FWD gain
#ifGainFactor	#ifGainFactor	Regulator gain factor from transmission
#fTemp	#fTemp	Temporary REAL
#fFilteredVelocity	#fFilteredVelocity	Filtered heave velocity
#fVelFWDFeed	#fVelFWDFeed	Velocity FWD feed
#Param.fFWD_VelMax	#Param.fFWD_VelMax	Maximum velocity FWD contribution (%)
#Param.fFWD_GAIN_Ka	#Param.fFWD_GAIN_Ka	Acceleration FWD gain
#ifHeave_Accel	#ifHeave_Accel	Heave acceleration
#fAccFWDFeed	#fAccFWDFeed	Acceleration FWD feed
#Param.fFWD_AccMax	#Param.fFWD_AccMax	Maximum acceleration FWD contribution (%)
#bDummy	#bDummy	Dummy bit

Network: 27      Position Regulator

Position regulator for ready and AHC modes.



Address	Symbol	Display format	Status value
1	//Oppdatering av parameterstillinger i funksjonsblokker		
2 M 100.7	"bParamIniSim"	BOOL	
3	//Presetting av tellekort		
4 M 100.4	"bPresetHookPos"	BOOL	
5	//Joystick operation = 0, AHC operation = 1		
6 M 100.5	"bAHCtoCtrlValve"	BOOL	
7	//Simulatoroutp. - Heave/Heave velocity/Roll/Pitch		
8 MD 512	"qfHeave"	FLOATING_POINT	
9 MD 516	"qfVelocity"	FLOATING_POINT	
10 MD 520	"qfPitch"	FLOATING_POINT	
11 MD 524	"qfRoll"	FLOATING_POINT	
12	//True heave param. - Delta T vel/Alpha vel/Delta T acc/Alpha acc		
13 MD 528	"ifDeltaTVelocity"	FLOATING_POINT	
14 MD 532	"ifAlphaVelocity"	FLOATING_POINT	
15 MD 536	"ifDeltaTAcc"	FLOATING_POINT	
16 MD 540	"ifAlphaAcc"	FLOATING_POINT	
17	//Simulatorsetp.		
18 MD 560	"ifHeaveAmplitude"	FLOATING_POINT	
19 MD 572	"ifPeriode"	FLOATING_POINT	
20 MD 564	"ifPitchAmplitude"	FLOATING_POINT	
21 MD 568	"ifRollAmplitude"	FLOATING_POINT	
22 M 100.3	"bSimulateOn"	BOOL	
23	//True heave outp. - True heave/True velocity/True acceleration		
24 MD 548	"fHeave"	FLOATING_POINT	
25 MD 552	"fHeaveVel"	FLOATING_POINT	
26 MD 556	"fHeaveAcc"	FLOATING_POINT	
27	//Actual hook position		
28 MD 576	"ifHookPosition"	FLOATING_POINT	

	Modify value
1	
2	true
3	
4	
5	
6	false
7	
8	
9	
10	
11	
12	
13	0.05
14	0.3
15	0.05
16	0.3
17	
18	2.0
19	10.0
20	0.0
21	0.0
22	false
23	
24	
25	
26	
27	
28	

Address	Symbol	Display format	Status value
29	//Regulator		
30	M 100.0 "bRegOn"	BOOL	
31	M 100.1 "bRegStop"	BOOL	
32	M 100.2 "bAHCActive"	BOOL	
33	DB98.DBD 2904 "Param".MW.AHC.AT.RegParam.fFWD_GAIN_Kv	FLOATING_POINT	
34	DB98.DBD 2908 "Param".MW.AHC.AT.RegParam.fFWD_GAIN_ka	FLOATING_POINT	
35	DB98.DBD 2924 "Param".MW.AHC.AT.RegParam.AHC_GAIN	FLOATING_POINT	
36	DB98.DBX 2932.1 "Param".MW.AHC.AT.RegParam.AHC_I_SEL	BOOL	
37	DB98.DBD 2928 "Param".MW.AHC.AT.RegParam.AHC_Tt	TIME	
38	DB98.DBD 3128 "Param".MW.AHC.fFWD_Kv_hoisting	FLOATING_POINT	
39	DB98.DBD 3296 "Param".MW.AHC.fFWD_Kv_lowering	FLOATING_POINT	
40	//Linearisert utgang fra regulator		
41	M 100.6 "bSelectLinOut"	BOOL	
42	//Regulatorpådrag		
43	MD 544 "fCtrlValveDrive"	FLOATING_POINT	
44			
45			
46			

Address	Symbol	Display format	Status value
29			
30			
31			
32			
33			
34			
35			
36			
37			
38			
39			
40			
41			
42			
43			
44			
45			
46			

# Appendix D

## Hose Table

APPENDIX D. HOSE TABLE

---

Table D.1: Hose table

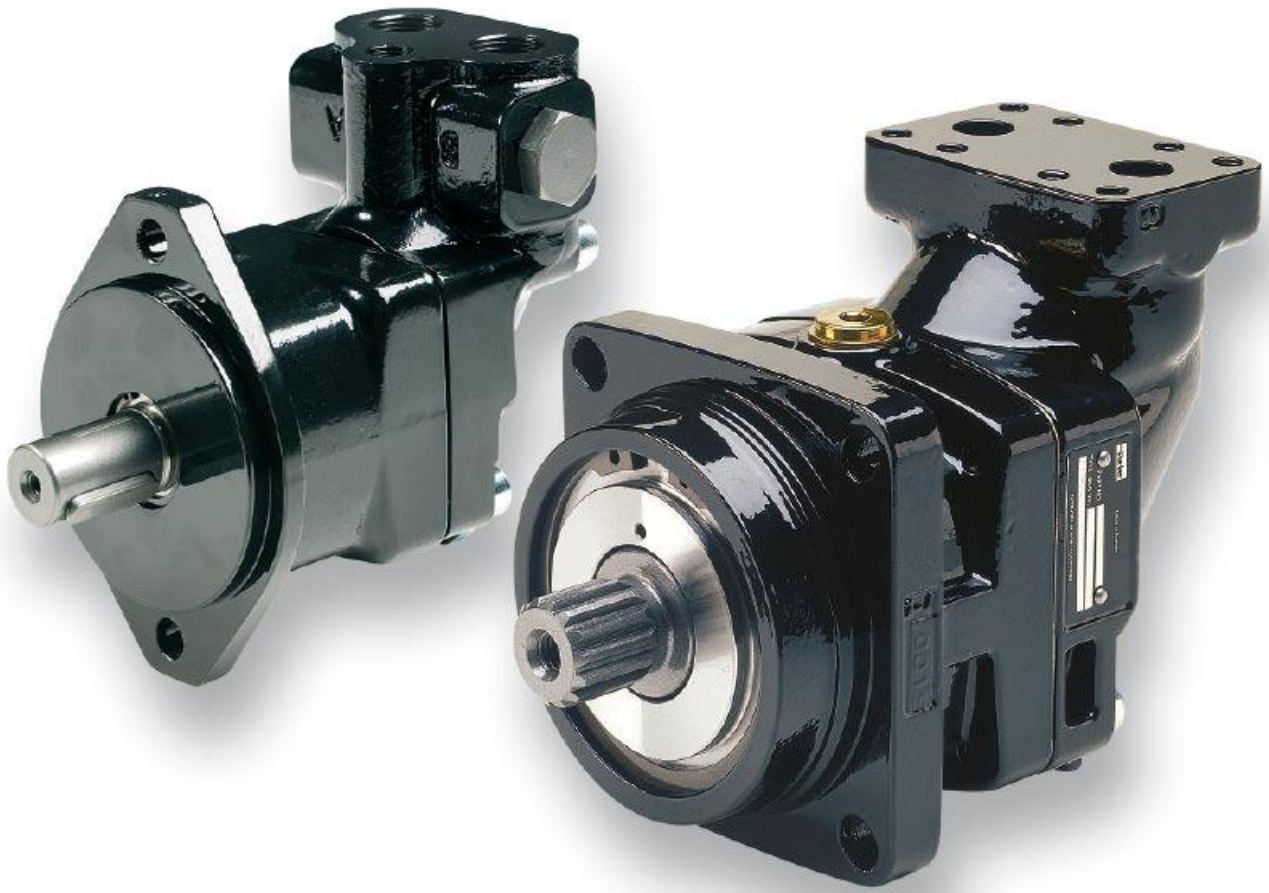
Hose Number	Size	Length [mm]	Coupling 1	Coupling 2
1	3/4"	1200	G536-25-12	G538-25-12
2	3/4"	1100	G536-25-12	G538-25-12
3	3/4"	900	G536-25-12	G538-25-12
4	1"	1100	G536-25-12	G538-25-12
5	3/8"	1500	G333-12-06	G334-12-06
6	1"	950	G336-30-16	G336-30-16
7	3/4"	1200	G536-25-12	G538-25-12
8	3/4"	1100	G536-25-12	G538-25-12
9	1/4"	400	G333-10-04	G334-10-04
10	1/4"	250	G333-10-04	G334-10-04
11	1/4"	700	G333-10-04	G334-10-04
12	3/8"	950	G333-12-06	G334-12-06
13	3/8"	550	G333-12-06	G334-12-06
14	3/8"	1000	G333-12-06	G334-12-06

# Appendix E

## Technical Datasheets

### E.1 Parker Hydraulic Motor





# Hydraulic Motor/Pump

Series F11/F12  
Fixed Displacement

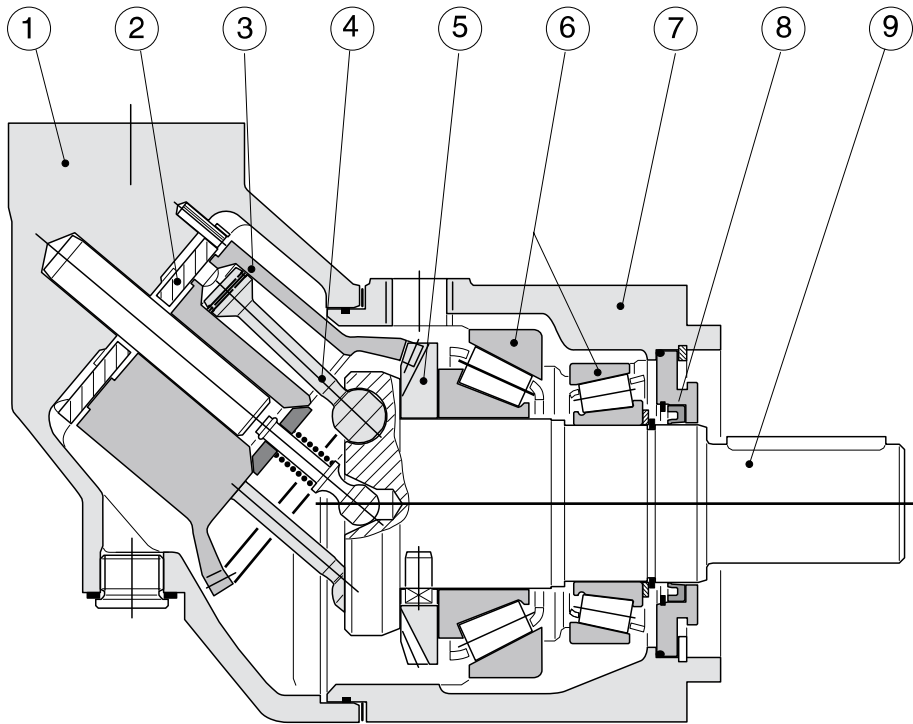
aerospace  
climate control  
electromechanical  
filtration  
fluid & gas handling  
**hydraulics**  
pneumatics  
process control  
sealing & shielding



ENGINEERING YOUR SUCCESS.

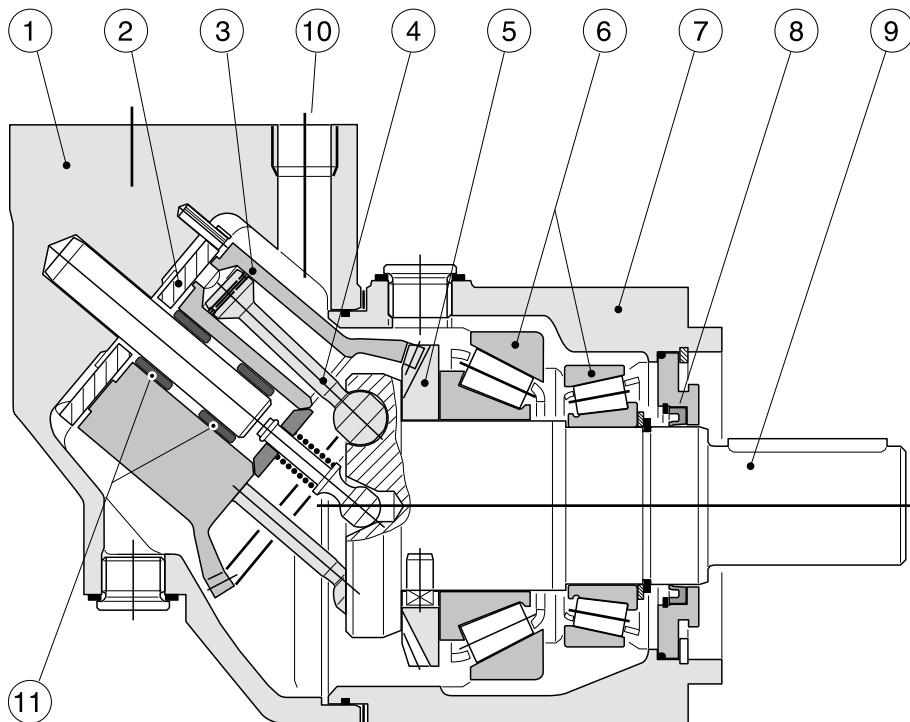
**F12 cross sections**

**F12-30, -40, -60, -80 and -90**  
 (F12-60 shown)



- Legend:
- |                            |                            |  |
|----------------------------|----------------------------|--|
| 1. Barrel housing          | 5. Timing gear             | 9. Output/input shaft                  |
| 2. Valve plate             | 6. Tapered roller bearings | 10. Port E (F12-110 and -125)          |
| 3. Cylinder barrel         | 7. Bearing housing         | 11. Needle bearings (F12-110 and -125) |
| 4. Piston with piston ring | 8. Shaft seal              |  |

**F12-110 and -125**  
 (F12-110 shown)



**Specifications**

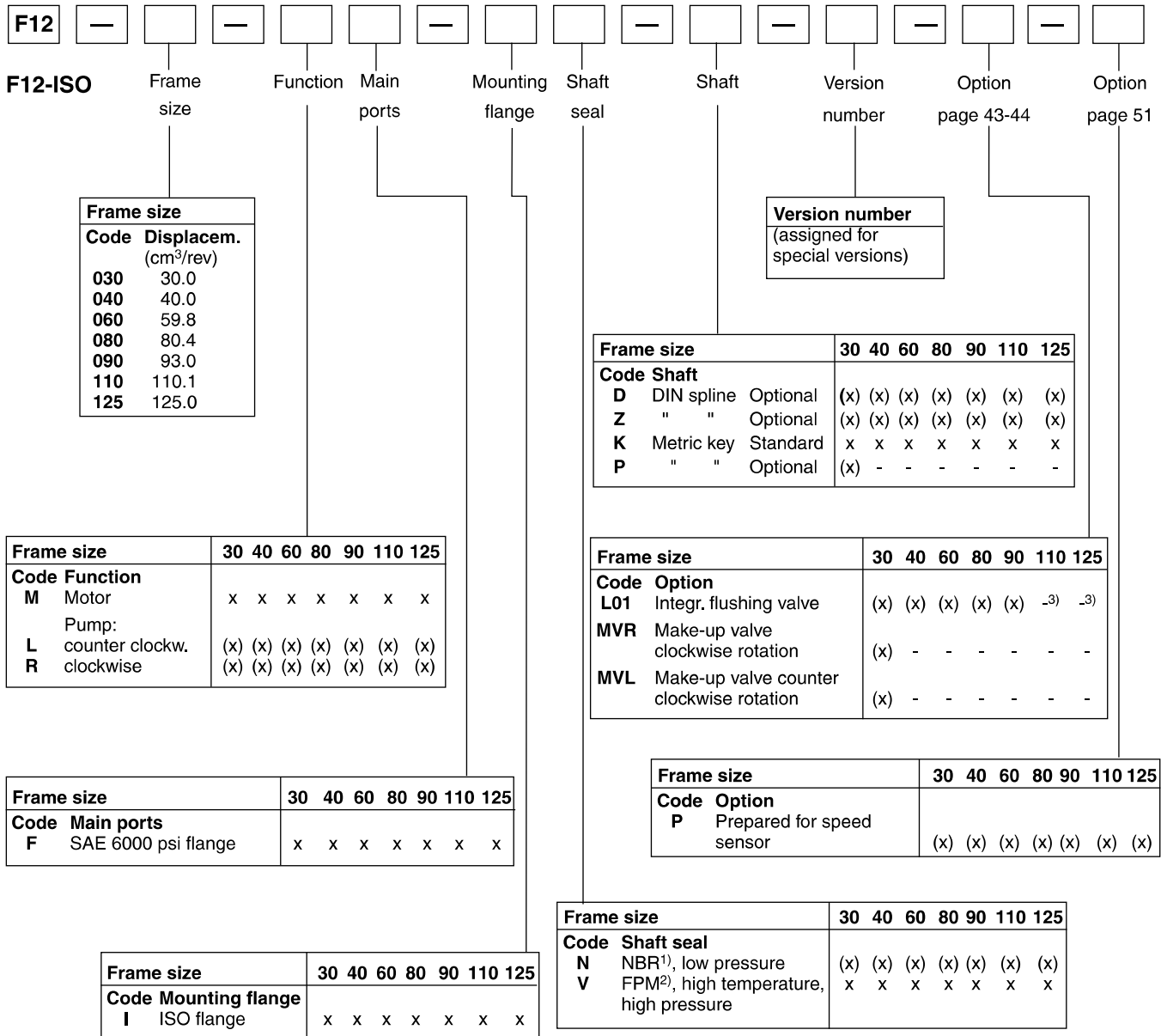
Hydraulic motor/pump

**Series F11/F12**

Frame size F11	-5	-6	-10	-12	-14	-19
<b>Displacement</b> [cm <sup>3</sup> /rev]	4.9	6.0	9.8	12.5	14.3	19.0
<b>Operating pressure</b>						
max intermittent <sup>1)</sup> [bar]	420	—————				420
max continuous [bar]	350	—————				350
<b>Motor operating speed</b> [rpm]						
max intermittent <sup>1)</sup>	14 000	11 200	11 200	10 300	9 900	8 900
max continuous	12 800	10 200	10 200	9 400	9 000	8 100
min continuous	50	—————				50
<b>Max pump selfpriming speed<sup>2)</sup></b>						
L or R function; max [rpm]	4 600	—	4 200	3 900	3 900	3 500
<b>Motor input flow</b>						
max intermittent <sup>1)</sup> [l/min]	69	67	110	129	142	169
max continuous [l/min]	63	61	100	118	129	154
<b>Main circuit temp.<sup>3)</sup>, max</b> [°C]	80					80
min [°C]	-40					-40
<b>Theoretical torque at 100 bar</b> [Nm]	7.8	9.5	15.6	19.8	22.7	30.2
<b>Mass moment of inertia</b>						
(x10 <sup>-3</sup> ) [kg m <sup>2</sup> ]	0.16	0.39	0.39	0.40	0.42	1.1
<b>Weight</b> [kg]	4.7	7.5	7.5	8.2	8.3	11

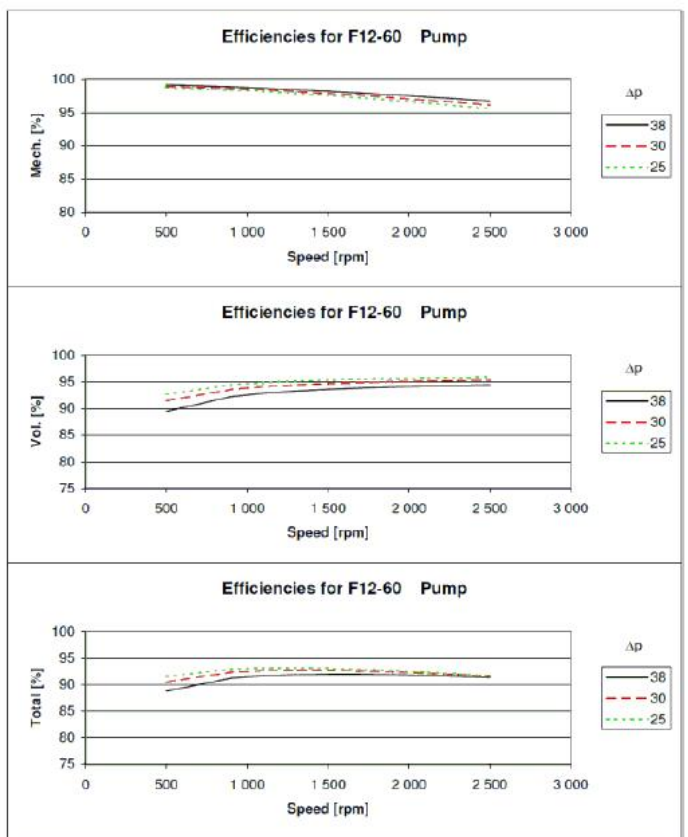
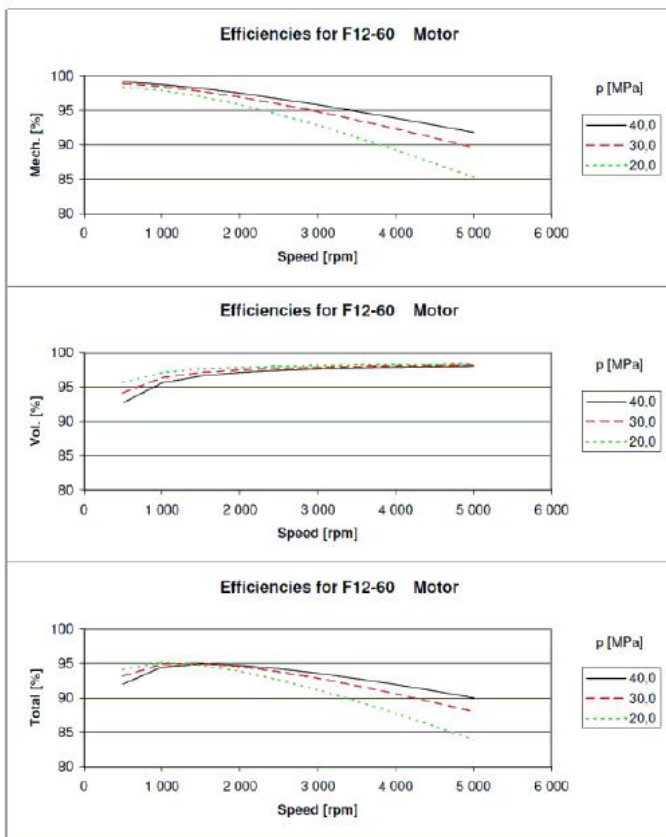
Frame size F12	-30	-40	-60	-80	-90	-110	-125	-150	-250	
<b>Displacement</b> [cm <sup>3</sup> /rev]	30.0	40.0	59.8	80.4	93.0	110.1	125.0	150	242	
<b>Operating pressure</b>										
max intermittent <sup>1)</sup> [bar]	480	—————			480	420	480	480	420	420
max continuous [bar]	420	—————			420	350	420	420	350	350
<b>Motor operating speed</b> [rpm]										
max intermittent <sup>1)</sup>	7 300	6 700	5 800	5 300	5 000	4 800	4 600	3 500	3 000	
max continuous	6 700	6 100	5 300	4 800	4 600	4 400	4 200	3 200	2 700	
min continuous	50	—————							50	
<b>Max pump selfpriming speed<sup>2)</sup></b>										
L or R function; max [rpm]	3150	2870	2500	2300	2 250	2200	2 100	1 700	1 500	
<b>Motor input flow</b>										
max intermittent <sup>1)</sup> [l/min]	219	268	347	426	465	528	575	525	726	
max continuous [l/min]	201	244	317	386	428	484	525	480	653	
<b>Main circuit temp.<sup>3)</sup>, max</b> [°C]	80								80	
min [°C]	-40								-40	
<b>Theoretical torque at 100 bar</b> [Nm]	47.6	63.5	94.9	127.6	147.6	174.8	198.4	238.1	384.1	
<b>Mass moment of inertia</b>										
(x10 <sup>-3</sup> ) [kg m <sup>2</sup> ]	1.7	2.9	5	8.4	8.4	11.2	11.2	40	46	
<b>Weight</b> [kg]	12	16.5	21	26	26	36	36	70	77	

1) Intermittent: max 6 seconds in any one minute.  
 2) Selfpriming speed valid at sea level.  
 3) See also installation information, operating temperature.



x: Available      (x): Optional      -: Not available  
 1) NBR - Nitrile rubber  
 2) FPM - Fluor rubber  
 3) F12-110 and -125: Accessory valve block (page 45)

## F12-060



## **E.2 Parker Servo Valve**

**Characteristics**

**Direct Operated Proportional DC Valve  
Series D3FP**

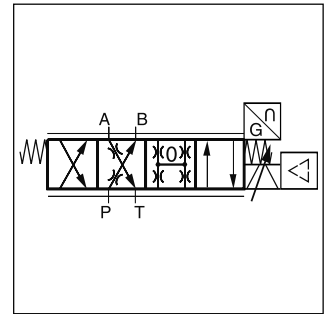
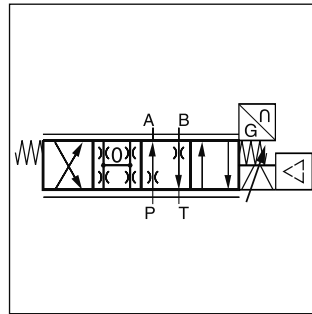
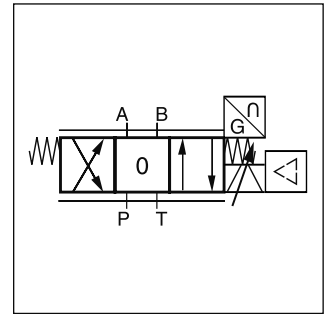
The direct operated control valve D3FP of the nominal size NG10 (CETOP05) shows extremely high dynamics combined with high flow. First of all it is used for highest accuracy in positioning of hydraulic axis and controlling of pressure and velocity.

Driven by the new patented VCD® actuator the D3FP reaches the frequency response of real servovalves.

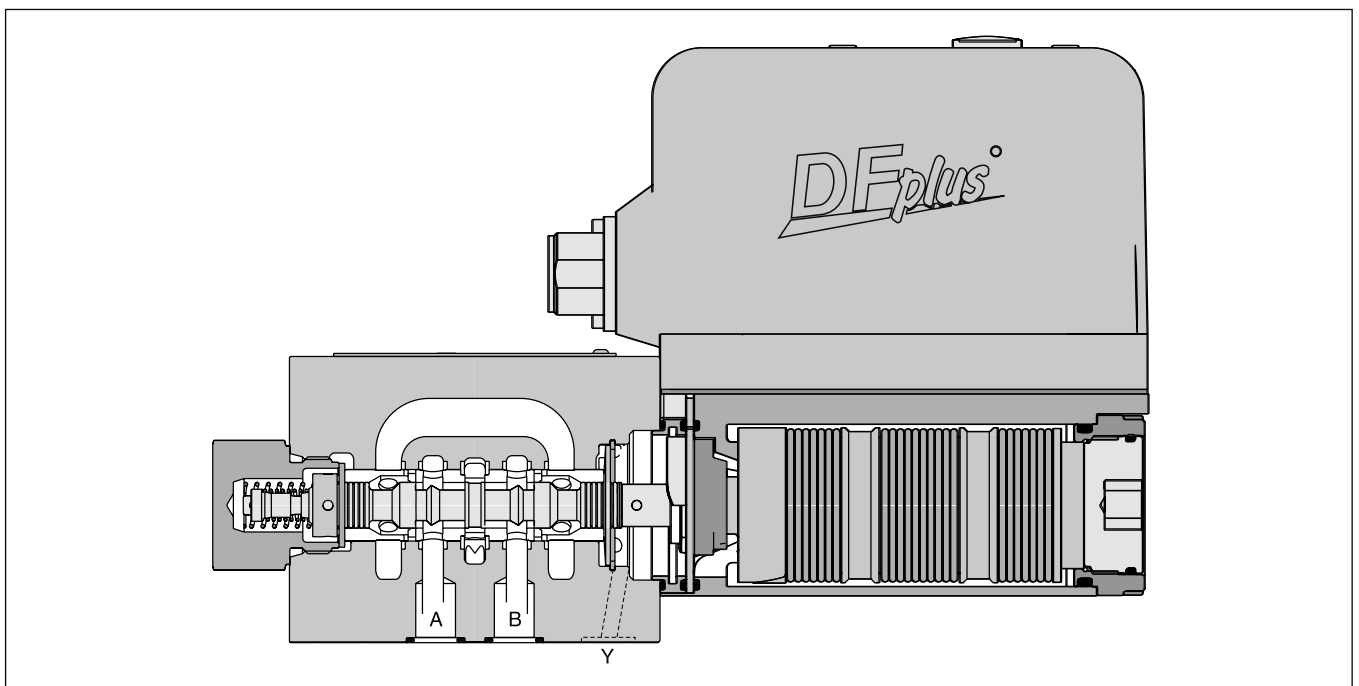
At power-down the spool moves in a defined position. All common input signals are available.

**Technical features**

- Real servovalve dynamics (-3dB/350Hz at ±5% input signal)
- Max. tank pressure 350 bar (with external drain port Y)
- Defined spool positioning at power-down - optional P-A/B-T or P-B/A-T or center position (for overlapped spools)
- Onboard electronics
- Spool / sleeve design

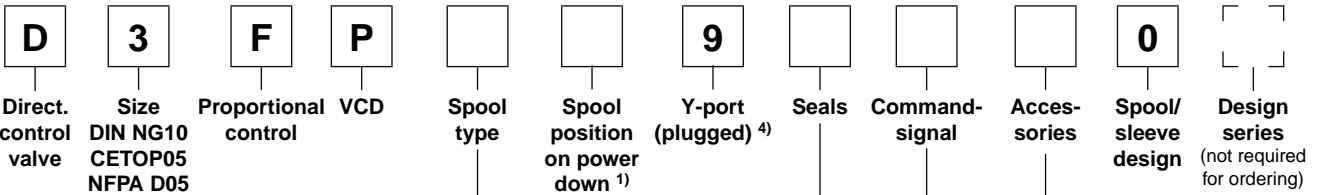


**3**



D3FP UK.INDD RH 15.08.2011

Ordering Code



3

Code	Spool type	Flow [l/min] at Δp 35bar per metering edge
Zerolap		
E50Y		100
E50P		50
B60Y	$Q_B = Q_A / 2$ 	100
B60P	$Q_B = Q_A / 2$ 	50
Underlap approx. -0.5%		
E55Y		100
E55P		50
Overlap 18%		
E01Y		100
E01P		50
E02Y		100
E02P		50
B31Y	$Q_B = Q_A / 2$ 	100 / 50
B31P		50 / 25
B32Y	$Q_B = Q_A / 2$ 	100 / 50
B32P		50 / 25

Code	Connection type
0	6 + PE acc. EN175201-804
5	11 + PE acc. EN175201-804
7	6 + PE + Enable

Code	Signal	Function
B	+/- 10V	0...+10V -> P-A
E	+/- 20mA	0...+20mA -> P-A
S	4...20mA	12...20mA -> P-A

Code	Seals
N	NBR
V	FPM
H	for HFC fluid

Code	Spool pos. at power down
A <sup>2)</sup>	
B <sup>2)</sup>	
C <sup>3)</sup>	

- 1) On power down the spool moves in a defined position. This cannot be guaranteed in case of single flow path on the control edge A – T resp. B – T with pressure drops above 120 bar or contamination in the hydraulic fluid.
- 2) approx. 10% opening, only zerolapped spools and underlapped spools.
- 3) only for overlapped spools
- 4) needs to be removed at tank pressure >35 bar

Please order connector separately.  
See chapter 3 accessories.

**Bold letters =**  
Short-term availability



<b>General</b>			
Design	Direct operated proportional DC valve		
Actuation	VCD® actuator		
Size	NG10/CETOP05/NFPA D05		
Mounting interface	DIN 24340 / ISO 4401 / CETOP RP121 / NFPA		
Mounting position	unrestricted		
Ambient temperature	[°C]	-20...+50	
MTTF <sub>D</sub> value	[years]	75	
Weight	[kg]	6.5	
Vibration resistance	[g]	10 Sinus 5...2000 Hz acc. IEC 68-2-6 30 Random noise 20...2000 Hz acc. IEC 68-2-36 15 Shock acc. IEC 68-2-27	
<b>Hydraulic</b>			
Max. operating pressure	[bar]	Ports P, A, B 350	
	[bar]	Port T max. 35, port Y max. 35 <sup>1)</sup>	
Fluid	Hydraulic oil as per DIN 51524...535, other on request		
Fluid temperature	[°C]	-20...+60	
Viscosity	permitted [cSt] / recommended [cSt]	[mm <sup>2</sup> /s]	20...380
		[mm <sup>2</sup> /s]	30...80
Filtration	ISO 4406 (1999) 18/16/13 (meet NAS 1638: 7)		
Flow nominal at Δp=35bar per control edge <sup>2)</sup>	[l/min]	50 / 100	
Flow maximum	[l/min]	150	
Leakage at 100 bar	[ml/min]	<400 (Zerolap spool); <100 (Overlap spool)	
<b>Static / Dynamic</b>			
Step response at 100% step <sup>3)</sup>	[ms]	<6	
Frequency response (±5% signal) <sup>3)</sup>	[Hz]	200 (amplitude ratio -3dB), 200 (phase lag -90°)	
Hysteresis	[%]	<0.05	
Sensitivity	[%]	<0.03	
Temperature drift	[%/K]	<0.025	
<b>Electrical characteristics</b>			
Duty ratio	[%]	100	
Protection class	IP65 in accordance with EN 60529 (with correctly mounted plug-in connector)		
Supply voltage/ripple	[V]	22 ... 30, ripple <5% eff., surge free	
Current consumption max.	[A]	3.5	
Pre-fusing	[A]	4.0 medium lag	
Input signal			
Voltage	[V]	10...0...-10, ripple <0.01% eff., surge free, 0...+10V P->A	
Impedance	[kOhm]	100	
Current	[mA]	20...0...-20, ripple <0.01% eff., surge free, 0...+20mA P->A	
Impedance	[Ohm]	250	
Current	[mA]	4...12...20, ripple <0.01% eff., surge free, 12...20mA P->A	
Impedance	[Ohm]	250	
Differential input max.			
Code 0	[V]	30 for terminal D and E against PE (terminal G)	
Code 5	[V]	30 for terminal 4 and 5 against PE (terminal ⊥)	
Code 7	[V]	30 for terminal D and E against PE (terminal G)	
Enable signal (only code 5/7)	[V]	5...30, Ri = 9 kOhm	
Diagnostic signal	[V]	+10...0...-10 / +Ub, rated max. 5mA	
EMC		EN 61000-6-2, EN 61000-6-4	
Electrical connection	Code 0/7	6 + PE acc. EN 175201-804	
	Code 5	11 + PE acc. EN 175201-804	
Wiring min.	Code 0/7	[mm <sup>2</sup> ]	7 x 1.0 (AWG 18) overall braid shield
	Code 5	[mm <sup>2</sup> ]	8 x 1.0 (AWG 18) overall braid shield
Wiring length max.	[m]	50	

<sup>1)</sup> For applications with p<sub>p</sub>>35 bar the Y-port has to be connected and the plug in the Y-port has to be removed.

<sup>2)</sup> Flow rate for different Δp per control edge:

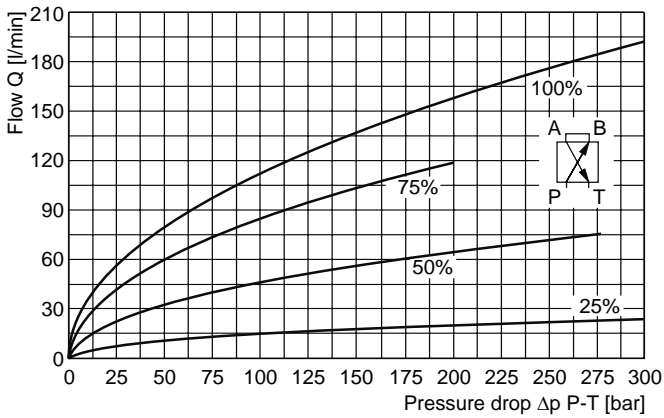
$$Q_x = Q_{Nom.} \cdot \sqrt{\frac{\Delta p_x}{\Delta p_{Nom.}}}$$

<sup>3)</sup> Measured with load (100 bar pressure drop/two control edges)

**Functional limits\***

at 25%, 50%, 75% and 100% command signal

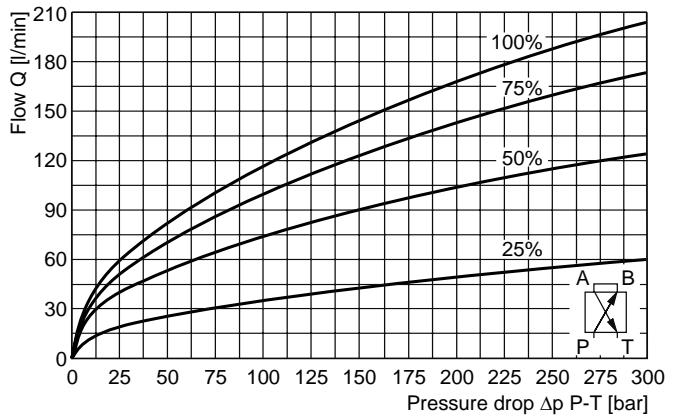
Spool type **E01/E02**



**Functional limits\***

at 25%, 50%, 75% and 100% command signal

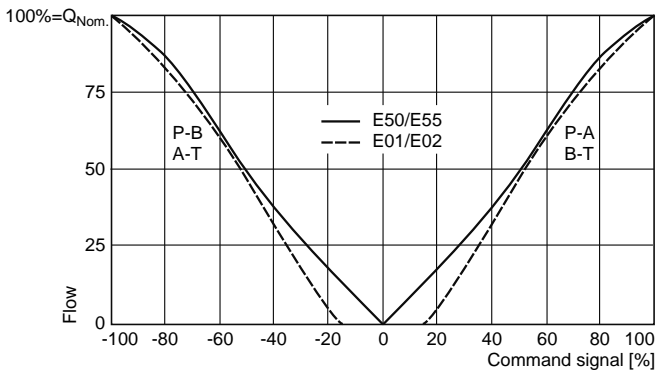
Spool type **E50/E55**



**Flow curves**

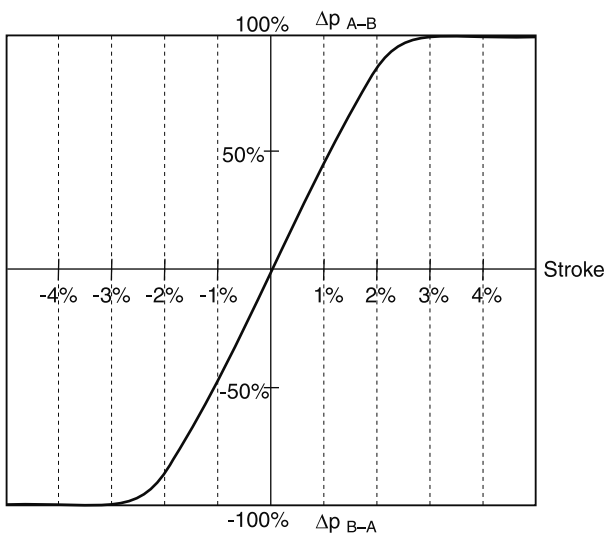
at  $\Delta p = 35$  bar per metering edge

Spool type **E50/E55, E01/E02**



**\* When exceeding the functional limits, for a period of time the valve will go into fail safe and power supply needs to be switched off/on to re-enable the valve.**

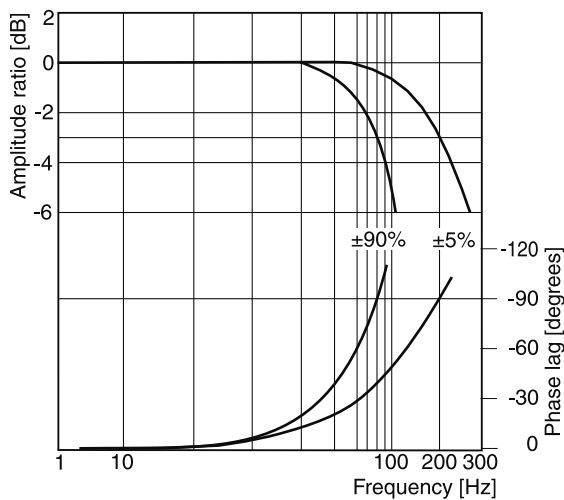
**Pressure gain**



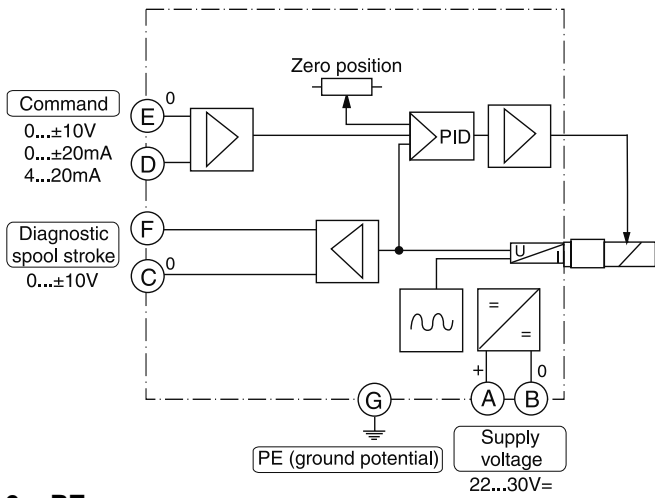
**Frequency response**

$\pm 5\%$  command signal

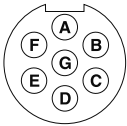
$\pm 90\%$  command signal



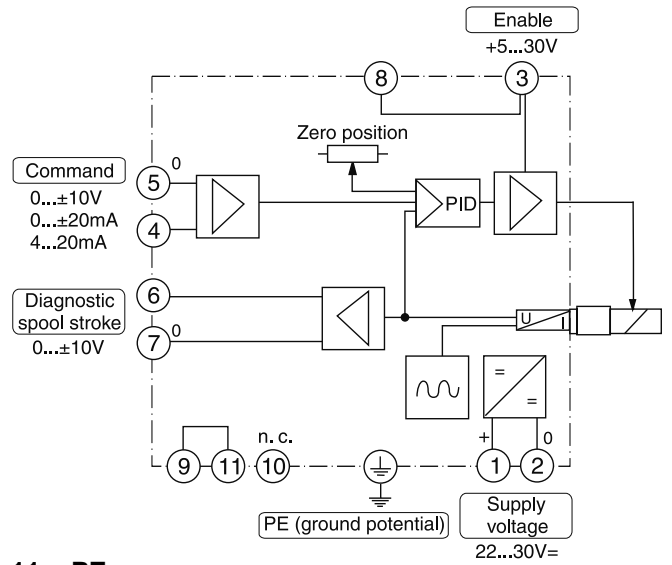
**Code 0**



**6 + PE**



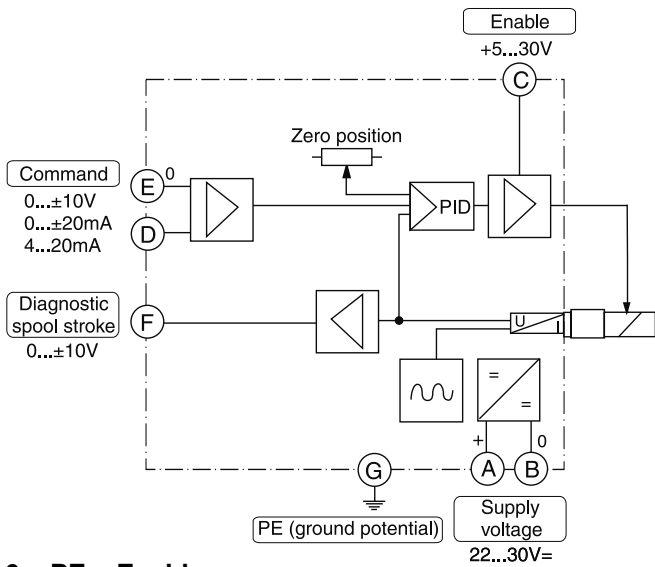
**Code 5**



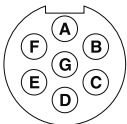
**11 + PE**



**Code 7**



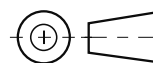
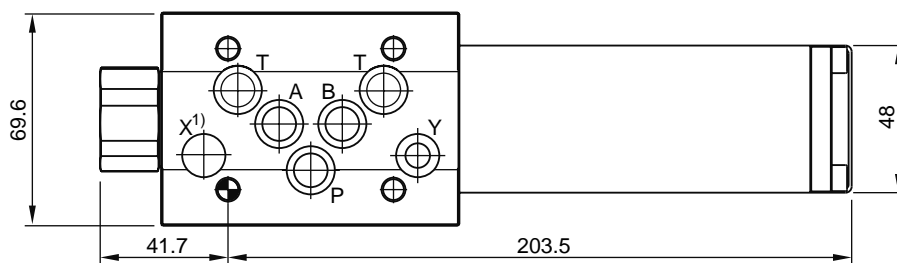
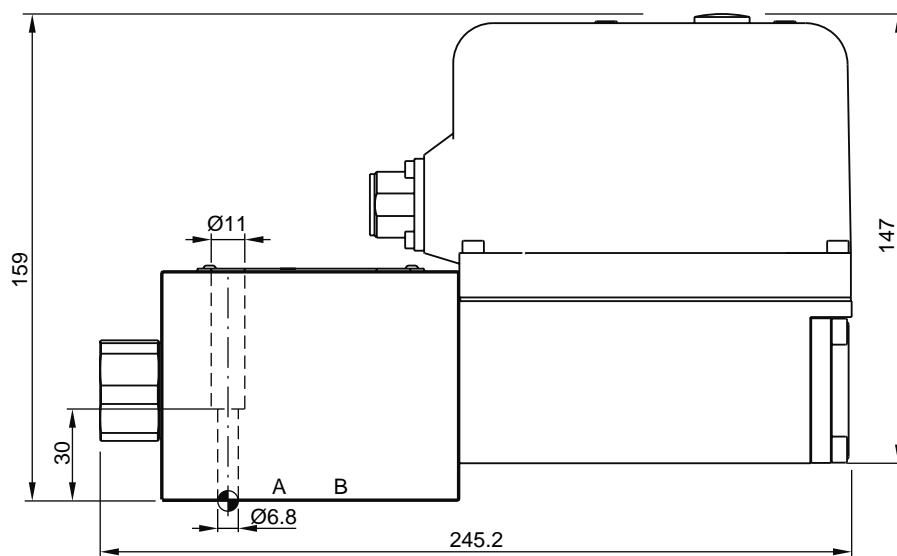
**6 + PE + Enable**







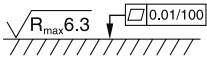
**3**

**Dimensions**

3



<sup>1)</sup> O-ring recess diameter on valve body.

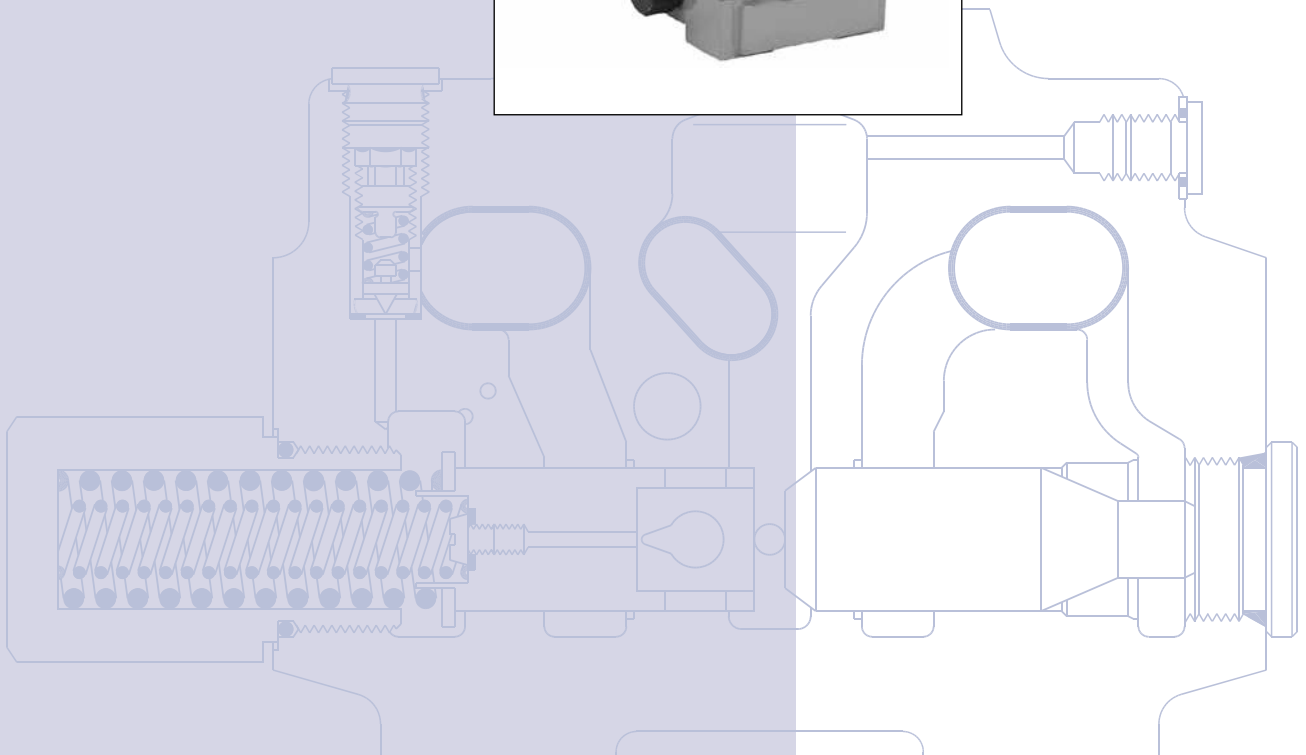
Surface finish	 Kit	 Kit	 Kit	 Kit
	BK385	4xM6x40 DIN 912 12.9	13.2 Nm ±15%	NBR: SK-D3FP FPM: SK-D3FP-V HFC: SK-D3FP-H

### **E.3 Sauer Danfoss PVG120**



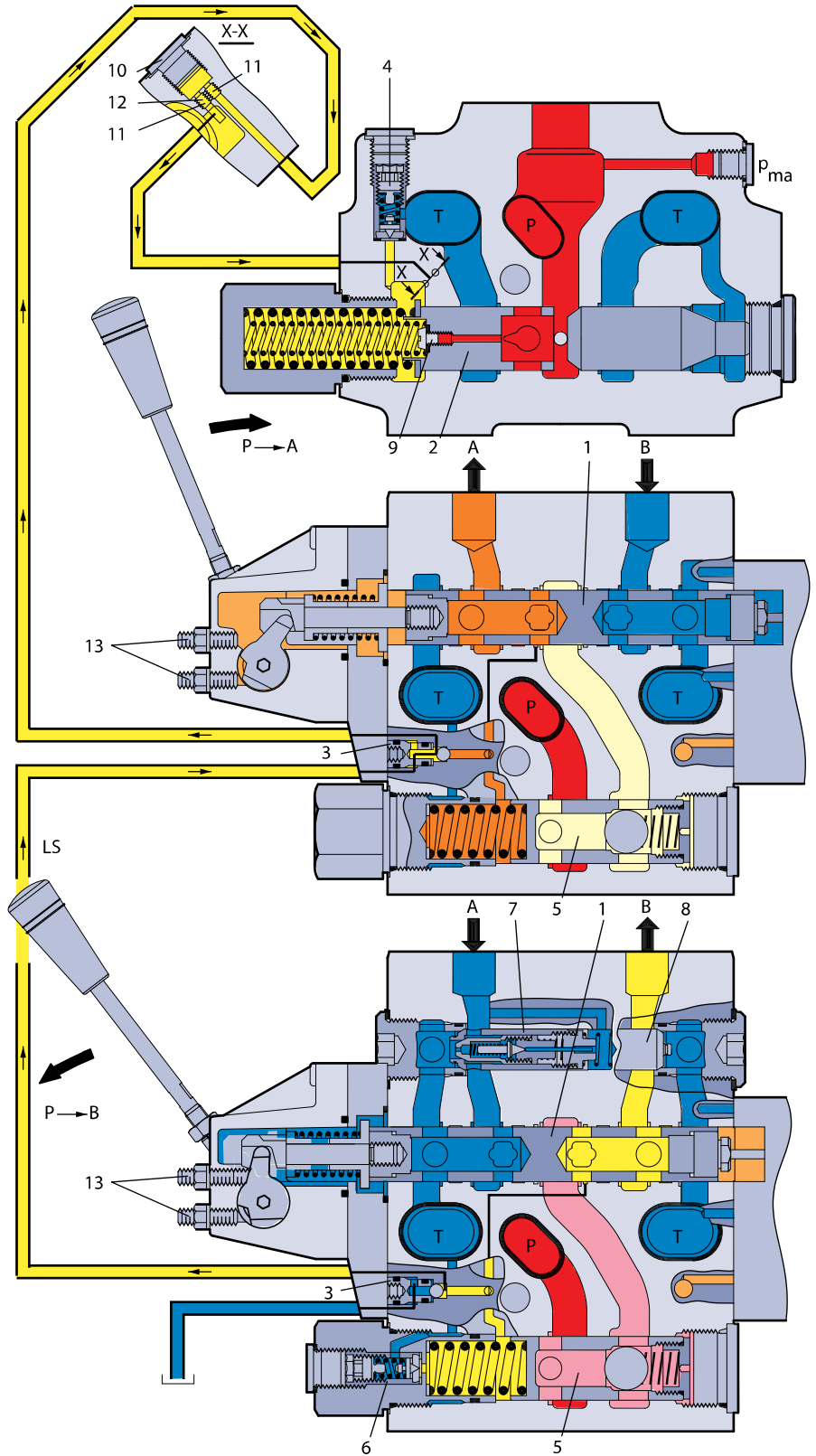
# PVG 120 Proportional Valves

## Technical Information



**PVG 120 Sectional Drawing**

1. Main spool
2. Pressure adjustment spool in PVP
3. Shuttle valve
4. Pressure relief valve in PVP
5. Pressure compensator in PVB
6. LS pressure relief valve in PVB
7. Shock and suction valve PVLP
8. Suction valve PVLA
9. Orifice, closed centre PVP  
Plug, open centre PVP
10. LS connection
11. Orifice, open centre PVP
12. Plug, closed centre PVP



V310100.A

PVG 120 Valve Group

<b>Max. pressure</b>	<b>Port P</b>	<b>continuous</b>	350 bar	[5075 psi]
		<b>intermittent<sup>1)</sup></b>	400 bar	[5800 psi]
	<b>Port A/B</b>		400 bar	[5800 psi]
	<b>Port T, static/dynamic</b>		25 bar/40 bar	[365/580 psi]
<b>Oil flow, (see characteristics page 27)</b>	<b>Port P, rated max.</b>		240/300 l/min	[63.4/79.3 gpm]
	<b>Port A/B</b>		65/95/130/180/ 210/240 l/min <sup>2)</sup>	[17.2/25.1/34.3/47.6/ 55.5/63.4 gpm <sup>2)</sup>
<b>Spool travel</b>			± 8 mm	[± 0.32 in]
<b>Dead band (± 25%)</b>			± 2 mm	[± 0.08 in]
<b>Max. internal leakage at 100 bar, 21 mm<sup>2</sup>/s</b>	<b>A/B → T, without shockvalve</b>		90 cm <sup>3</sup> /min	[5.5 in <sup>3</sup> /min]
	<b>A/B → T, with shockvalve</b>		95 cm <sup>3</sup> /min	[5.6 in <sup>3</sup> /min]
<b>Oil temperature (inlet temperature)</b>	<b>Recommended temperature</b>		30 to 60°C	[86 to 140°F]
	<b>Min. temperature</b>		-30°C	[-22°F]
	<b>Max. temperature</b>		+90°C	[+194°F]
<b>Ambient temperature</b>			-30 to +60°C	[-22 to +140°F]
<b>Oil viscosity</b>	<b>Operating range</b>		12 to 75 mm <sup>2</sup> /s	[65 SUS to 347 SUS]
	<b>Min. viscosity</b>		4 mm <sup>2</sup> /s	[39 SUS]
	<b>Max. viscosity</b>		460 mm <sup>2</sup> /s	[2128 SUS]
<b>Filtering (See page 39)</b>	<b>Max. contamination (ISO 4406)</b>		23/19/16	
<b>Oil consumption in pressure reduction valve for PVT at PVE pilot-oil supply</b>			0.4 l/min	[0.1 gpm]

1) Intermittent operation: the permissible values may occur for max. 10% of every minute.

2) See page 25 regarding the ordering or conversion of valve groups for oil flows exceeding 180 l/min [47.6 gpm].

**Mechanical Actuation PVM**

<b>Operating force</b>	<b>PVM + PVMD</b>	Neutral position	2.8 ± 0.2 N·m	4.0 ± 0.2 N·m
			[24.8 ± 1.8 lbf·in]	[35.5 ± 1.8 lbf·in]
	<b>PVM + PVE (without voltage)</b>	2.8 ± 0.2 N·m	4.0 ± 0.2 N·m	
		[24.8 ± 1.8 lbf·in]	[35.5 ± 1.8 lbf·in]	
	<b>PVM + PVH</b>	4.7 ± 0.2 N·m	12.8 ± 0.2 N·m	
		[41.6 ± 1.8 lbf·in]	[113.3 ± 1.8 lbf·in]	
<b>Possible control lever positions</b>	<b>Number</b>	2 × 5		
<b>Regulation range, control lever</b>		±19,5°		

**Hydraulic Actuation PVH**

<b>Control range</b>	5 to 15 bar	[75 to 220 psi]
<b>Max. pilot pressure, static</b>	35 bar	[510 psi]
<b>Max. pressure on port T *</b>	3 bar	[45 psi]

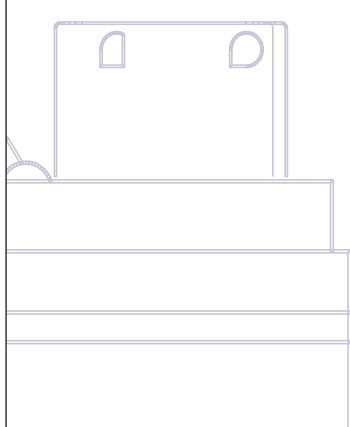
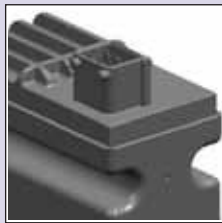
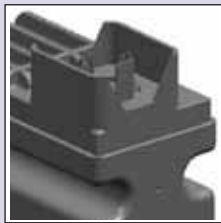
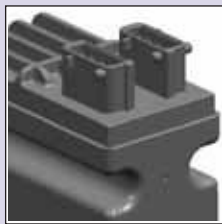
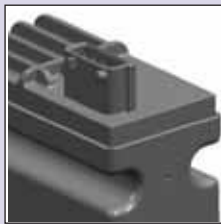
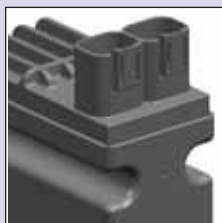
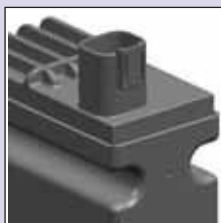
\* It is recommended that the tank connection from the hydraulic remote control unit PVRH is taken direct to tank.





PVE – Series 4  
for PVG 32, PVG 100  
and PVG 120

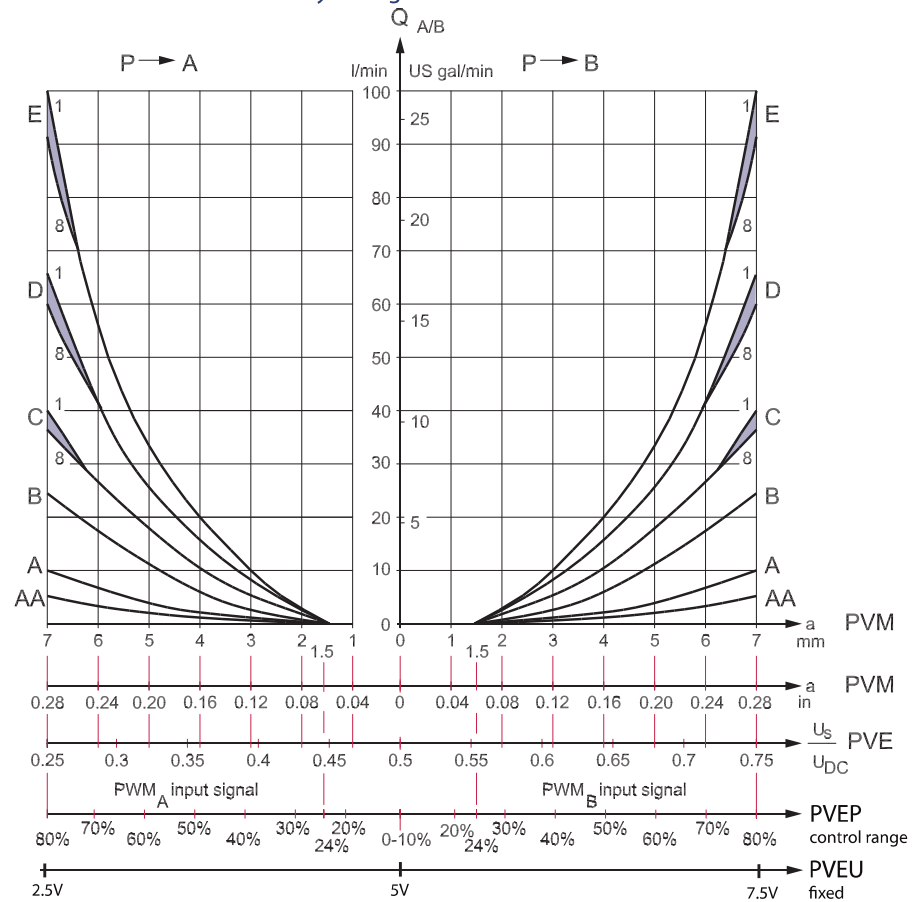
Technical  
Information



**PVE Control by Voltage**

- The standard PVE is controlled with a low current voltage signal.
- The spool stroke is proportional to the control voltage ( $U_s$ ).
- The power is supplied via the supply wire ( $U_{BAT}$  or  $U_{DC}$ ).
- The ratio  $U_s / U_{DC}$  define the actuation.
- A not connected  $U_s$  pin (floating) is recognized as  $U_s = \frac{1}{2}U_{DC}$

*PVE characteristic – control by voltage*



*Values for standard mounted PVE (PVEA/M/H/S)*

Function	Signal voltage ( $U_s$ )
Neutral	$U_s = 0.5 \cdot U_{DC}$
Q: P → A	$U_s = (0.5 \rightarrow 0.25) \cdot U_{DC}$
Q: P → B	$U_s = (0.5 \rightarrow 0.75) \cdot U_{DC}$

**PLUS+1™ compliance**

PVEA, PVEH, PVES, PVEO, PVEP and PVED can be controlled by PLUS+1.

The  $U_{DC}$  has a capacitance of 2,2uF which can give problems with some micro-controller power supply. To eliminate this problem Sauer-Danfoss has designed a special resistance supply and control cable.

**ATEX PVE**

The Sauer-Danfoss PVE ATEX portfolio has the same monitoring and control characteristics as the equivalent standard PVE.

**Operating Parameters  
 (continued)**

*PVEP*

Supply voltage $U_{DC}$ range	11 ÷ 32 V
Supply voltage $U_{DC}$ max. ripple	5%
Supply voltage $U_{DC}$ over voltage (max. 5 min)	36 V
PWM control range (duty cycle)	10 ÷ 80%
PWM frequency	100 ÷ 1000 Hz
PWM input voltage swing	0 - $U_{DC}$
PWM Trigger point	70% of $U_{DC}$
Input impedance (standard pull down)	5 k $\Omega$
Input capacitor	---
Power consumption	7 W
Error voltage: Fault	$U_{DC}$
Error voltage: No Fault	< 2 V

All connector terminals are short-circuit protected, protected against reverse connection and their combinations. Connecting error pins from two or more PVE's will cause the surveillance system to malfunction.

*Reaction time PVEA, PVEH and PVES (minus PVG 120)*

Supply voltage	Function		PVEA Prop. fine s	PVEH Prop. high s	PVES Prop. super s	PVEP PWM Ctrl s
Disconnected by means of neutral switch	Reaction time from neutral position to max. spool travel	max.	0.500	0.230	0.230	0.230
		rated	0.320	0.150	0.150	0.150
		min.	0.250	0.120	0.120	0.120
	Reaction time from max. spool travel to neutral position	max.	0.550	0.175	0.175	0.175
		rated	0.400	0.090	0.090	0.090
		min.	0.300	0.065	0.065	0.065
Constant voltage	Reaction time from neutral position to max. spool travel	max.	0.500	0.200	0.200	0.200
		rated	0.320	0.120	0.120	0.120
		min.	0.250	0.050	0.050	0.050
	Reaction time from max. spool travel to neutral position	max.	0.250	0.100	0.100	0.100
		rated	0.200	0.090	0.090	0.090
		min.	0.150	0.065	0.065	0.065
Hysteresis*	rated	2%	4%	0%	5%	

\* Hysteresis is indicated at rated voltage and  $f=0.02$  Hz for one cycle (one cycle = neutral → full A → full B → neutral).

## **E.4 Brevini Hydraulic Winch**

